Final Technical Report (FTR)

a. *Federal Agency*	Department of Energy	
b. *Award Number*	DE-EE0008351	
c. *Project Title*	Modular HF Isolated MV String Inverters Enable a New Paradigm for Large PV Farms	
d. *Recipient Organization*	Georgia Institute of Technology	
e. *Project Period*	*Start:* 08/01/2018	*End:* 07/31/2022
f. *Principal Investigator (PI)*	Name: Deepak Divan Title: Professor Email address: ddivan@gatech.edu Phone number: 404-385-4036	
g. *Business Contact (BC)*	Name: Douglas Feller Title: Sponsored Accountant II, Grants & Contracts Accounting Email address: douglas.feller@business.gatech.edu Phone number: (404) 385-4195	
h. *Certifying Official (if different from the PI or BC)*		

_____ _____

Signature of Certifying Official *Date*

By signing this report, I certify to the best of my knowledge and belief that the report is true, complete, and accurate. I am aware that any false, fictitious, or fraudulent information, misrepresentations, half-truths, or the omission of any material fact, may subject me to criminal, civil or administrative penalties for fraud, false statements, false claims or otherwise. (U.S. Code Title 18, Section 1001, Section 287 and Title 31, Sections 3729-3730). I further understand and agree that the information contained in this report are material to Federal agency's funding decisions and I have any ongoing responsibility to promptly update the report within the time frames stated in the terms and conditions of the above referenced Award, to ensure that my responses remain accurate and complete.

1. Acknowledgment

"This material is based upon work supported by the U.S. Department of Energy's Office of Energy Efficiency and Renewable Energy (EERE), and the Solar Energy Technologies Office (SETO) under the Advanced Power Electronics Design For Solar Applications (DE-FOA-0001740) Award Number(s) DE-EE0008351."

2. Disclaimer

3. Executive Summary

The “Modular HF Isolated MV String Inverters Enable a New Paradigm for Large PV Farms” project focuses on exploring alternative power converter and system-level plant configurations to achieve the lowest cost and highest energy output for a given solar plus storage (e.g., PV + battery) plant, including the use of medium voltage (MV) collection while taking into account detailed models of all elements. To realize this objective, four approaches were utilized (i) employ a novel Medium Voltage String Inverter (MVSI) topology (soft switching solid state transformer – S4T) to convert 1000 Vdc to 4.16 kVac; (ii) plant collection using standard, low-cost overhead MV distribution network; (iii) enable energy storage integration without additional converter cost to achieve dispatchability of the PV resource; and (iv) provide advanced functionality (autonomous operation, track ISO signals for dynamic balancing and ancillary services, and PV farm operation as a virtual grid resource). Subsequently and in alignment with the previously mentioned approaches, the project was structured in five efforts (i) S4T MVSI simulation and design; (ii) system analysis and storage optimization; (iii) financial analysis; (iv) power converter prototype build and test; and (v) regulatory and commercial impact study. The outcomes provided by each effort can be summarized as follows (i) Project explored the use of MV AC distribution architecture for hybrid PV+storage utility-scale PV farms; (ii) Detailed loss and LCOE analysis for AC and DC side BESS architecture, including multiple converter topologies, as well as for proposed MVSI/MDCT systems; (iii) MVSI was built and holds promise but needs lower-cost high-voltage Si-C devices, which does not seem possible in the near term; (iv) MDCT provides a simpler modular building block – validated through HIL and farm level modeling, simulation and experimental validation; (v) 300 kVA MDCT prototype built and tested, technology is being commercialized; and (vi) Regulatory model of utility building PV plants, where PV panels are treated as DC generation (IPP), seems viable and can allow improved grid integration.

4. Glossary

BESS	**Battery Energy Storage System**
BOM	**Bill of Materials**
BOS	**Balance of System**
CI	**Central Inverters**
EBOS	**Electrical Balance of System**
EMI	**Electromagnetic Interference**
HF	**High Frequency**
HIL	**Hardware-in-the-Loop**
IGBT	**Insulated-gate bipolar transistor**
ILR	**Inverter-Loading-Ratio, defined as a ratio of peak PV DC power to inverter AC power.**
ISO	**Independent System Operator**
LCOE	**Levelized Cost of Energy**
LVRT/ZVRT	**Low/Zero Voltage Ride Through**
MDCT	**Multi-Port DC Transformer**
MV	**Medium Voltage**
MVSI	**Medium Voltage String Inverter**
PCS	**Power Conversion System**
PCS	**Power Conditioning Unit, including inverters and 60 Hz transformers (if appropriate)**
PEBB	**Power Electronics Building Block**
PRD	**Preliminary Requirements Document**
PV	**Photovoltaic**
RB	**Reverse-blocking**
S4T	**Soft Switching Solid State Transformer**
SCADA	**Supervisory Control and Data Acquisition**
SI	**String Inverters**
SiC	**Silicon Carbide**
SLD	**Single-Line-Diagram**
SPS	**Solar-Plus-Storage**
THD	**Total Harmonic Distortion**

5. Table of Contents

1. Background

Prices for photovoltaic energy have been dropping exponentially for decades, driven by dropping prices for PV panels. This has, in turn, been accompanied by a major focus on driving the cost of 'balance of systems' (BOS) down as well. One major component of BOS cost is the electrical system, including current collection, power conversion, transformer isolation, and breakers. Large PV farms span a large area of around 1 km x 1 km area for a 50 MW farm. This necessitates current collection through the entire farm area, with increasing current density near the inverters. There are two basic approaches in the collection, conversion, and connection– central inverters and string inverters. While central inverters had a cost advantage initially, recent trends show dramatic reductions in the cost of string inverters, with CAPEX cost parity seemingly imminent[1]. Another trend of moving towards higher voltage strings, DC collection voltages have moved from 690 to 1000 volts, with 1500 volts now being explored by many key players[2].

The primary DC/AC inverter technology used is the two-level voltage source inverter, with newer designs using the three-level inverter to achieve higher voltages and efficiencies. Central inverters are rated at up to 2 MW each [3],[4], translating into 2000 Amps on both the DC and AC sides and 25,000 A for a 25 MW cluster. Each inverter is connected to a transformer which raises the AC voltage to, say 33 kV, with one or two substation transformers to connect to transmission voltage at 69 kV to 500 kV. String inverters, typically rated around 60 kW, eliminate the need for combiner boxes and the central inverter. However, available inverters limit the AC side voltage to 400-600 volts [5],[6], requiring high current collection on the AC side. As a result, most comparisons between central and string inverters assume that similar levels of copper are required.

Moreover, as PV becomes a higher percentage of the overall generation, it is important to integrate it directly into the grid. By way of example, First Solar and CAISO have demonstrated the use of a 300 MW PV plant to provide frequency regulation, ACE error, and other ancillary services [7]. In the years ahead, it will be increasingly important to include energy storage for dispatchability, ramp-rate control, grid forming capability that allows black start following a blackout, and grid support functions, including voltage, VARs, and power flow control.

Lastly, this project aims to address to aforementioned challenges for hybrid PV systems by investigating and articulating the power converter/system-topology required to minimize cost while maximizing energy output. The proposed solution addresses the voltage-source converter challenges, AC/DC collection, and system losses while providing a solution that can provide multiple value streams, as previously mentioned.

---

[1] Evan Vogel, Schneider Electric, *Comparing Central Inverters and String Inverters in Utility Scale Solar Systems in North America*. Available: http://www.renewableenergyworld.com/articles/2016/12/comparing-central-inverters-and-string-inverters-in-utility-scale-solar-systems-in-north-america.html

[2] R. Garabedian, "Technology Update," First Solar shareholder analyst day presentation, 2014.

[3] ABB Central Inverters, Available:http://new.abb.com/power-converters-inverters/solar/central/pvs980

[4]Schneider Central Inverters, Available: http://cdn.solar.schneider-electric.com/wp-content/uploads/2016/06/conext-smartgen-brochure-201609013.pdf

[5] ABB String Inverters, Available: http://new.abb.com/power-converters-inverters/solar/string/three-phase

[6] Schneider String Inverters, Available: https://solar.schneider-electric.com/solution/decentralized/

[7] GreentechMedia. (2017). First Solar Proves That PV Plants Can Rival Frequency Response Services From Natural Gas Peakers. Available: https://www.greentechmedia.com/articles/read/pv-plants-can-rival-frequency-response-services-from-natural-gas-peakers

2. Project Objectives

Explore alternative converter and plant configurations to achieve the lowest cost and highest energy output for a given PV + storage plant, including the use of medium voltage (MV) collection while taking into account detailed models of all elements.

Approach:

- Employ a novel Medium Voltage String Inverter (MVSI) topology (soft switching solid state transformer – S4T) to convert 1000 Vdc to 4.16 kVac.
- Plant collection using standard, low-cost overhead MV distribution network.
- Enable energy storage integration without additional converter cost to achieve dispatchability of the PV resource.
- Provide advanced functionality: autonomous operation, track ISO signals for dynamic balancing and ancillary services, and PV farm operation as a virtual grid resource.
- By agreement between DOE/SETO and CDE at GT, this project has pivoted to build and test a 300 kVA Multiport DC Transformer (MDCT) to 13 kV in budget period 3 instead.

The primary objective of this project is to develop and demonstrate a new approach for larger commercial and utility-scale PV farms which reduces the 'balance of systems' (BOS) cost by: (1) Employing a novel medium voltage string inverter (MVSI) topology (based on soft-switching-solid-state-transformer – S4T) 1000 Vdc to 4.16 kVac (as shown in Figure 1); (2) Making use of standard, low-cost overhead MV distribution network; (3) Providing advanced functionalities: autonomous operation, track ISO signals for dynamic balancing and ancillary services, and the ability to operate the PV farm as a virtual resource; and (4) Enabling energy storage integration without any additional converter and cost.

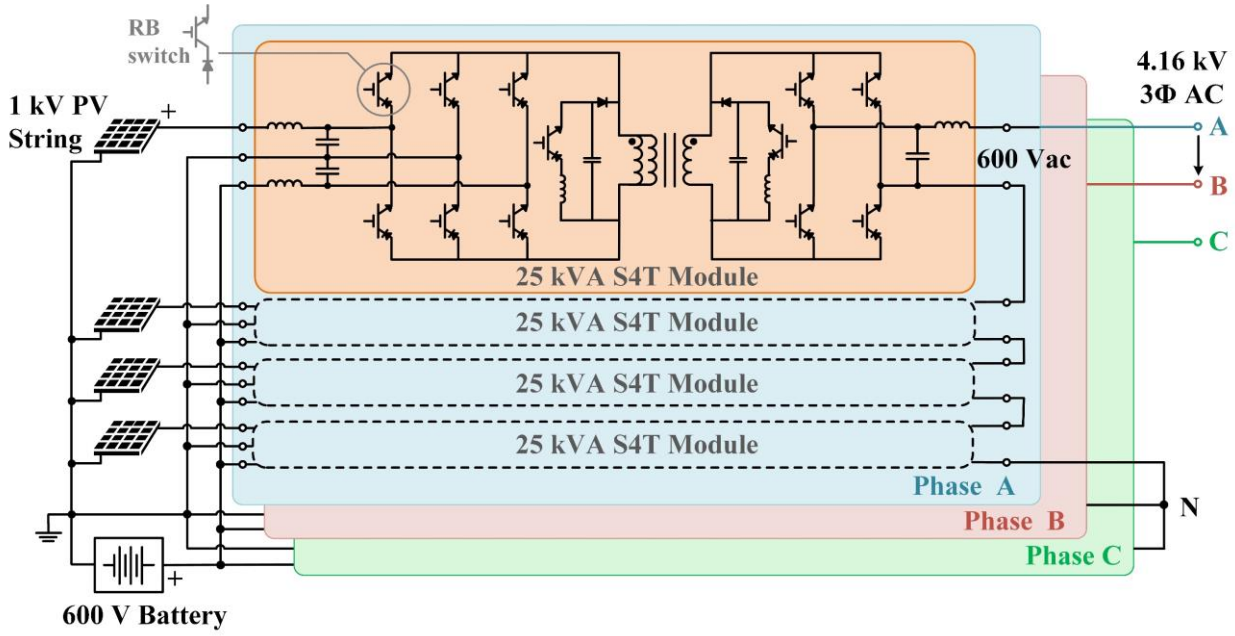

Figure 1: MVSI based on S4T to realize 1000 V PV with integrated energy storage to 4.16 kV grid interface.

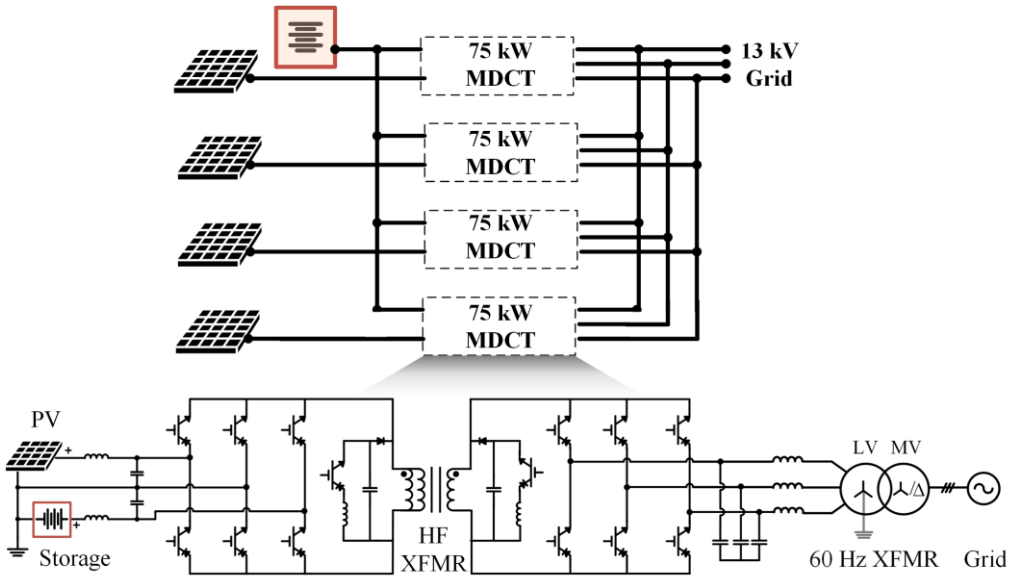

Figure 2: MDCT based on S4T to realize 1000 Vdc PV with integrated energy storage to 13 kVac grid interface.

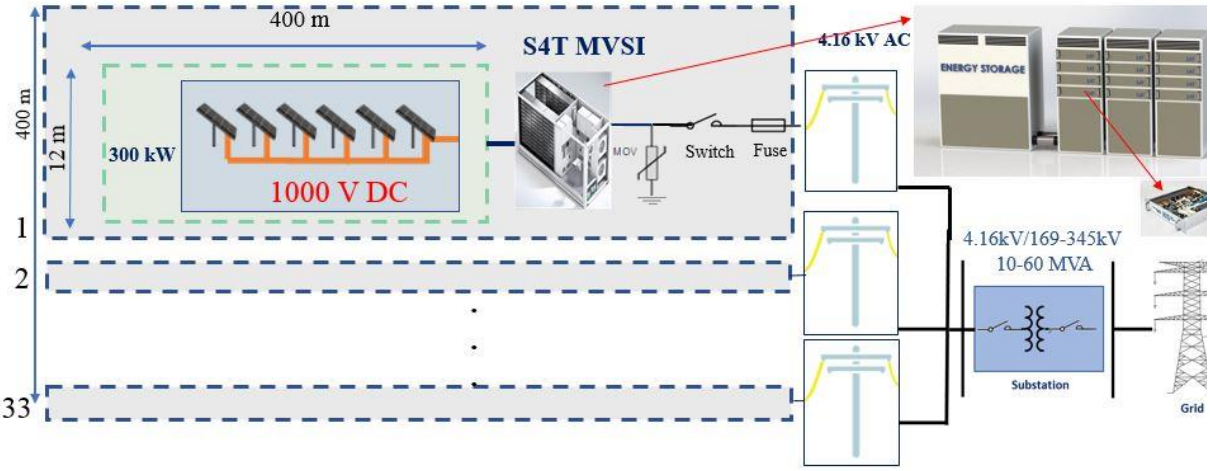

Figure 3: 10-60 MVA system schematic with proposed S4T MVSIs.

At the end of BP-2, the scope of the project was modified to shift to a Multiport DC Transformer (MDCT) implementation of the desired functionality – i.e., the interface of a PV string and battery to the medium voltage grid, now at 13 kV. This change was agreed upon between DOE/SETO and CDE at Georgia Tech based on the technical viability and economic analysis in the near term, which suggests MDCT is a better design option, and the final deliverables are still aligned with the overall objective of the original proposal. Based on the aforementioned pivot, the focus of work during the third budget period was to demonstrate a 300 kVA MDCT prototype (instead of MVSI), followed by the regulation and commercial impact study.

Figure 2 shows the schematic of MDCT-based implementation, where four 75-kW MDCT modules are connected in an input-parallel-output-series (IPOS) manner. Each MDCT

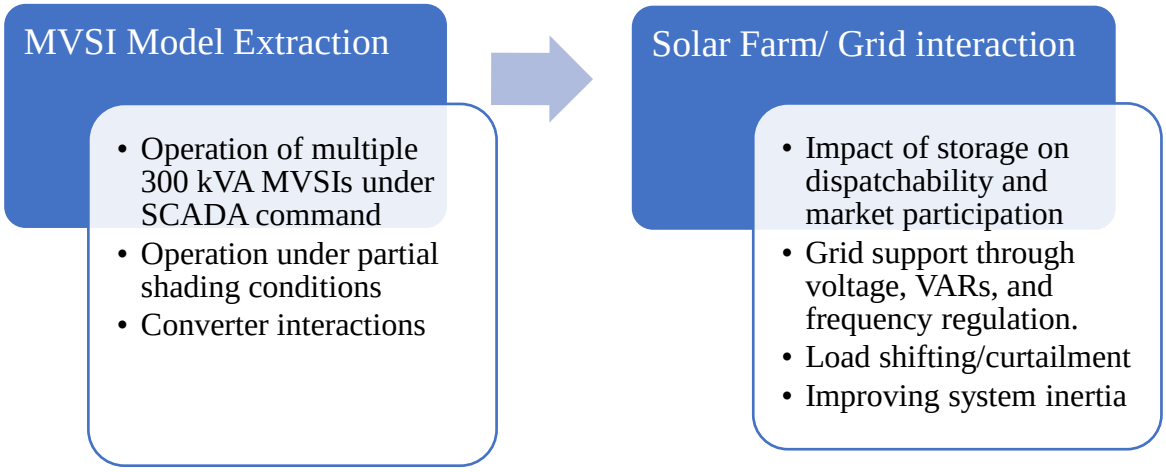

Figure 5: Functionalities to be verified from the system analysis effort.

comprises a cascaded S4T converter with a 13 kV 60 Hz transformer, integrating 1 kV PV and storage to 13 kV medium voltage AC distribution inside the PV farms. The megawatt-level system schematic is presented in Figure 3.

3. Efforts

The technical scope of this project was carried under *five efforts/thrusts/work areas* (which encompass 14 sequentially numbered tasks). The key tasks per effort are summarized below.

Effort 1: S4T MVSI Simulation and Design (BP1: Tasks 1-3, BP2: Tasks 7,8)

- Generate a product specifications document that led to a detailed design of the MVSI — these tasks were performed in Budget Period (BP)1 and BP 2, focusing on identifying objectives, defining specifications of the MVSI, design of the MVSI, and design of a 20 MW solar farm based on the proposed MVAC distribution architecture.
- MVSI operation validation through simulation studies.
- A complete design of the MVSI, including high-frequency transformer, selection of switching devices, thermal design, controller design, layout and packaging, 4.16 kV AC and 1000 V DC disconnect, and protection design.
- MVSI hardware-in-loop (HIL) simulations.

Effort 2: System analysis and Storage Optimization (BP2: Task 9)

- Validate the system-level benefits of the proposed MV distribution architecture based on MVSI inverters through system analysis.
- Simulation of the 20 MW solar farm (like the architecture shown in Figure 3 and Figure 4), modeling parameters such as cable and transformer impedances, partial shading, etc., using the OpenDSS or equivalent platform.
- Verify the functionalities listed in Figure 5 with models obtained from Effort 1.
- Identify the optimum storage level required.

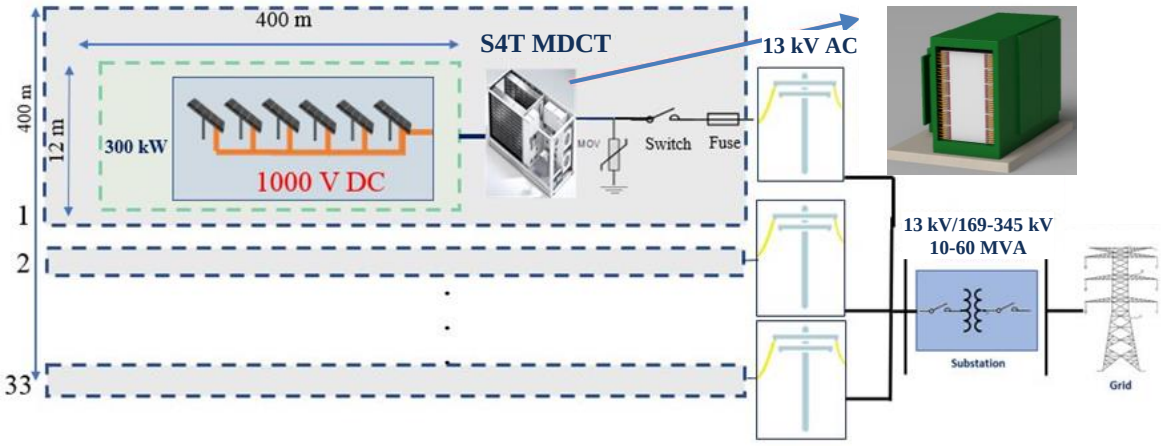

Figure 4: 10-60 MVA system schematic with proposed MDCTs.

Effort 3: Financial analysis (BP1: Task 4, BP2: Task 10)

- Quantify the benefits of the proposed MV distribution architecture based on MVSI inverters.
- Generate a Financial analysis of state-of-art approaches with and without integrated storage.
- Calculate the LCOE and the First Cost of proposed approaches with and without integrated storage.

Effort 4: Prototype Build and Test (BP1: Task 5; BP2: Task 11, BP3: Task 13)

- Build a 300 kVA prototype and validate the functionality.
- Evaluate the ability of the proposed S4T MVSI to provide grid services.

Effort 5: Regulatory and Commercial Impact Study (BP1: Task 6, BP2: Task 12, BP3: Task 14)

- Explore different regulatory models to increase Utility participation in solar PV farms.
- Commercial analysis to develop (a) Commercial and regulatory mechanisms that can lead to new business models and (b) Evaluation of new commercial, regulatory, and business models enabled by the proposed MVSI approach were performed.

4. Project Results and Discussion

In this section, the project results for each task are presented together with their corresponding analysis.

a. Budget Period 1

Task 1: S4T MVSI – Converter Simulation: The proposed S4T MVSI is realized by stacking S4T modules. The operation of stacked converters with triport functionality is challenging. It is necessary to simulate the S4T MVSI with integrated storage to understand and demonstrate the required functionalities and to design the 300 kVA system.

Approach

- Subtask 1.1: Develop a preliminary requirements document (PRD), including device and system specifications of the MVSI for storage-integrated PV farm, in consultation with industrial and utility partners.
- Subtask 1.2: Simulation of 300 kVA MVSI with integrated storage.

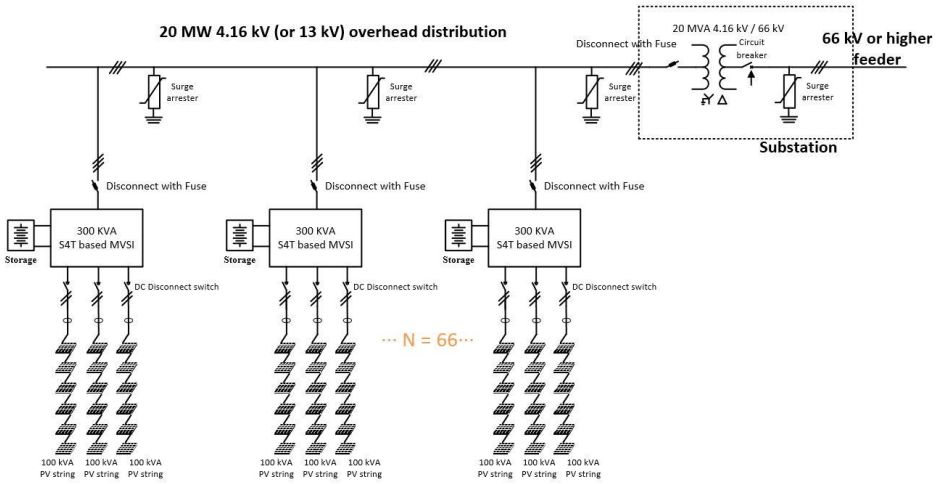

Figure 6: System layout of 20 MW MVSI-based PV farm with battery.

- Subtask 1.3: Generate transient and steady-state models of the MVSI.
- Subtask 1.4: 300 kVA MVSI HIL simulation.

Results and Discussion:

Subtask 1.1: A typical utility-scale PV farm with proposed MVSIs is shown in Figure 2, with 4.16 kVac (eventually 13 kV) overhead distribution lines coming out of the substation fed from the transmission network.

Each S4T module, shown in Figure 1, is rated at 25 kVA and connects to a PV string of up to 1000 V DC. The AC side of the converter realizes single-phase AC at 600 V. Four of these S4T modules can be series-connected to realize 2.4 kV line-neutral voltage, with three such cascaded strings realizing three-phase 4.16 kV L-L voltage. The overall MVSI would have a rating of 300 kVA, much more than would be feasible with traditional 480 V string inverters.

On the DC side of each module, an additional terminal is seen that interconnects all the modules in the MVSI. This common terminal allows the exchange of power between modules as needed to allow for occasional cloud shading on individual solar panel strings and provides the mechanism to connect a battery in the 600-1000 VDC range without any additional power converters. This feature reduces the cost dramatically. This can also reduce curtailment and improve the dispatchability of the PV farm. Individual S4T modules can interface with individual PV strings, allowing optimization and maximum power tracking at the string level. Alternatively, DC trunk buses could be used to simplify wiring from the panels to the MVSI. The high-frequency switching provides unprecedented control capability with low harmonics and a fully controllable power factor on the AC side.

Lastly, Table 1 outlines the final product requirement documents for the MVSI developed throughout this project, whereas Figure 6 shows the system architecture of a 20 MW PV farm with the proposed MVSIs to realize MV distribution with its preliminary specifications listed in Table 2.

Table 1: Product Requirement Document (PRD) for MVSI

AC Side	
AC grid connection	Three-phase (Neutral Point grounded)
Rated AC Power	300 kVA at unity PF
Maximum AC output Power Smax	300 kVA at unity PF
Rated AC grid voltage	2400 V (L-N) 4160 (L-L)
AC voltage range	+/- 10%
Maximum AC output current	42 Arms
Current THD	<3%
Rated output frequency	60 Hz
Output frequency range	57 to 63 Hz
Nominal Power Factor and range	0.995, 0 to +/- 1 with Smax
AC connection type	Bushing
Over voltage Protection	Varistor
Over current Protection	Fuses and main breakers at rated current
PV Side	
Rated DC input voltage	1000 V
Operating voltage range	800V to 1200V
Rated DC input power	300 kW
Max DC Power Connected	300 kW
Number of DC input pairs	12 strings
Maximum DC input current per pair	36 A
Number of independent MPPT	12
DC connection type	Input lugs, conduit entry
Overvoltage protection	varistor
Storage Integration (typical)	

Rated DC input voltage	600 V
Operating voltage range	540-660 V
Number of DC input pairs	1
DC connection type	Input lugs, conduit entry
Overvoltage protection	varistor
Operating Performance	
Peak Efficiency	97.4 % at 100% load
Isolation level	High-frequency transformer – 30 kV
Control	Bidirectional and independent power flow - Set point control through communication protocols
Communication	
User Interface	LEDs/ HMI Comm port
Set-point communication	CAN/ Modbus TCP
Event logger	High-Speed Fault data recorder
Environmental	
Ambient Operating Temperature	-20 to 50 C (full range not tested under this project)
Relative Humidity	<95% non-condensing
Altitude	<4,000 m (13,123 ft.) (full range not tested under this project)
Physical	
Enclosure	Pad-mounted Steel high/low voltage compartment HV cable entry on top, LV cable entry on bottom
Thermal Management	Forced air cooling
Minimum Degree of Protection *	IP54
Modular – 25 kVA converter units	
Dimensions (HxWxD)	7in x 15in x 36in
Weight	< 25 lbs
Mounting options	Rack-mountable

Applicable Standards and Codes*	UL Standard 1741SA NERC PRC-024 and IRPTF Guideline applicable for BES plants IEEE 1547 and 519

*Certification was not carried out throughout this project.

Table 2: Preliminary Product Requirement Document (PRD) for Solar Farm

Grid Side	
AC grid connection	Three-phase Delta – 66 kV
Transformer	20 MVA 4.16 (or 13) kV Y / 66 kV Delta
Protection	Circuit breaker and Surge arrester
MV AC Distribution	
Voltage	4.16 (or 13) kV
Distribution type	radial
Protection	MV AC Disconnect with fuses and Surge arresters
PV Side	
Voltage	1000 V dc
PV String rating	100 kW each (3 per MVSI)
Protection	DC Disconnect with fuses

Subtask 1.2: Based on the PRD, a simulation model of 300 kVA MVSI as shown in Figure 1, was built in PLECS. The simulation parameters are summarized in Table 3. Different test cases were demonstrated.

Table 3: Simulation Parameters of 300 kV/4 kVac MVSI

Parameters	***Values***	***Parameters***	***Values***
Vpv	1000 Vdc	Vbattery	600 Vdc
Vac	600 Vrms	Fsw	16 kHz
L_m	340 uH	L_{lk}	0.35 uF (0.1%)
L_r	2 uH	C_r	60 nF
L_{dc}	324 uH	C_{dc}	217 uF
L_{ac}	584 uH	C_{ac}	51 uF

The three-phase MVSI is realized by connecting three single-phase stacked modules in Y with neutral grounded. The S4T MVSI allows having independent PV input per 25 kVA module or one 100 KW input for each phase leg or even 300 kW single input for the MVSI. The choice depends on the system design.

The simulation results of the three-phase MVSI with three PV inputs and one Battery input are shown in Figure 7. In this case, the PV power is constant, and the remaining demanded Grid power (300 kVA) is taken from the Battery terminal. A step-change in the demanded grid power simulated at simulation time t = 0.05 seconds shows that the balanced operation is maintained. It is shown that the voltage THD at the ac side is around 1.3% which is below the metric of 5%.

Figure 8 shows the simulation results of the MVSI to demonstrate the ability to control the power from PV, battery, and the grid independently under partial shading conditions. To show this case, three independent PV lines connecting to each phase of the S4T MVSI are simulated. It is to be noted that the PV terminals can be one for all 12 modules, 3 for one phase each, or one for each module. If three strings of PV panels were assumed to be connected to the MVSI, and if due to partial shading, the voltage of each string will be different. This scenario is simulated, showing that even though the PV inputs/ phase of the inverter are at different voltages, the grid voltage and current are balanced at a fixed power, and the additional power is used to charge the battery. A step reduction in the grid power command is simulated at 0.5 s simulation time, showing the dynamic change in the battery power. The THD of the grid voltage is maintained under 5% metric even during the unbalanced power operation. It is to be noted that the simulation results in Figure 7 show the battery is being discharged, and the results in Figure 8 indicate that the battery is being charged. This shows the bidirectional power flow capability of the converter. In principle, the battery can be charged from the grid as well if needed.

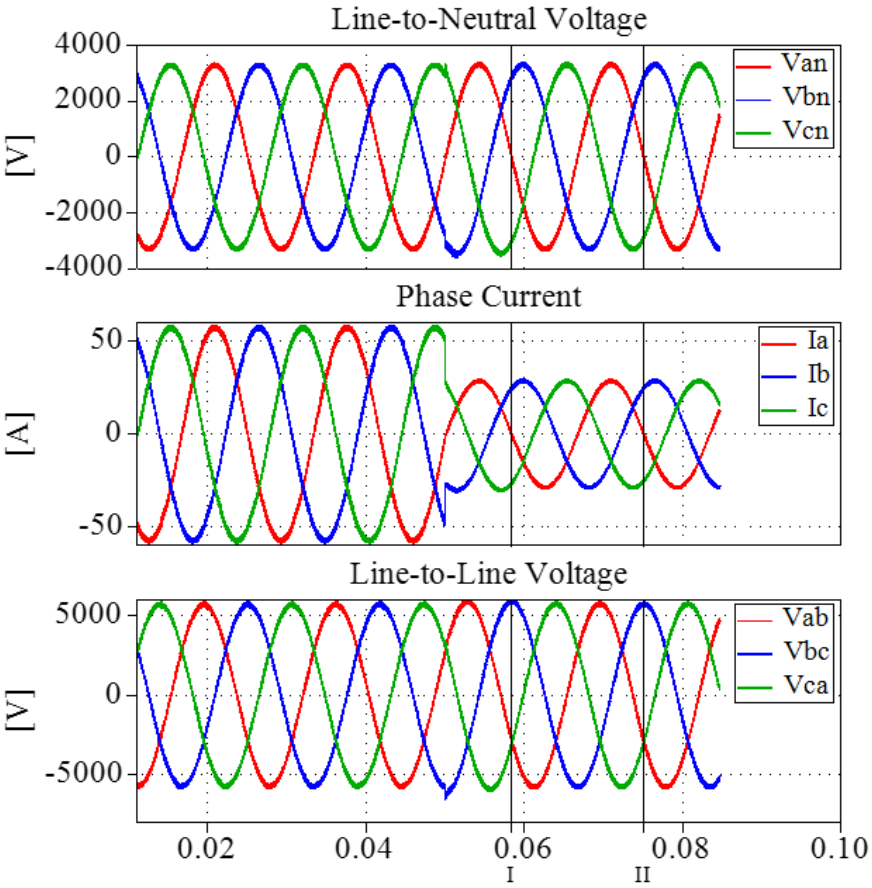

(a) 300 kVA MVSI simulation with 50% load step change.

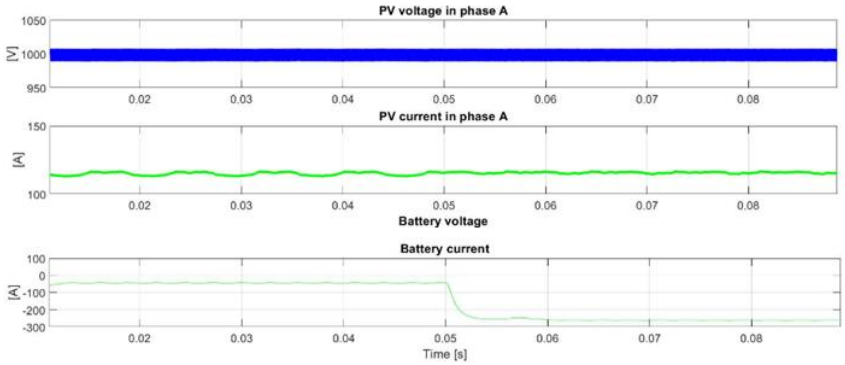

(b) PV and battery voltage/current in simulation.

Data

Name	Cursor 1	Cursor 2	Delta	RMS	THD
Time	0.0583802	0.0750469	0.0166667		
Line-to-Neutral Voltage					
Van	*40.2112*	16.8025	*23.4087*	2345.77	0.0133378
Vbn	*2877.67*	2772	*105.667*	2345.87	0.0133273
Vcn	*-3075.94*	-2874.38	*-201.557*	2357.34	0.0195566
Phase Current					
Ia	*0.349055*	0.145855	*0.2032*	20.3625	0.0133378
Ib	*24.9798*	24.0625	*0.917247*	20.3635	0.0133273
Ic	*-26.7009*	-24.9512	*-1.74963*	20.463	0.0195566
Line-to-Line Voltage					
Vab	*-2837.46*	-2755.2	*-82.2582*	4062.96	0.0111288
Vbc	*5953.61*	5646.39	*307.224*	4079.78	0.0131635
Vca	*-3116.15*	-2891.19	*-224.966*	4065.88	0.0135517

(c) RMS and THD measurement of AC outputs.

Figure 7: Simulation results MVSI with integrated storage delivering 300 kVA.

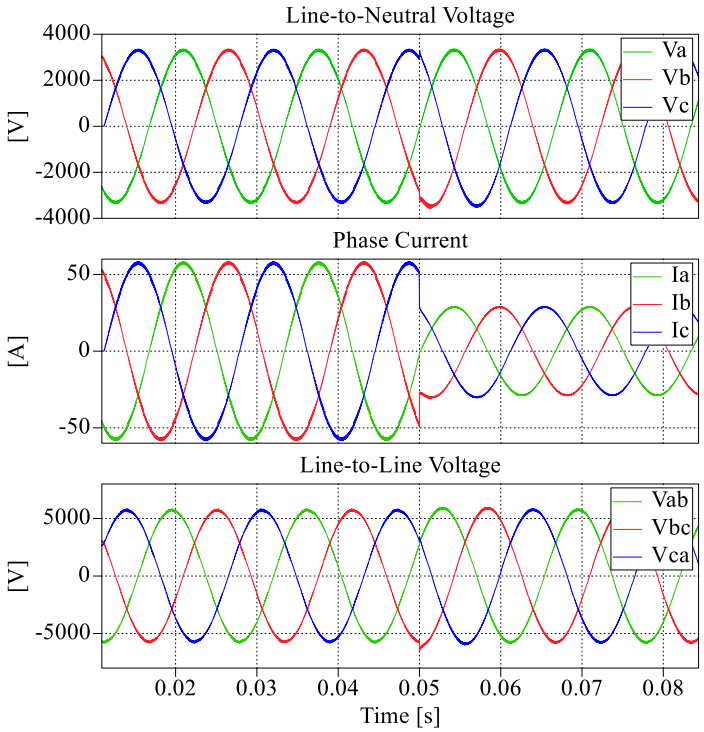

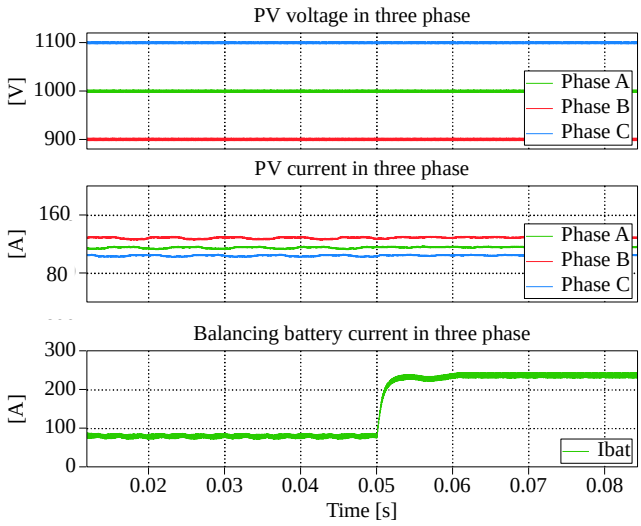

Name	Cursor 1	Cursor 2	Delta	RMS	THD
Time	0.0213481	0.0380142	0.0166661		
Line-to-Neutral Voltage					
Va	3273.41	*3258.61*	*14.8048*	2335.49	0.0137334
Vb	-1188.51	*-1202.31*	*13.8037*	2336.45	0.0136817
Vc	-1987.44	*-2058.23*	*70.7891*	2334.53	0.0139553
Phase Current					
Ia	56.83	*56.573*	*0.257028*	40.5467	0.0137334
Ib	-20.6338	*-20.8734*	*0.239647*	40.5634	0.0136817
Ic	-34.5042	*-35.7332*	*1.22898*	40.53	0.0139553
Line-to-Line Voltage					
Vab	4461.92	*4460.92*	*1.00117*	4045.89	0.0104819
Vbc	798.938	*855.924*	*-56.9855*	4044.96	0.0107064
Vca	-5260.85	*-5316.84*	*55.9843*	4044.26	0.0109465

Figure 8: Simulation results of 300 kVA MVSI under partial shading conditions.

Subtask 1.3: The steady-state model is similar to the standard PV inverter model. The transient model of the MVSI was developed and verified in PLECS simulation. The small-signal model well matches the switched model in time-domain simulation under both steady-state and load step change conditions.

State-space model of the S4T Module

Figure 9 shows the circuit schematic of tri-port S4T converters, which is the basic building block of the proposed 300 kVA MVSI.

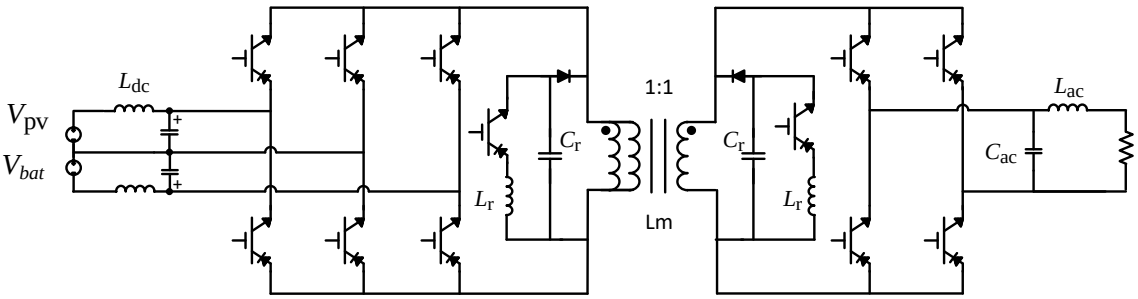

Figure 9: Circuit schematic of tri-port S4T module.

The state-space averaging technique is applied to the full switching model presented in Figure 9, with the state variables **x**, input variables **u**, and output variables **y** defined in

$$\mathbf{x} = \begin{bmatrix} i_m \\ v_{ac} \end{bmatrix}, \quad \mathbf{u} = \begin{bmatrix} v_{pv} \\ v_{cap} \end{bmatrix}, \quad \mathbf{y} = v_{ac}$$

The small-signal model of the tri-port S4T converter, after neglecting the second-order term, is given by:

$$\dot{i}_m = \frac{1}{L_m} \cdot (d_{pv} \cdot v_{pv} + d_{cap} \cdot v_{cap} - d_{ac} \cdot v_{ac})$$
$$\dot{v}_{ac} = \frac{1}{C_{grid}} \cdot (d_{ac} \cdot i_m - \frac{v_{ac}}{R_L})$$

Figure 10 presents the derived small-signal model of the tri-port S4T module. Its effectiveness has been validated in PLECS. Figure 11 (a)-(g) shows the verifications results of the small-signal model and the switched model in time-domain simulation under both steady-state and 50% load step change conditions. The small-signal model matches the switched model well in both conditions in terms of magnetizing current, AC voltage/current, PV voltage/current, and balancing battery voltage/current.

The high-fidelity small-signal model also applies to the 300 kVA MVSI that consists of 12 tri-port S4T converter modules. Its effectiveness is shown in the results for Task 9 – simulation for system analysis.

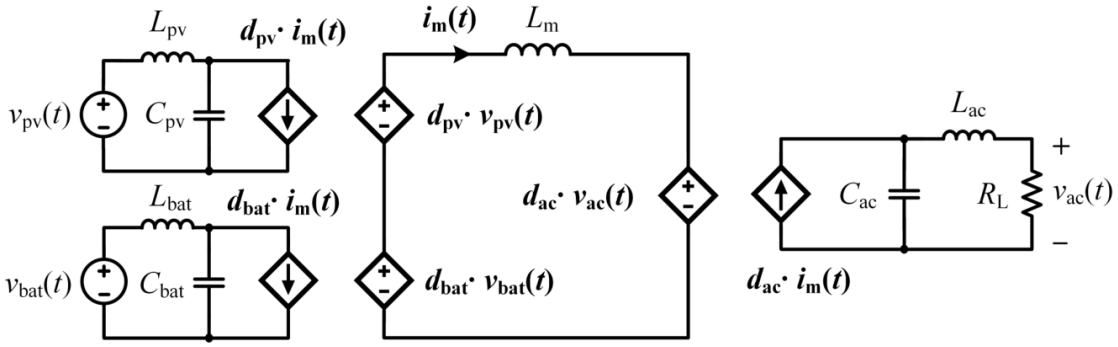

Figure 10: Small Signal Model of the triport S4T module.

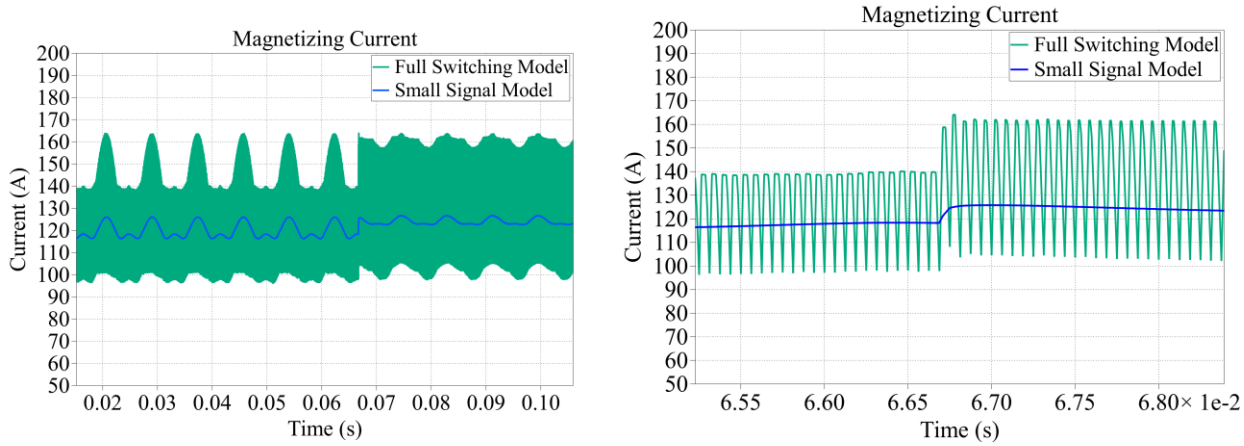

(a) Magnetizing current

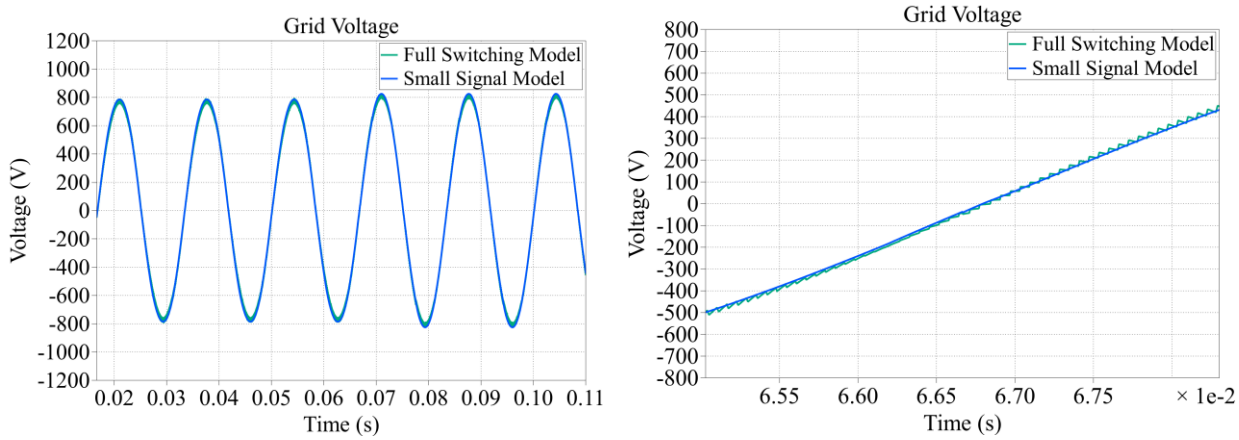

(b) AC voltage

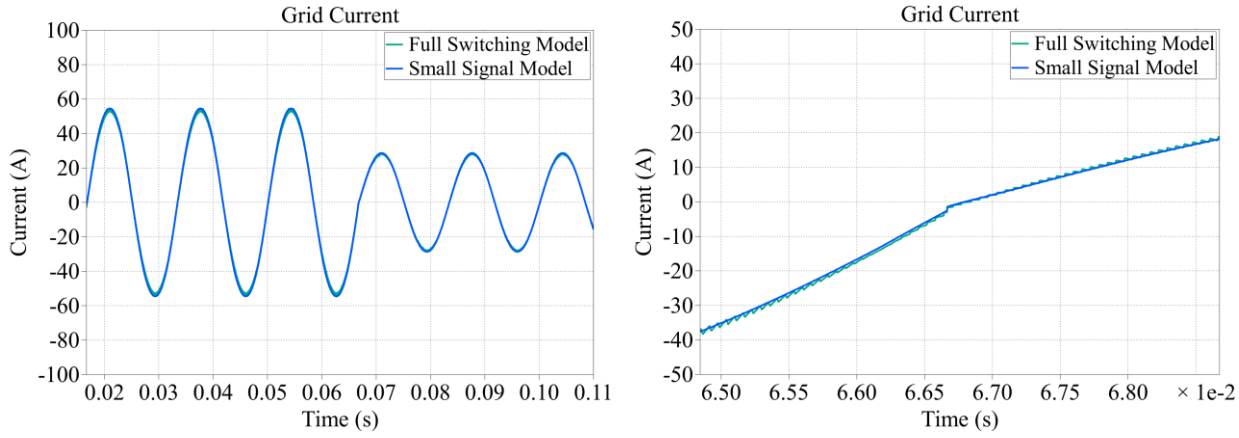

(c) AC current

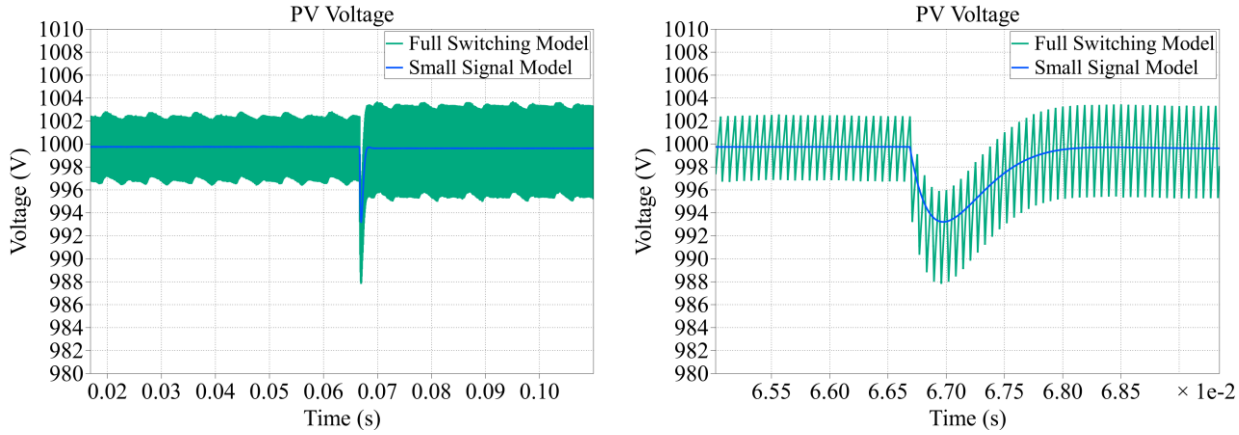

(d) PV voltage

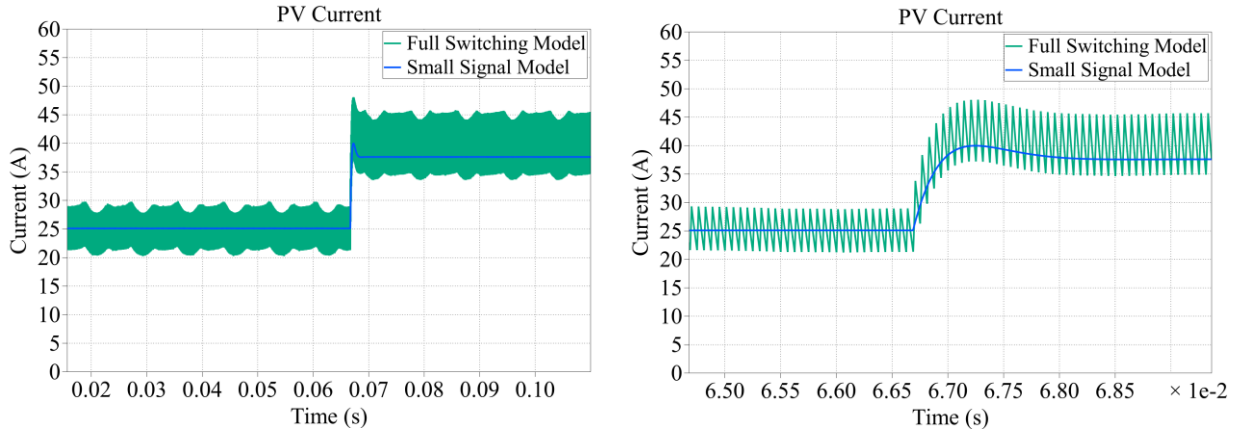

(e) PV current

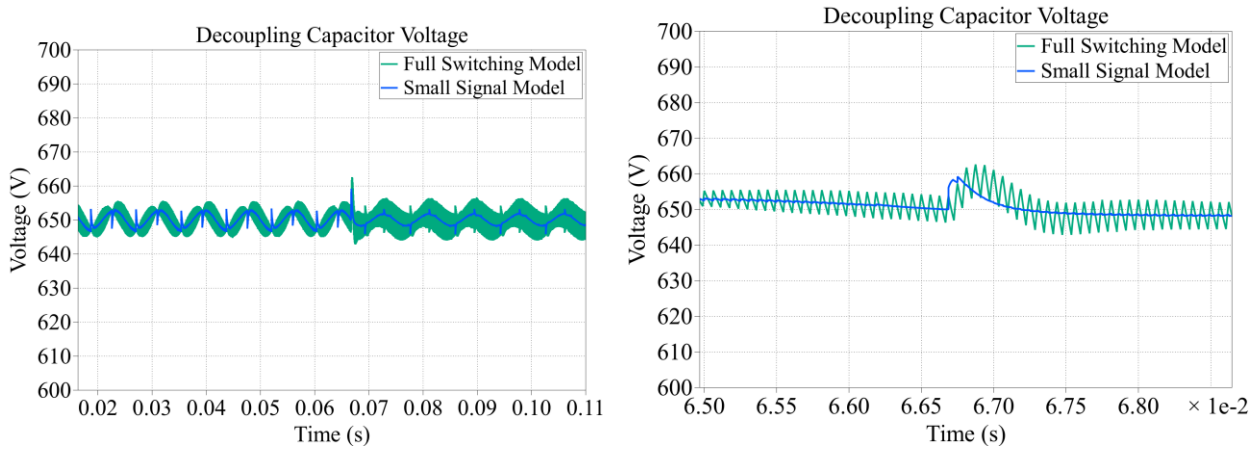

(f) Battery voltage

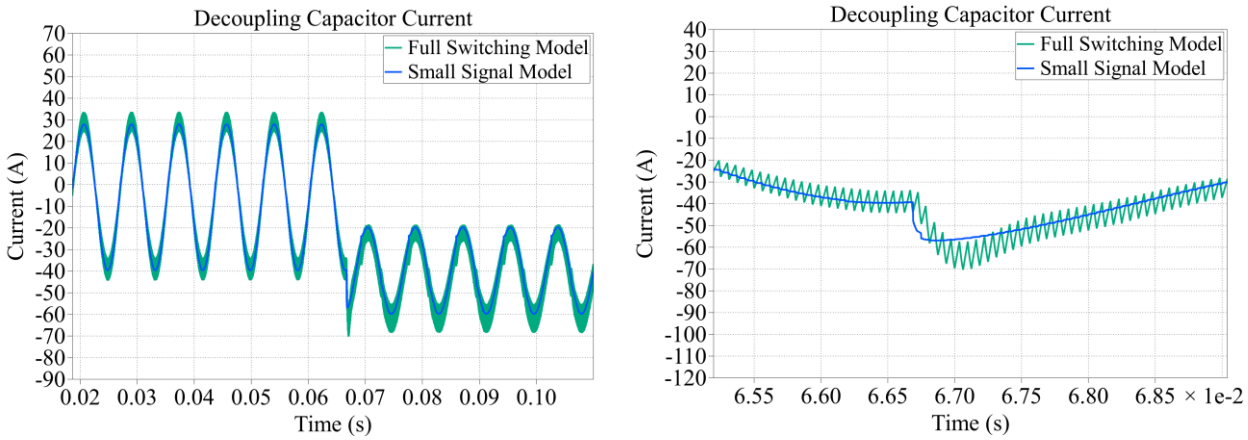

(g) Battery current

Figure 11: Verification of derived small-signal model in PLECS.

Subtask 1.4: The model predictive-based priority switching control (MPPS) algorithm for the low inertia stacked S4T modules were implemented in DSP/FPGA-based control card. Four modules stacked with an independent control card were simulated in quasi-real-time using an OPAL-RT platform.

Control Architecture

Multiple converter modules (25 kVA) require a control card in the proposed MVSI. A distributed Master-Slave Controller Architecture using a daisy chain is employed. Each slave controller controls one module, and all controllers are grounded on the LV side. Signals that are communicated with each controller are switching frequency synchronization signal to ensure interleaving; Reference grid voltage signal synchronized at line frequency; Health signal; Startup/shutdown signal; Info signal.

The latency of the signals between each module is less than 100ns. The master controller manages the generation of the synchronization signal, startup, shutdown, and info signal. Two types of architecture are being investigated – (a) multiple fiber optic cable; (b) single fiber optic cable, as shown in Figure 12. Eight communication wires/fibers are required for each controller and are identical designs of slave controllers.

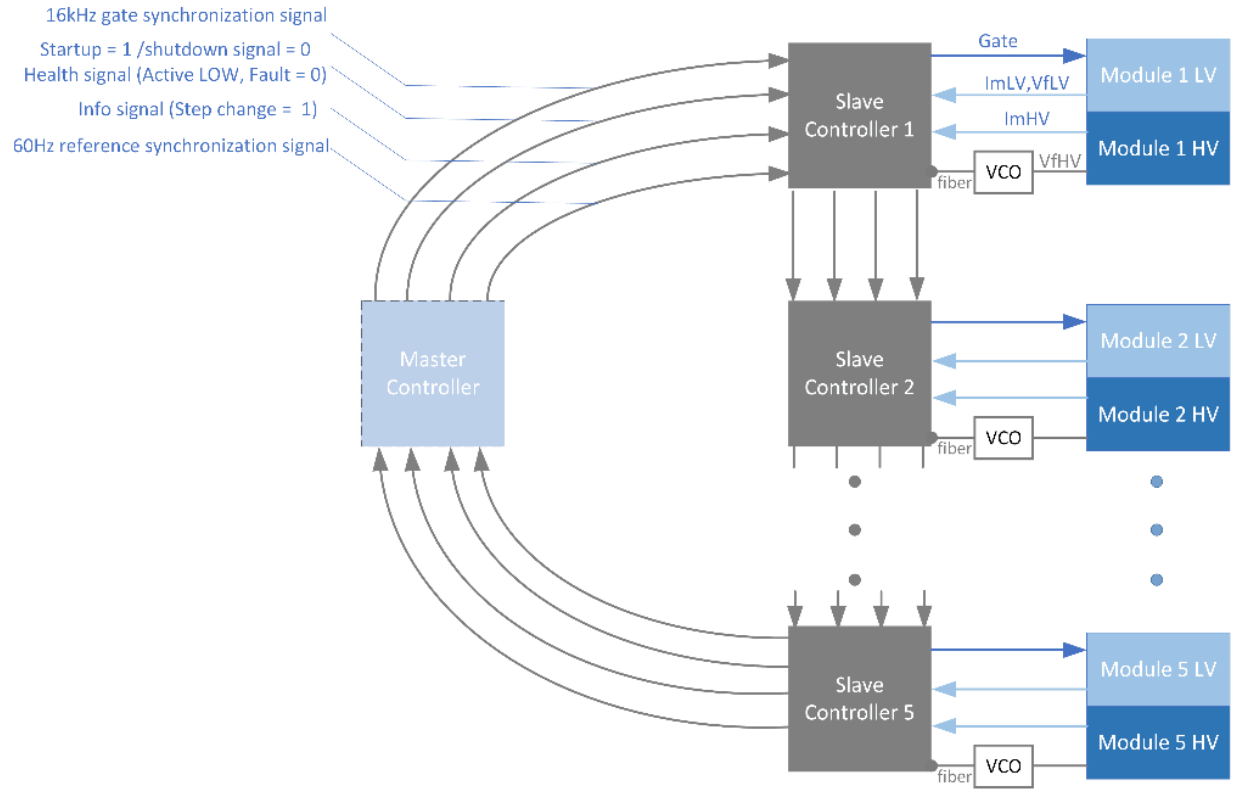

(a)

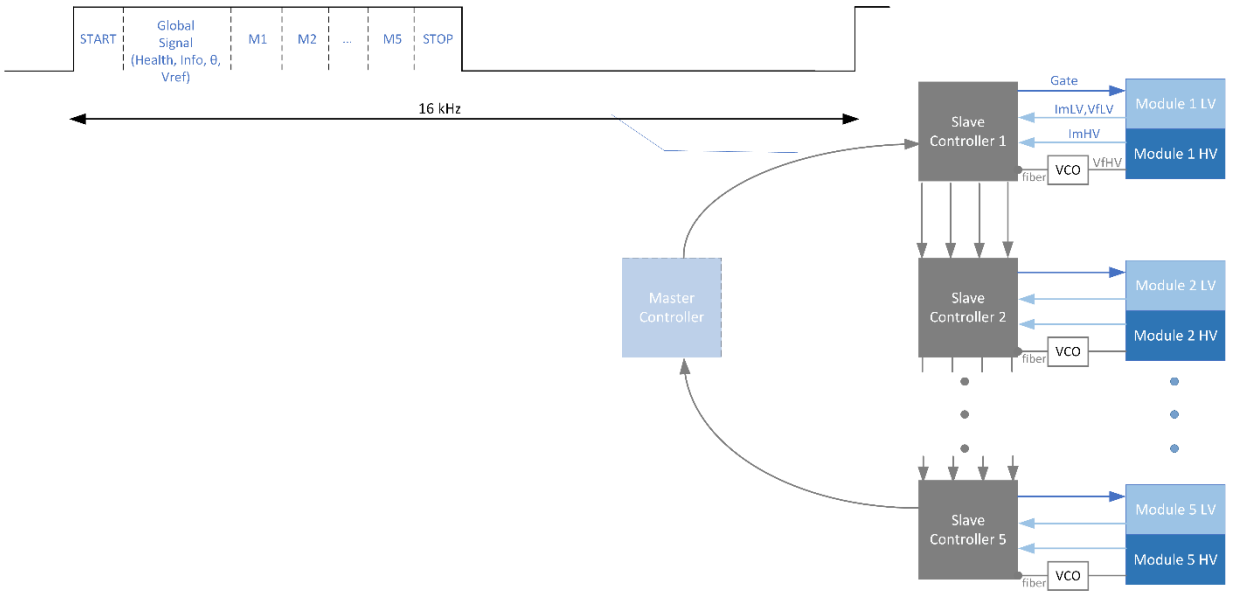

(b)

Figure 12: Daisy-chained control architecture. (a) Multi-Fiber solution. (b) Single Fiber Solution.

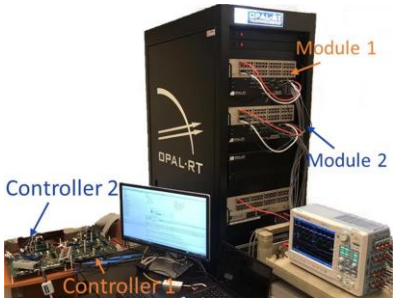

(a)

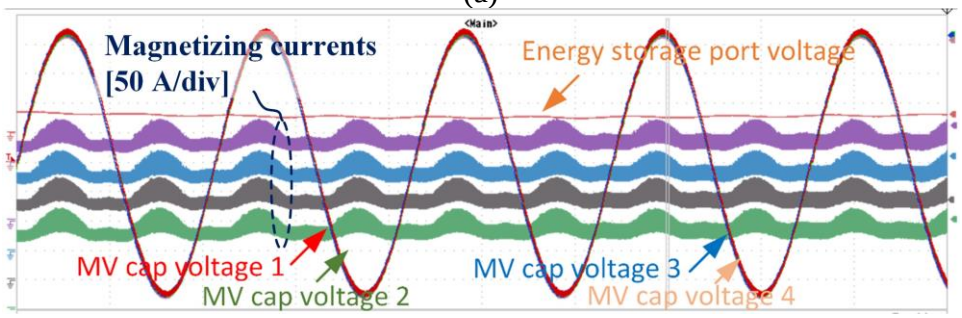

(b)

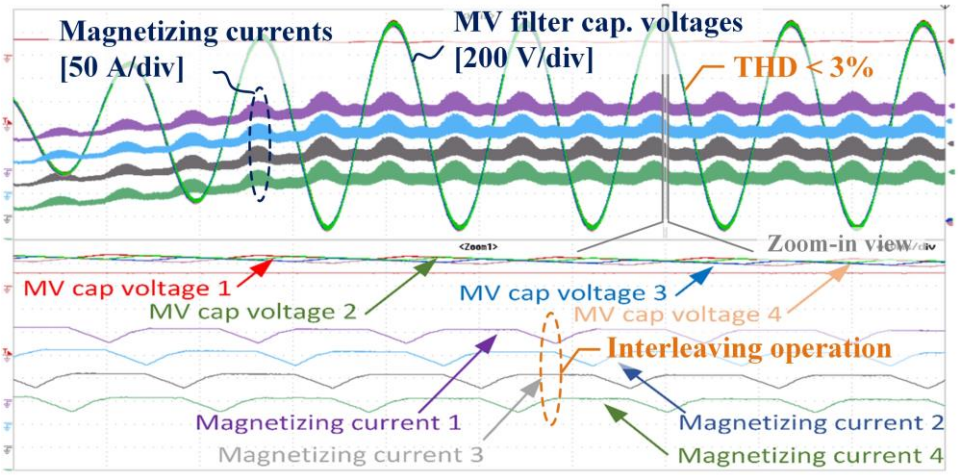

(c)

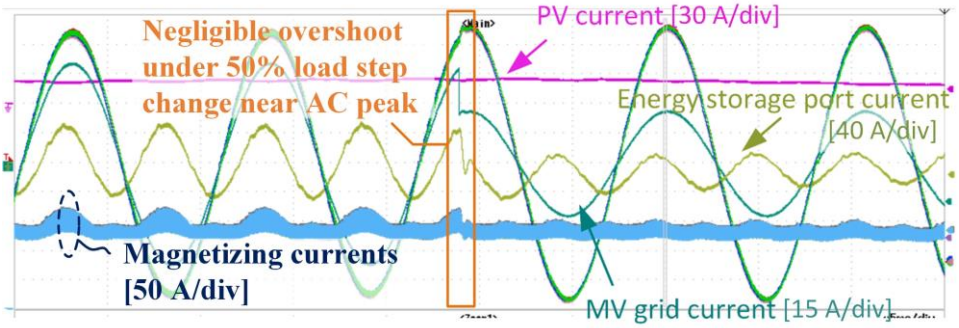

(d)

Figure 13: HIL OPAL-RT validation. (a) HIL workbench. (b) Steady-state. (c) Power ramp-up. (d) Load change.

A hardware-in-the-Loop (HIL) simulation was implemented on the OPAL-RT platform to validate the stack operation of four S4T converter modules stacked in one phase with the developed daisy chain communication algorithm. Figure 13 presents three case studies to validate the performance, including steady-state, power ramps with interleaving operation, and load step-change near AC peak. The four modules in one phase were synchronized well in different operating conditions and featured a smooth transition with negligible overshoot during load step change near AC peak, validating the efficacy of the communication algorithm and thus laying a solid foundation for its application in hardware tests.

Task 2: 300 kVA S4T MVSI bronze prototype design: The design of the S4T MVSI bronze prototype, including the high-frequency transformer.

Approach:

- Subtask 2.1: Design of 300 kVA MVSI bronze prototype with integrated storage.

Results and Discussion:

The converter design includes the medium-frequency transformer, resonant circuits, reverse-blocking switch modules, and filters. The proposed 300 kVA MVSI consists of twelve 25 kVA 600 V modules. The design for the 25 kVA module is described in the following pages. The schematic of the 25 kVA module is shown in Figure 14. The converter specifications are listed in Table 4.

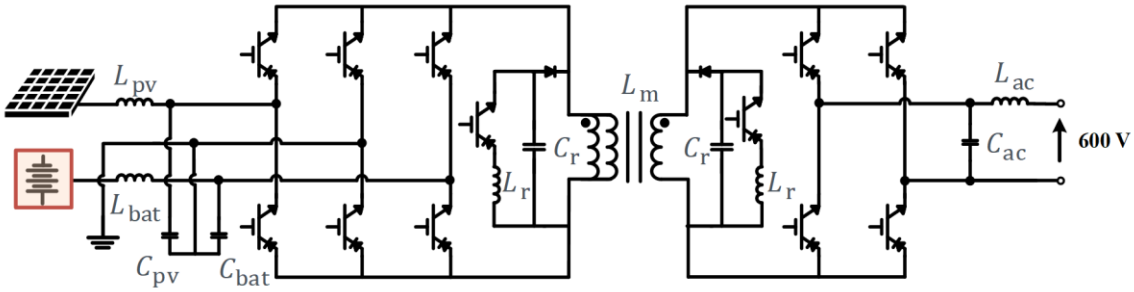

Figure 14: Schematic and specifications of the 25 kVA/600 Vac S4T module.

Table 4: Specifications of 25 kVA/600 Vac MVSI modules

Parameters	Values	Parameters	Values
PV voltage	1000V	Battery voltage	650V
Grid voltage	600 Vrms	Switching frequency	16 kHz
Mag. Ind. L_m	330 uH	Leakage ind. L_{lk}	0.33 uF
Resonant ind. L_r	2 uH	Resonant cap. C_r	60 nF
PV filter ind. L_{pv}	324 uH	PV filter cap. C_{pv}	78 uF
Battery filter ind. L_{bat}	117 uH	Battery filter cap. C_{bat}	217 uF
Grid filter ind. L_{ac}	584 uH	Grid filter cap. C_{ac}	43.5 uF

Table 4 shows the bill of materials (BOM) of selected key components. The semiconductor devices are 1.7 kV Silicon IGBT from IXYS and 1.7 kV SiC diodes from Genesic. The

medium-frequency (MF) transformer was built with a Nanocrystalline core from MK magnetics.

Table 5: BOM of key selected components for the 25 kVA/600 Vac MVSI module.

Components	Part number	Manufacturer	Quantity
1.7 kV Si IGBT	IXBK75N170	IXYS	24
1.7 kV SiC diode	GB50MPS17-247	GeneSiC	28
HF XFMR cores	SC2065M1	MK Magnetics	2
Coaxial winding cables	N32-33E-00003-2	New England	N/A
Resonant capacitor	B32672L8103J000	TDK	12
Resonant inductor	N/A	Customized	2
600 Vrms sensor	CV3-1200	LEM	1
PV voltage sensor	LV 25-P/SP5	LEM	1
Battery voltage sensor	LV 25-P/SP5	LEM	1
I/O current sensor	LF 210-S	LEM	3
Mag. Current sensor	LF 510-S	LEM	1

MF Transformer Design

The main criterion for transformer design is to achieve the required magnetizing inductance, peak current at the lowest possible leakage inductance, parasitic capacitance and losses. Please note that in the case of S4T, the transformer behaves more like a flyback transformer with predominantly DC flux superimposed with switching frequency flux ripple [1]. Leakage inductance has a significant effect on the device stress should be minimized as much as possible [2].

The final design consists of 2 sets of AMCC 630 nanocrystalline cores and 6 layers of 14 AWG equivalent / 60 kV isolation coaxial cable in parallel connection for the transformer winding. Each layer contains 16 turns of windings. The custom coaxial cable provides a low leakage option while achieving high isolation voltage between primary and secondary. The selection of Nanocrystalline is to minimize the losses. Table 6 lists the design specifications of the 25 kVA MF transformer for the MVSI, and Figure 15 shows the selected components and winding pattern to fulfill the design.

Table 6: Design specifications of 25 kVA MF transformer

Parameters	Values	Parameters	Values
Avg. Im	110 A	Mag. Inductance L_{m}	330 uH
Current ripple	60 A	Leakage ind. L_{lk}	0.33 uH
Switching freq.	16 kHz	Saturation current	170 A

(a) (b)

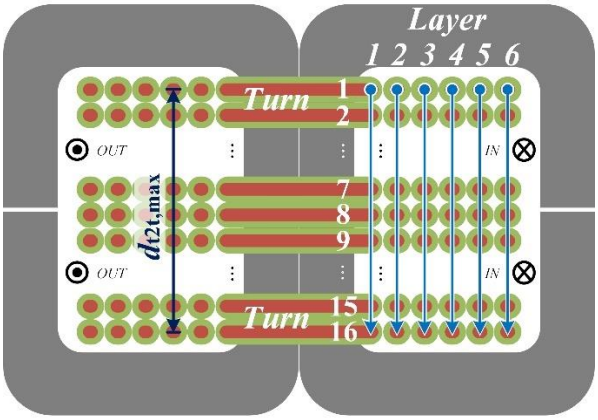

(c)

Figure 15: 25 kVA MF transformer design. (a) The selected nanocrystalline core. (b) Custom coaxial Litz-wire. (c) Winding pattern.

Resonant circuit design

Another major element is the resonant circuit. The design criteria for the resonant tank is to limit the peak voltage and current stress within device limits and reduce resonant time to maximize the effective duty cycle for power transfer.

Optimization was performed to select the resonant capacitor and inductor values. Finally, a resonant capacitor Cr = 60 nF and a resonant inductor Lr = 2 uH were selected, leading to a controlled $dv/dt = 1\ kV/us$ and resonant time duration $t_{res} = 1.1\ us$. The performance of the resonant circuit is verified through simulation studies, as summarized in Table 7.

Table 7: Resonant circuit design verification

Parameters	Design	Calculation	Simulation
dv/dt	1 kV/us	0.92 kV/us	1.2 kV/us
Peak current (pulse)	< 400 A	322 A	233 A
Peak voltage	< 1360 V	1254 A	1136
Effective duty cycle	> 0.9	0.96 A	0.94 A

In practice, six capacitors of 10 nF were paralleled to reduce equivalent series inductance (ESL). Film capacitors were selected owing to their relatively high root-mean-square (RMS) current ratings and excellent capacitance stability. A toroidal air-core inductor in the donuts-shape was designed and built with magnet wire AWG #12 for the resonant inductor, featuring a radius of 0.75 inches. Figure 16 shows the pictures of resonant capacitors and the inductor.

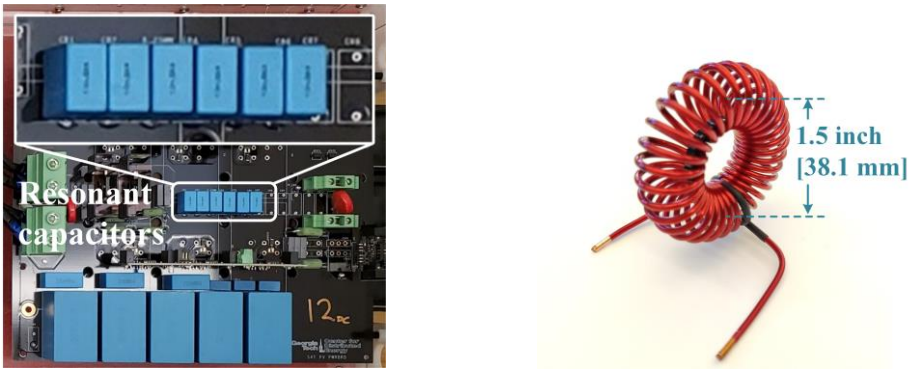

(a) (b)

Figure 16: Prototype pictures of (a) resonant capacitors and (b) resonant inductor.

Reverse-Blocking switch module design

As a current-source converter, reverse-blocking(RB) devices are required for MVSI's operation. Due to the nonavailability of reverse-blocking(RB) modules in the market, a custom design with discrete devices was implemented.

To guarantee the ZVS conditions for all devices across the entire load range, the peak voltage in each module has to be higher than the maximum port voltage with a reasonable safety margin. Based on Table 4, a peak voltage of 1.1 kV was finalized for the 25 kVA MVSI module. Hence, 1.7 kV devices were selected to provide a sufficient safety margin. To balance cost and efficiency, each RB switch consists of a silicon IGBT and a silicon carbide (SiC) Schottky diode. Two RB switches are connected in parallel to safely accommodate the peak magnetizing current, as shown in Figure 17.

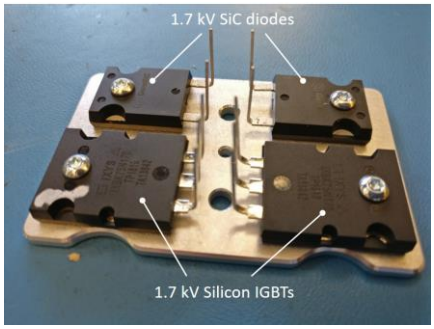

Figure 17: Prototype of custom 1.7 kV RB switch module.

Filters

Second-order LC filters were applied to filter out the switching harmonics and maintain a smooth input/output current profile. Figure 18 shows the schematic, where a damping resistor R_{damp} was used to damp output self-resonance between the filter inductor L_f and filter capacitor C_f.

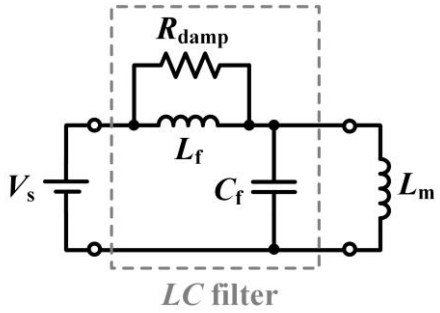

Figure 18: Schematic of selected second-order LC filters.

For the PV and battery ports on the DC side, the voltage ripple was selected to be 1% of their rated voltage, leading to the filter capacitance. The filter inductor is calculated based on the corner frequency of 1 kHz. On the AC side, the voltage ripple was determined to be 5%. The final values of second-order LC filters for the MVSI are summarized in Table 8.

Table 8: Second-order LC Filters Design for the 25 kVA/600 Vac MVSI modules

Parameter	Value	Parameter	Value
Switching frequency	16 kHz	Corner frequency	1 kHz
PV filter capacitor	78 μF	PV filter inductor	324 μH
PV damping resistor	2.0 Ω	Battery filter capacitor	217 μF
Battery filter inductor	117 μH	Battery damping resistor	0.7 Ω
AC filter capacitor	43.5 μF	AC filter inductor	584 μH
AC damping resistor	3.7 Ω		

Task 3: Solar PV Farm design based on MVSI: The S4T MVSI-based PV farm will have a significant impact if the farm size is above 20 MW, and it is necessary to perform a detailed design of such larger farms using S4T MVSI.

Approach:

- Subtask 3.1: (M1-M12) Detailed system design.

Results and Discussion:

Working with Southern Company and First Solar, an optimum farm design with 4 kV (or any MVAC) distribution was finalized. The details of the design of the farm are presented below.

Figure 19 shows the architecture and schematic of a 20 MW solar farm based on the central inverter configuration. The First Solar Series 4 PV module with 115 W max was used in this design. The farm has 7 arrays of solar panels, each feeding to the inverter at a power conversion station (PCS) at 1000V. Each array comprises of 20 rows on the North-side and 10 rows on the South-side. Each row comprises of 6 or 8 structural tables of panels (with each structural table having 6 electrical tables) connected to the trunk cable, as shown on the right-hand side in Figure 19(a). PV harnessing each electrical table is 10*3 strings, which is 10 panels in series with three strings in parallel. The total area of the farm is 700mx420m, with the substation located at the northeast corner of the farm. The farm has 7 power conversion stations (PCS); each has a 3 MVA inverter and a 3 MVA 480V/35kV transformer. Typically, 4 or 5 rows in the array are combined using a DC combiner box, and a DC feeder cable connects the combiner box to the inverter terminal. The farm is divided into two sections in terms of AC line (35 kV buried cable) running from the substation to each of the PCS, as shown in the figure. The overall schematic is depicted in Figure 19 (b).

Figure 20 shows the 20 MW solar farm based on the string inverter configuration. The plant layout is the same as that in the central inverter case, with each centralized PCS having 25 string inverters of 125 kVA. Each row comprising of 8 structural tables is connected to one string inverter. The ac output of 25 inverters is combined in an ac combiner box and then connected to the 60 Hz transformer.

Figure 21 shows the 20 MW solar farm based on the proposed 300 kVA/4 kVac MVSI configuration. The plant layout is modified to make better use of the 4 kV distribution. The 4 kV distribution line goes in the north-south (N-S) direction collecting the power from MVSI along the way. The N-S 4 kV lines feed into the east-west collection feeder, which runs all the way to the substation.

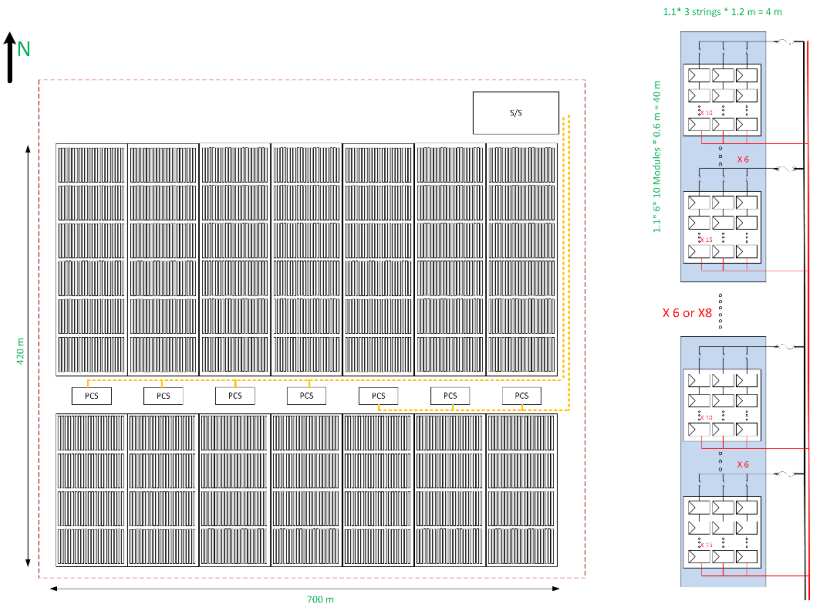

(a) Farm layout and PV Harnessing Strings

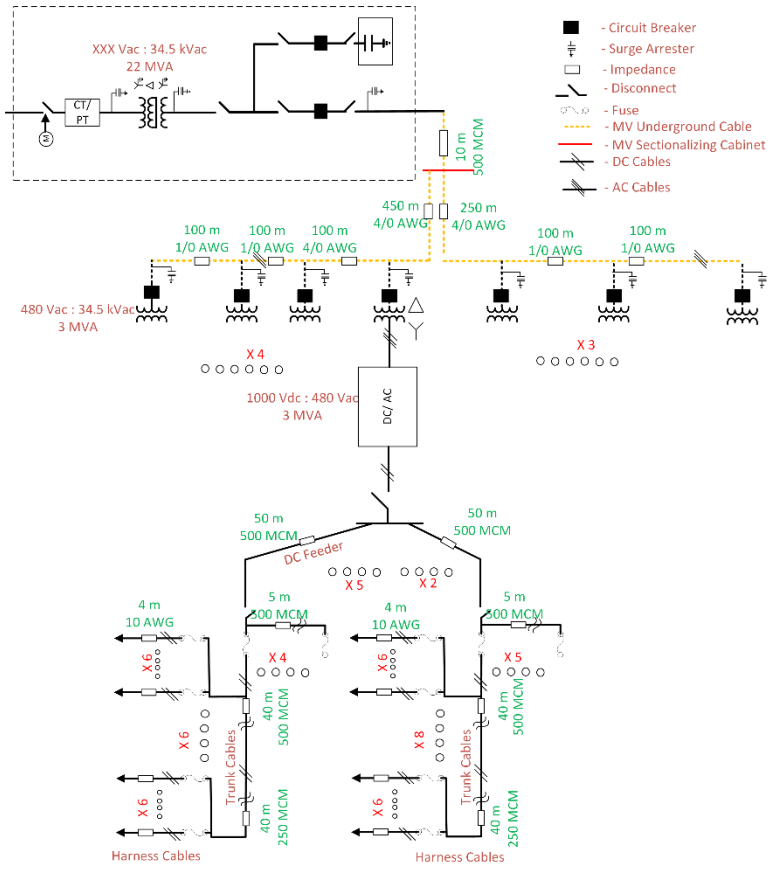

(b) Schematic

Figure 19: 20 MW solar farm architecture with central inverters.

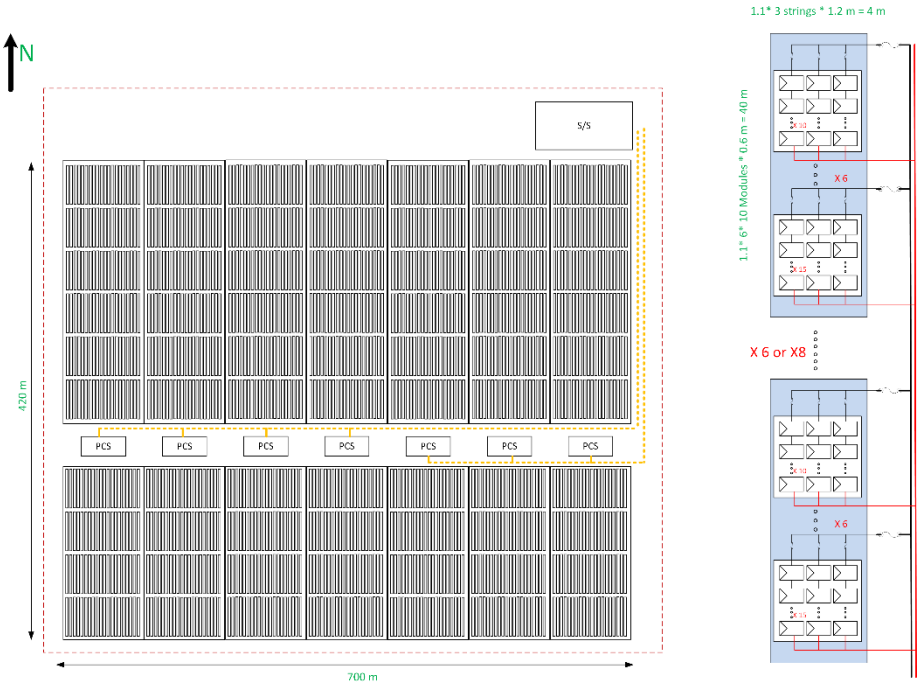

(a) Farm layout and PV Harnessing Strings

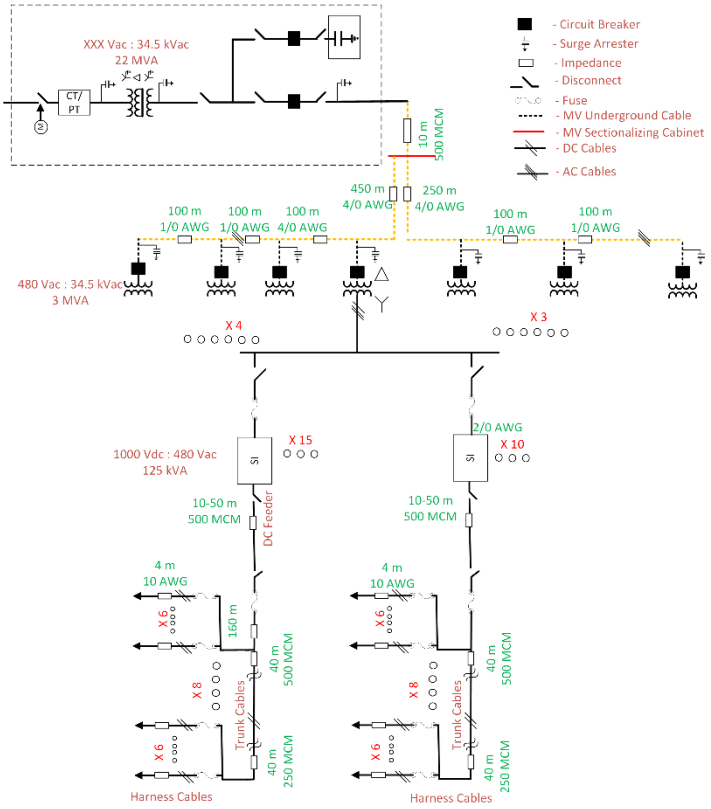

(b) Schematic

Figure 20: 20 MW solar farm architecture with string inverters.

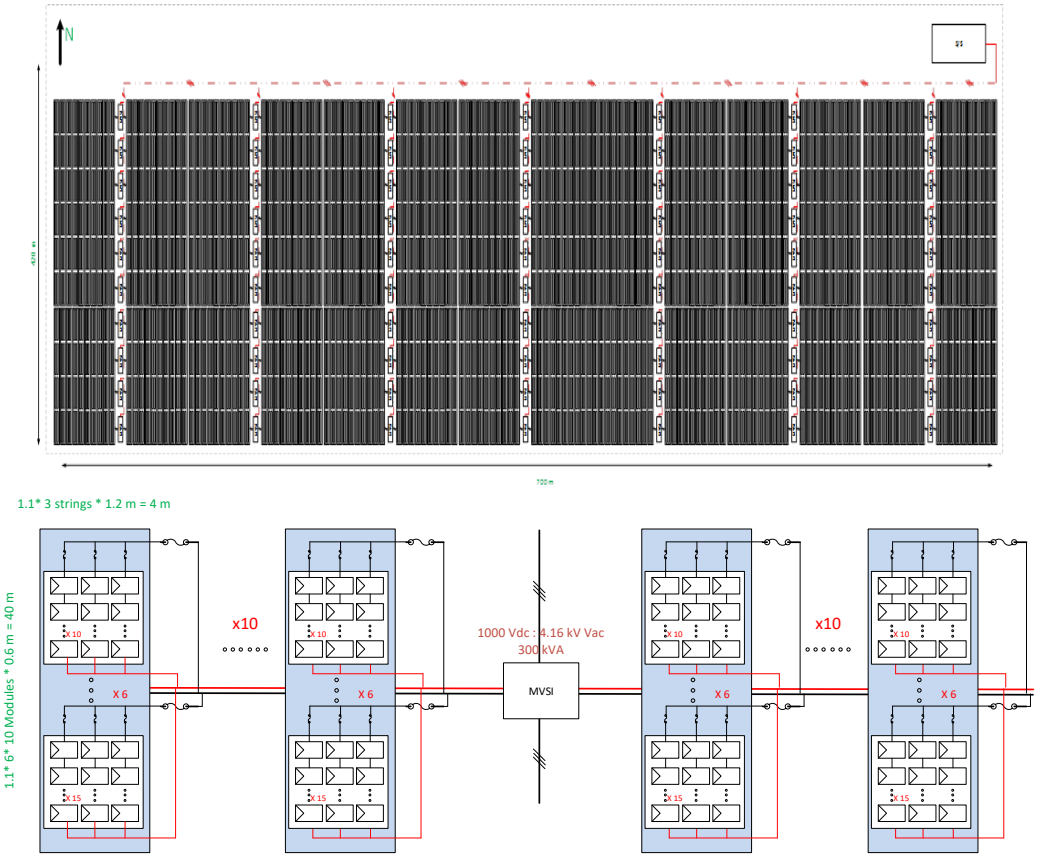

(a) Farm layout and PV Harnessing Strings

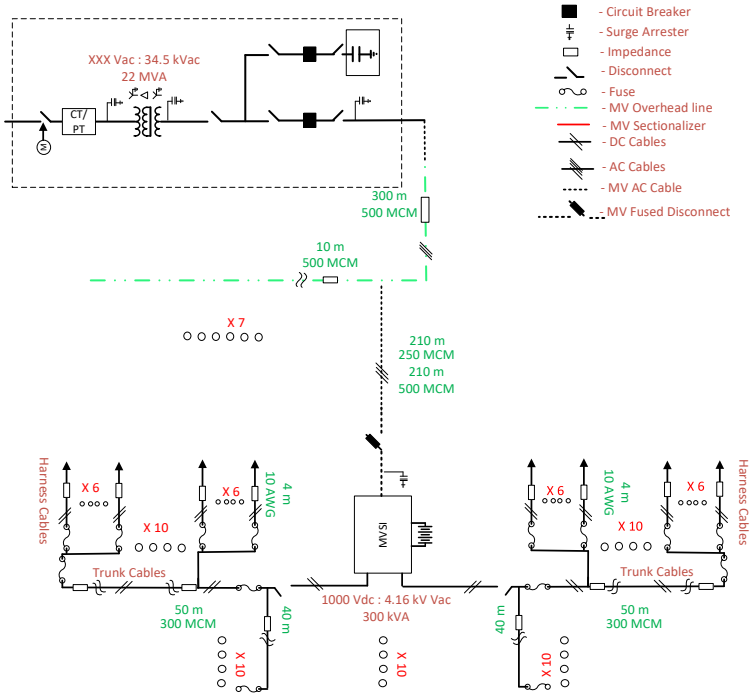

(b) Schematic

Figure 21: 20 MW solar farm architecture with the proposed 300 kVA/4 kVac MVSI.

For the loss comparison, the following assumptions have been made.

- Similar current densities in cables and overhead lines of different segments are assumed for the central inverter and MVSI scenario to balance the cable cost and losses.
- The overhead lines (bare aluminum conductor) are selected based on the same current density, and the price comes from the vendor.

Table 9: Assumptions in the cost vs. loss analysis for the central inverter and MVSI-based approaches

	Central	MVSI- 4kV	MVSI-13kV	MVSI-35kV
Trunk cable	90 A/mm^2	99 A/mm^2	99 A/mm^2	99 A/mm^2
AC side	170 A/mm^2	160 A/mm^2	155 A/mm^2	175 A/mm^2

Cable	Cost($/m)*	Cable	Cost($/m)**
10 AWG Cu	1.148	2 AWG AL 35 kV	13
12 AWG Cu	0.951	1 AWG AL 35 kV	15.5
14 AWG Cu	0.84	1/0 AWG AL 35 kV	18.24
2/0 AWG AL, 2kV	2.82	2/0 AWG AL 35 kV	20.96
3/0 AWG AL, 2kV	3.04	3/0 AWG AL 35 kV	22
4/0 AWG AL, 2kV	3.31	4/0 AWG AL 35 kV	22.86
250 MCM AL, 2kV	8.72		
350 MCM AL, 2kV	10.50		
400 MCM AL, 2kV	11.25		
500 MCM AL, 2kV	12.92		

Overhead line	Cost ($/m)***
1/0 AWG AL	1.25
2/0 AWG AL	1.28
3/0 AWG AL	1.61
4/0 AWG AL	2.53
250 MCM AL	2.20
300 MCM AL	2.76
350 MCM AL	2.76
400 MCM AL	3.18
500 MCM AL	4.79

The loss vs. cost results at 1000 V DC and 1500 V DC are shown in Figure 22. With MVSI, we get advantages with both cost and loss reduction. At 4 kV distribution, the main loss reduction is because of the reduction in one 60 Hz transformer. At 13 kV, the loss reduction because of copper loss reduction becomes significant. Moving to higher voltages, the benefits saturate as, at this point, the copper loss is mainly in the dc collection.

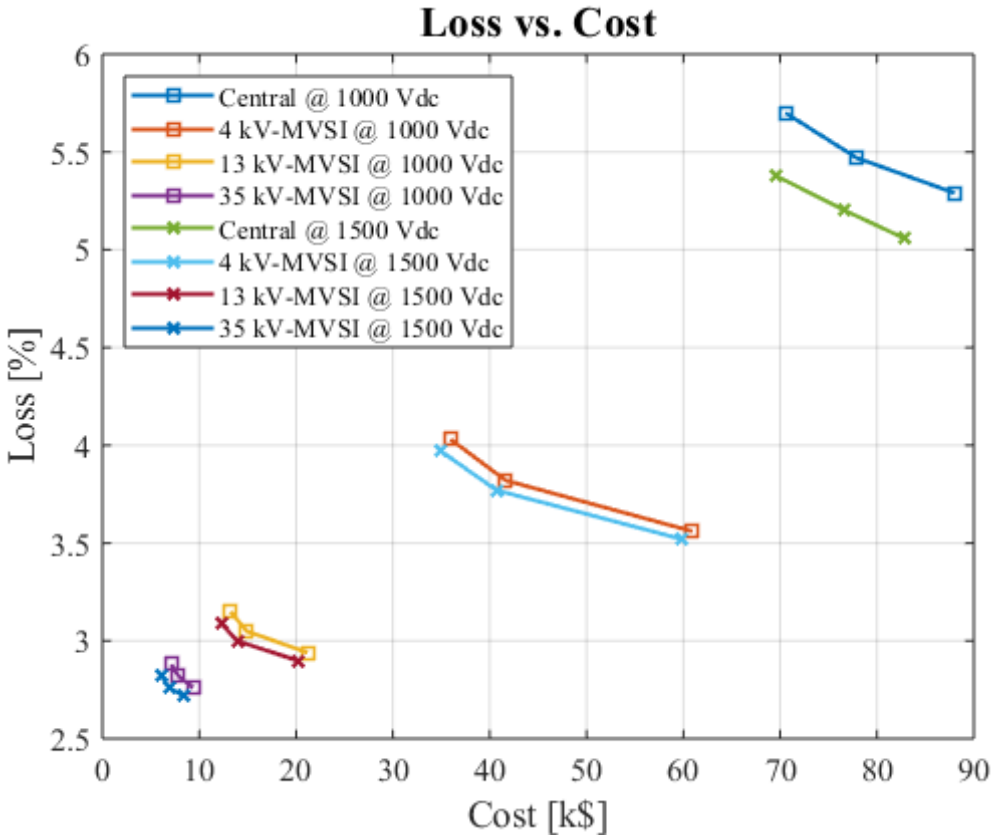

Figure 22: Loss comparison of 20 MW solar farms with central inverter and proposed MVSI approaches. Both 1000 V and 1500 V dc collection are presented.

Task 4: Financial Analysis: The S4T MVSI-based PV farm can reduce the Levelized Cost of Energy, and it is necessary to quantify and compare with technologies used in state-of-the-art PV farms. This task defines the procedure to obtain the LCOE and First Cost values.

Approach

LCOE and First cost are affected by the ability to add storage to the PV farm, which enables the PV farm's participation in ancillary markets like frequency regulation. In this task, the financial analysis was carried out based on the EBOS and storage medium-cost itself and potential revenue from ancillary services. NREL's LCOE Model and calculator were used for the analysis of the following use cases:

1. Current state-of-art based on central converter at 1000 V - 1500 V DC collection
2. Current state-of-art based on string converter at 1000 V - 1500 V DC collection and 480 V AC distribution

- Subtask 4.1: LCOE and First cost analysis of state-of-art based approaches.
- Subtask 4.2: Converter Cost estimation

Results and Discussion:

Subtask 4.1: We worked with First Solar to collect all the data required to calculate the LCOE for the base case.

Cost of 20 MW PV farm based on central inverters

Table 10 presents the inverter cost and EBOS cost of a 20 MW PV farm based on central inverters, which is the state-of-the-art approach and is taken as the base case for comparison. These data are obtained from a reference design by First Solar.

LCOE Analysis Framework

NREL's ATB tool was used to calculate LCOE, keeping the assumptions similar. The method to factor in the change in capacity factor due to the added battery storage needs to be investigated. Final LCOE analysis and comparison of the 20 MW PV farm with state-of-art and proposed MVSI approaches are presented in Task 10.

Table 10: LCOE calculation for the base case

Net Capacity Factor (%)	20%
Annual Energy Production (kWh/ kW)	1725
OCC ($/ kW)	1426
Fixed O&M ($/ kW-yr)	14
Variable O&M ($/ MWh)	$ -
LCOE from NREL Tool ($/MWhr)	68
LCOE $/kWh	0.07

	CAPEX ($/Wdc)	
		Benchmark
	Module	$ 0.69
BOS	Inverter	$ 0.04
BOS	EBOS	$ 0.096
BOS	SBOS	$ 0.20
Others	Labor	$ 0.14
Others	Design & Engineering	$ 0.01
Others	Permitting & Interconnection	$ 0.02
Others	Civil	$ 0.02
Others	Supply Chain, Logistics & Misc	$ 0.03
Others	Taxes	$ 0.04
Others	Overhead & Margin	$ 0.14
	Total	$ 1.426

EBOS	
Transformer	0.019
Combiner (Fuse)	0.006
DC Cable	0.055
AC Cable	0.007
Disconnect	Part of combiner
Circuit breakers	N/A
Instrumentation	0.009
Comm	Part of isntrumentation
Total	0.096

Subtask 4.2: The price for each 25 kVA module is shown in Table 11. It is expected to be around $1.38/VA. The main cost is for the semiconductors (driven by the SiC diodes) and the MF transformer (driven by the Nanocrystalline cores).

The cost of semiconductors is expected to reduce further in the next few years, which will bring the cost to around $1/VA. Please note that this includes the cost of the transformer and also includes the capability to integrate storage.

Table 11: Estimated BOM cost of 25 kVA MVSI module

Index	Quantity	Part Number	Manufacturer Part Number	Description	Available	Price USD/ 1000n	Total
			1700 V 150 A modules		7	$ 250.00	$ 1,750.00
3	12	495-3232-ND	B32672L8103J000	CAP FILM 10000PF 5% 2KVDC RADIAL	12	$ 0.25	$ 2.99
4	12	399-12795-ND	PHE845VF6220MR30L2	CAP FILM 0.22UF 20% 1.5KVDC RAD	12	$ 1.46	$ 17.46
5	12	495-3234-ND	B32672L8153J000	CAP FILM 0.015UF 5% 2KVDC RADIAL	12	$ 0.34	$ 4.04
6	5	495-3937-ND	B32778G0406K000	CAP FILM 40UF 10% 1.1KVDC RADIAL	5	$ 15.36	$ 76.81
7	3	495-3933-ND	B32778G1276K000	CAP FILM 27UF 10% 1.3KVDC RADIAL	3	$ 13.03	$ 39.10
8	6	399-16982-ND	C4AQSBW5170A3MJ	CAP FILM 17UF 5% 1500V RADIAL	6	$ 3.75	$ 22.48
9	14	399-12616-ND	R76UI04704000J	CAP FILM 470PF 5% 2KVDC RADIAL	14	$ 0.24	$ 3.40
10	4	ATS2089-ND	ATS-PCB1047	HEATSINK TO-218/TO-247 W/TAB	4	$ 1.11	$ 4.46
11	32	SAM10951-ND	CES-103-01-G-S	CONN RCPT 3POS 0.1 GOLD PCB	32	$ 0.40	$ 12.85
12	2	22112032	0022112032	CONN HEADER VERT 3POS 2.54MM	2	$ 0.29	$ 0.58
13	10	277-6038-ND	1704020	TERM BLOCK 1POS SIDE ENTRY PCB	10	$ 4.54	$ 45.38
14	4	F3046-ND	V1000LA160BP	VARISTOR 1.5125KV 6.5KA DISC	4	$ 1.36	$ 5.45
15	2	478-5046-1-ND	12105C475KAT2A	CAP CER 4.7UF 50V X7R 1210	2	$ 0.46	$ 0.93
16	16	SMBJ15CD-M3/HGICT-ND	SMBJ15CD-M3/H	TVS DIODE 15V 24V DO214AA	16	$ 0.12	$ 1.98
17	8	36-5018CT-ND	5018	PC TEST POINT COMPACT	8	$ 0.17	$ 1.34
18	2	F5413-ND	V660LA10P	VARISTOR 1.08KV 2.5KA DISC 10MM	2	$ 0.46	$ 0.93
19	2	F3029-ND	V1000LA80AP	VARISTOR 1.65KV 4.5KA DISC 14MM	2	$ 1.17	$ 2.34
20	8	PPC5W180CT-ND	AC05000001800JAC00	RES 180 OHM 5W 5% AXIAL	8	$ 0.22	$ 1.76
21	4	PPC5W120CT-ND	AC05000001200JAC00	RES 120 OHM 5W 5% AXIAL	4	$ 0.22	$ 0.90
22	4	651-1856126	1856126	TERM BLK 2P SIDE ENT 17.48MM PCB	4	$ 13.13	$ 52.52
23	5	504-C2791	C2791	Barrier Terminal Blocks BLK (B008-2792/1)	5	$ 7.60	$ 38.00
24	1	*	customized design	reduced FPGA+DSP Control board	1	$ 200.00	$ 200.00
25	2	**		Power PCB board	2	$ 47.55	$ 95.10
26	2	**		Gate driver board LVGD	7	$ 14.00	$ 98.00
27	2	**		Gate driver board HVGD	5	$ 20.00	$ 100.00
28	2	**		Fiber optic adapter board	2	$ 30.85	$ 61.70
29	2		SC2065M1	XFMR core AMCC630 nano.	2	$ 225.00	$ 450.00
31	2		LV 25-P/SP5	[PV & cap] voltage sensor,1000 Vpv and 650 Vca	2	$ 49.30	$ 98.60
32	1		LF 510-S	I_m High speed current sensor A1, 800Arms AC,	1	$ 72.59	$ 72.59
33	3		LF 210-S	`	3	$ 38.57	$ 115.71
34	5		HFBR-2524Z	Fiber Optic Transmitter 660nm 2.02V 80mA Vers	5	$ 5.78	$ 28.89
35	5		HFBR-1524Z	Fiber Optic Receiver 1MBd -24dBm 4.75V ~ 5.25	5	$ 5.78	$ 28.89
36	5		HFBR-4513Z	CONN FIBER PLUG SMPLX 1000UM	5	$ 0.34	$ 1.71
37	5		HFBR-4503Z	CONN FIBER PLUG SMPLX 1000UM	5	$ 0.34	$ 1.71
	1		LRS-150-24	Power supply	1	$ 18.23	$ 18.23
			Unit price		**1**		**$ 3,456.82**

Task 5: Test Bed Setup: Demonstration of the proposed energy storage integrated S4T MVSI at 300 kVA.

Approach:

- Subtask 5.1: (M4-M12) Build test setup

Results and Discussion:

Figure 23 shows the schematic of the designed test bed. The PV was emulated by a three-phase rectifier and the battery with an NHR emulator. The overall setup is with looping the three-phase AC side so that 300 kVA can be circulated through the MVSI with only loss is taken from the main power supply. The required 300 kVA 4.16 kV/ 600 V transformer has to be custom-built because of the required K-factor. A transformer from Schaffner (transformer manufacturer) was procured for testing, and a 1000 V 50 kW rectifier was designed and developed, which is presented in Task 11 for the MVSI testing.

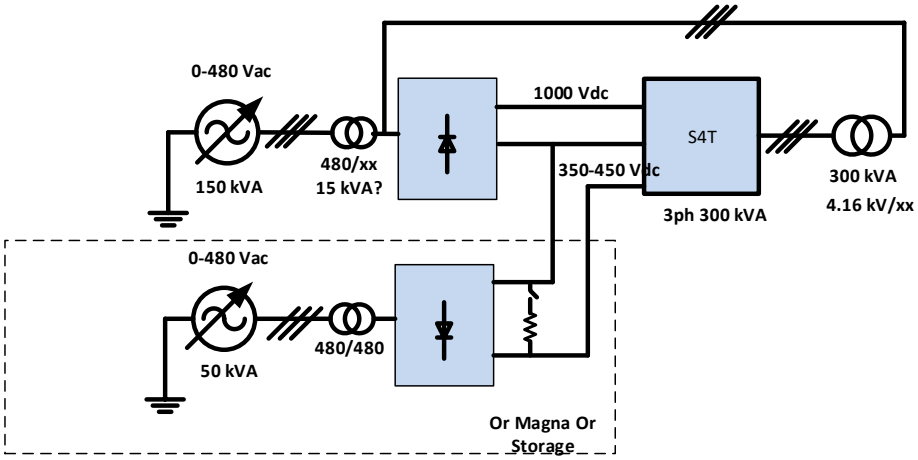

(a)

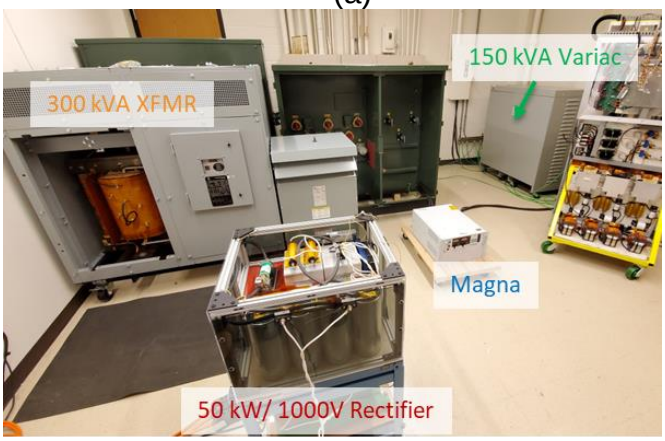

(b)

Figure 23: Proposed testbed setup. (a) Schematic. (b) Pictures of procured/built elements.

Task 6: Explore regulatory issues: It is necessary to identify the market opportunities, distribution channels, and any potential barriers to the commercialization of the proposed architecture.

Approach:

- Subtask 6.1 (M4-M12) Regulatory issues: Explore different regulatory models to increase Utility participation in solar PV farms.

Results and Discussion:

Regulatory models enabled by MVSI technology to increase utility participation in solar farms are discussed. Lastly, the final report delivered by the corresponding project sub-awardee is attached in the Appendix B section for reference.

Regulatory Models Enabled by MVSI Technology and Direct Current Service

The technologies demonstrated in this project could enable a utility to provide DC – AC conversion for solar and energy storage and efficiently manage the interconnection of the solar facility and the larger AC power grid. The MVSI technology enables the output of the facility to be managed in real-time, balancing the provision of real and reactive power, reserves, and storage. The technology can respond to real-time operator instructions or,

on a sub-cycle basis, to conditions in the power grid. By expanding the utility's role as a network operator to include power conversion and integration of the PV facility into the grid, the utility will be able to optimize the value provided by solar and storage based on changing system requirements. The MVSI and direct current capabilities demonstrated in this project could further change the role of the distribution utility from being a poles and wires company to becoming an active real-time system operator.

Utility operation of PV integration services could avoid the negative impacts that solar can have on power system operations. Customers and third parties may have an economic incentive to simply maximize the electrical output of their PV systems. In some cases, this may create congestion, limit circuit hosting capacity, increase losses and costs to the utility and adjacent customers, violate voltage standards, and/or require additional utility investment. Moreover, when third-party aggregators bid distributed generation into wholesale power markets without coordinating with the distribution network operator, they skip over an essential layer in the architecture of the power system. The third-party aggregator's dispatch of a specific resource has the potential to interfere with distribution operations and require interrupting service to distribution customers.

Additionally, utility management of a solar and storage facility's interconnection with the power system could allow it to offer additional services, including:

- Gathering service: Even a utility that faces regulatory limits on owning or operating generation may be able to collect DC energy, transport power on DC lines, and operate a switchable transformer to convert DC to AC power.
- DC as customer service: The utility may be able to provide a portion of the facility's DC output to a data center, charging facility for electric vehicle fleets, or another customer with DC power requirements.
- Enhanced reliability and ancillary services: MVSI control of the real-time output of solar panels, reserve solar capacity, and/or storage offers the potential to support adjacent microgrids or provide flexible reserves, black start, and other ancillary services.

With smart, flexible MVSI control, a utility operator of the solar and storage facility has the potential to support the real-time operation of an increasingly fractal and autonomous energy system. These values streams are achievable with only one converter in the case of the MVSI but can also be achieved with several converters with advanced controllers.

b. Budget Period 2

The focus of work during the second budget period was to build/test a prototype MVSI and perform Financial (LCOE and First Cost) analysis on the proposed PV farm with MV distribution.

Task 7: 300 kVA S4T MVSI HIL Simulation and Golden prototype design: Task 7 required the completion of Task 11 (Bronze prototype build and test) – was postponed until completion of Task 11. Not completed because of COVID-19 and pivot to MDCT (to be detailed later in this report)

Task 8: Solar PV Farm design based on MVSI: The S4T MVSI-based PV farm will have a significant impact if the farm size is above 20 MW, and it is necessary to perform a detailed design of such larger farms using S4T MVSI.

Approach:

- Subtask 8.1: (M19-M24) Revised system design based on learnings from system analysis in Effort 2 and converter testing in Effort 4.

Results and Discussion:

Figure 24 (a) shows the 20 MW PV farm layout with the proposed 300 kVA/4 kVac MVSI AC collection, featuring a length of 700 m and a width of 420 m. All 70 of 300 kVA S4T MVSI units with battery storage are connected with a 4.16 kV AC overhead line, which is fed into one substation to be elevated to 35 kV for power transmission.

Compared to the 3 MVA central inverter-based and 480V string inverter-based plants, it eliminates the need for multiple line frequency substation transformers and consequently saves first cost. In addition, along with the battery storage and PV array, the proposed MVSI enables scalable solar-plus-storage (SPS) farm building blocks, resulting in significant cost reductions in the design stage.

Figure 24(b) presents the configuration of a 300 kVA scalable SPS farm building block. PV array in each 300 kVA unit contains 3600 PV modules of First Solar Series 4, 115W to form the 1000 Vdc / 300 kVA input. The 3D prototype of 300 kVA S4T-based MVSI with storage is presented in Figure 25(a), which comprises of 12 of 25 kVA building blocks shown in Figure 25(b) in a three-phase configuration.

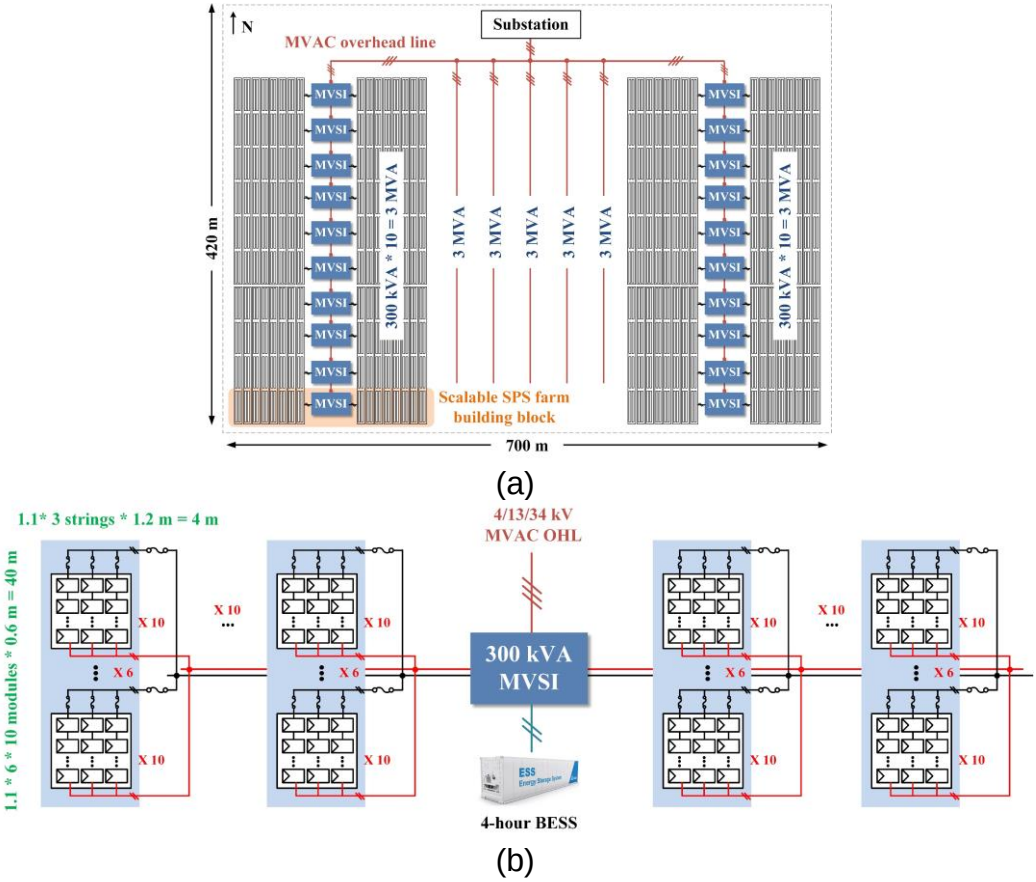

Figure 24: Farm layout of a 20 MW SPS farm based on the proposed 300 kVA/ 4 kVac MVSI units. (a) Distributed system layout. (b) 300 kVA SPS farm building blocks.

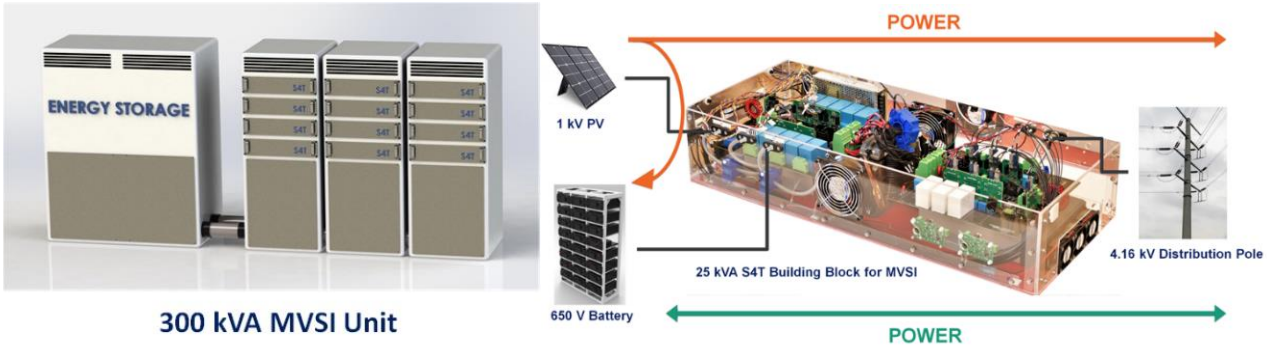

(a) (b)

Figure 25: (a) 3D prototype of 300 kVA/4 kVac S4T based MVSI with battery storage; (b) 25 kVA S4T building block for MVSI.

Task 9: Simulation for system analysis: The PV farm with MV distribution needs to be investigated to understand its impact and benefits on the grid at the system level. In addition, the integration of energy storage is a key benefit of the proposed MVSI, and it is necessary to analyze and identify the storage requirements of the PV farm.

Approach:

- Subtask 9.1: Farm-level simulation. Simulation of 20 MW solar farm, modeling parameters such as cable and transformer impedances and cloud cover, in OpenDSS or equivalent platform to verify the following:
  - Operation of multiple 300 kVA MVSIs operating together to respond to SCADA signals.
  - Operation under partial shading conditions.
  - Converter interactions.
- Subtask 9.2: Grid/Farm Interaction study. Simulate a large grid (>100 buses) with the proposed solar farm with integrated storage and evaluate the following
  - Impact of storage on dispatchability and market participation.
  - Grid support through voltage, VARs, and frequency regulation.
  - Load shifting/curtailment.
  - Improving system inertia.
- Subtask 9.3: Analysis of storage requirements for PV farm based on the proposed converter:

Results and Discussion:

Subtask 9.1: With the developed high-fidelity small-signal model of the proposed MVSI, a simulation model of a 20 MW/80 MWh SPS farm was built in Matlab/Simulink. The impedance of the grid and interconnection cables are included to study the converter interactions. Several case studies were completed to demonstrate the improved energy dispatchability under partial shading conditions and response to grid commands.

Figure 26 shows the circuit schematic of the 20 MW MVSI-based SPS farms. There are, in total, 70 of the proposed 300 kVA/4 kVac MVSI PEBBs. Without loss of generality, the derived high-fidelity small-signal model of the MVSI [cf. Figure 10] was used to save computational effort. The line impedance of interconnection cables and grid impedance were extracted based on the farm layout and specifications presented in Figure 21.

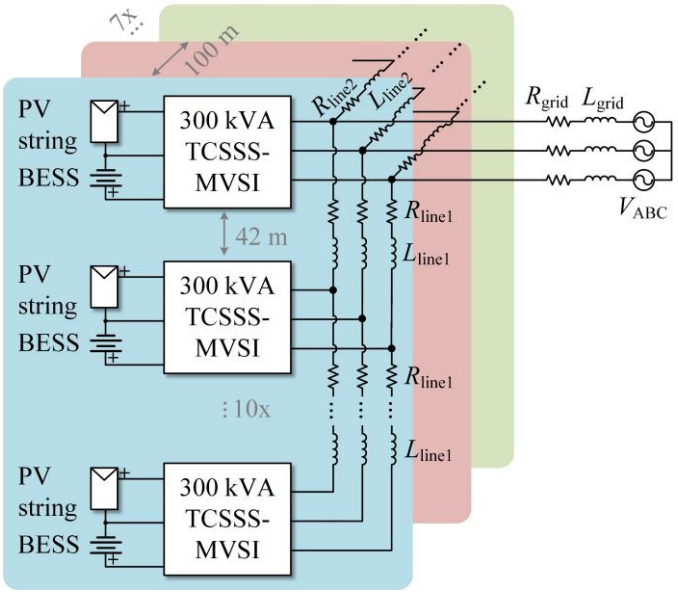

Figure 26: Simplified circuit schematic of the 20 MW SPS farm based on the proposed 300 kVA/ 4 kVac MVSI units.

Case 1: Improved Energy Dispatchability under partial shading conditions

Partial shading induces a volatile output power of solar farms at different times of scale and thus poses significant challenges to grid planning and operation. In SPS farms, the paired battery storage can balance out the energy deficit under partial shading conditions and lead to a smooth grid output.

Fig. 27 shows the simulation results of the 20 MW MVSI-based SPS farm, where constant output power on the grid side was achieved under a realistic PV irradiation profile. The MVSIs enable a dc-coupled battery to provide a responsive power balance between PV and the grid, suggesting an enhanced energy dispatchability of the SPS farm.

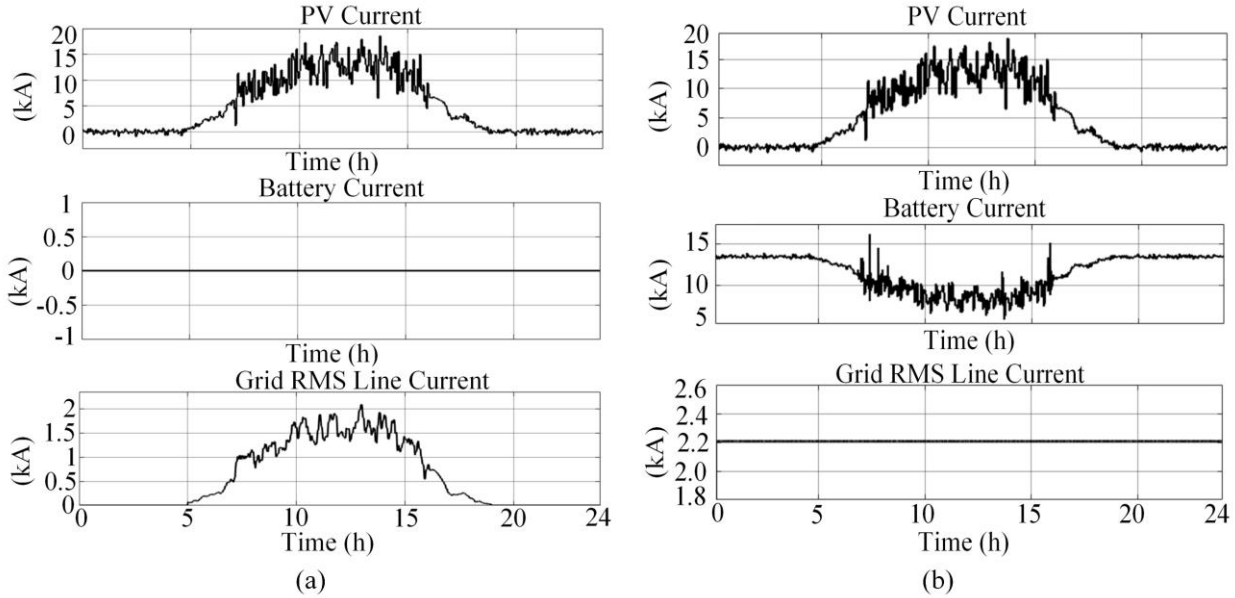

Figure 27: Improved energy dispatchability of the 20 MW MVSI-based SPS farm with a realistic PV irradiance profile.

Case 2: Reactive Power Support During Voltage Sags

In addition to the active power, reactive power also plays a critical role in reliable and efficient AC grid operation. With the increased penetration of DERs, reactive power (VAr) support provided by solar farms has become increasingly crucial to the voltage stability of the grid, leading to an increased value proposition of solar farms.

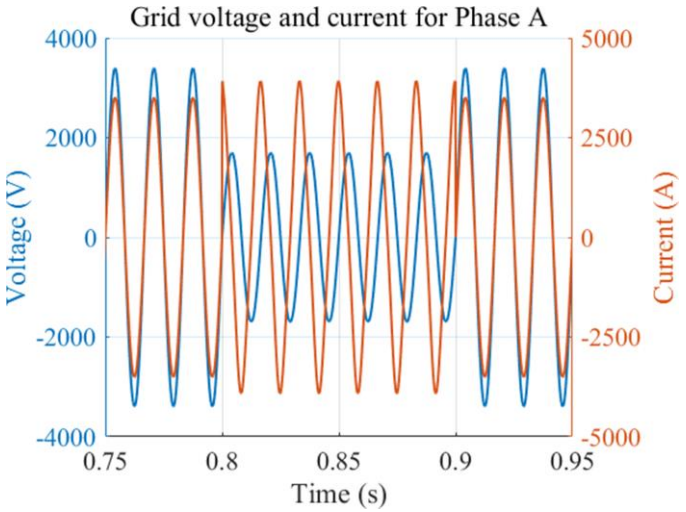

Figure 28: 0.5p.u. reactive power support provided by the 20 MW TCSSS-MVSI based SPS farm during single-phase-to-ground fault.

Figure 28 presents the VAr support of the 20 MW MVSI-based SPS farm, where phase A to ground fault on the grid side was created on purpose for the case study. The fault caused an unsymmetrical voltage sag and a phase shift between voltage and current in phase A, requiring 10 MVAr reactive power support from the SPS farm. With the DC-coupled BESS, the MVSI delivered 10 MVAr reactive power (0.5 p.u.) to the grid responsively for six consecutive line cycles before the fault was cleared and a normal operation was recovered, satisfying the requirements by IEEE Standard 1547 [3].

Case 3: Low-Distortion Output Under Grid Harmonics

The increased penetration of inverter-based resources (IBRs) and the numerous different types of loads generate ubiquitous harmonics in the grid, resulting in potential threats to critical loads sensitive to the grid output quality. Thus, a smooth grid output with low THD is of vital interest even under grid harmonics.

Figure 29 demonstrates the grid operation under grid voltage harmonics, where the harmonics profile listed in Table 12 was injected into the grid voltage. With the responsive MVSI, a smooth grid current with a THD < 3% was observed in this case.

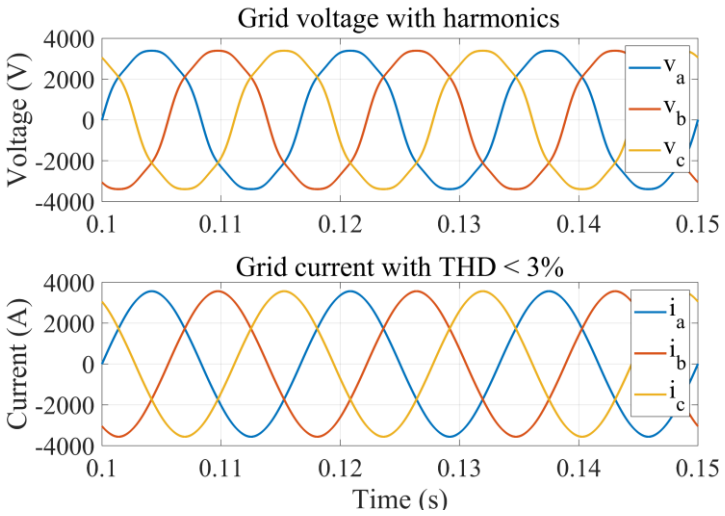

Figure 29: Low-THD AC output of the 20 MW MVSI based SPS farm under grid harmonics.

Table 12: Harmonics profile of the grid voltage

Harmonics	Percentage	Peak voltage
3rd order	7.5%	255 V
5th order	5.0%	170 V
7th order	4.0%	136 V

Subtask 9.2: This task was completed and delivered by Electric Power Research Institute (EPRI) in OpenDSS with several case studies. A separate report by EPRI has been submitted to SETO and included in this report for reference. The model behavior is modeled in Python, and the grid is modeled in OpenDSS. Figure 30 shows the flowchart for the Grid/Farm interaction study in OpenDSS. Three primary control objectives, i.e., grid-side power regulation, PV MPPT, and dc-link current regulation of MVSI, have been achieved.

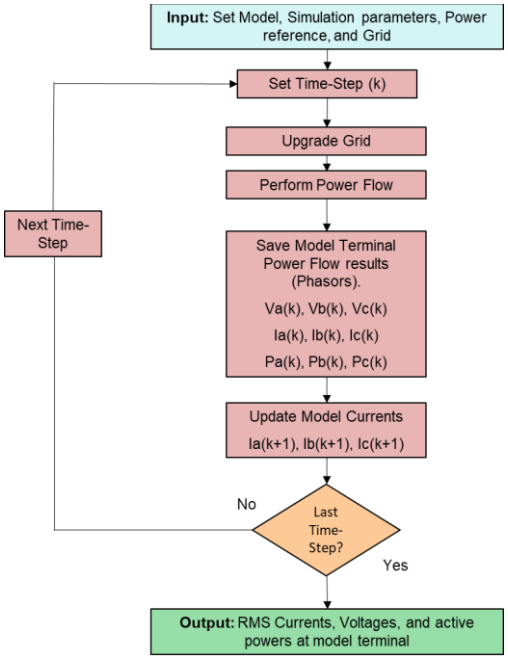

Figure 30: Flowchart for the Grid/Farm interaction study in OpenDSS.

The key takeaways of this task are summarized as follows:

- Farm-level properties were demonstrated using the small-signal model developed in Task 1 and implemented at the farm level.
- The scalability of the approach is shown by implementing the developed small-signal model in OpenDSS and showing similar performance.

Subtask 9.3: A separate report by Oak Ridge National Lab is included in the Appendix section of this report for reference. The key takeaways of this task are summarized as follows:

Explore different regulatory issues to increase Utility participation in solar PV farms (Consultant)

- We see expanded opportunities to take the concept to Clustered DC Loads (DC as a Service) that utilities can serve and can better integrate with grid operations

- There may be opportunities for utilities to play the role of building and owning make-ready infrastructure. There is nothing inherently anti-competitive that would prevent a distribution utility in a retail access jurisdiction from developing make-ready infrastructure.
- Such infrastructure might include all of the wires for gathering power and an MDCT and DC / AC converter used to connect the facility to the grid. A vertically integrated utility can own all or part of a solar facility.
- To build such infrastructure, both the vertically integrated utility and the distribution utility in a competitive market would face financing disadvantages. For example, a third-party developer could benefit from the full ITC credit on gathering, conversion, and interconnection portions of a solar project, while the utility would have to follow tax normalization rules.
- Nonetheless, it may prove viable for distribution utilities to offer access to solar as a service.
- There are many consumers who would like to purchase solar power but are unable to affordably do so because they live in multi-family housing, don't have a suitable site, or can't afford the up-front investment.

Task 10: Financial analysis of the proposed approach: The S4T MVSI-based PV farm can reduce the Levelized Cost of energy, and it is necessary to quantify and compare with technologies used in state-of-the-art PV farms.

- Subtask 10.1: LCOE and First cost analysis based on the proposed approach.
- Subtask 10.2: Reliability impact on the financial analysis.

Results and Discussion:

Subtask 10.1: Taking a 20 MW/80MWh SPS farm as a case study, the proposed MVSI and MDCT have shown significant advantages in reducing system LCOE compared with traditional central inverters and string inverters with AC- and DC-coupled BESS across inverter-loading-ratio from 1.3 to 2.0. The results are presented below:

Framework of System-Level LCOE Analysis

Table 13: Limited impact of inverter cost on LCOE of large-scale PV farms

(a) Breakdown of Overnight Capital Cost

	Overnight Capital Cost ($/Wdc)	Benchmark ($)
	PV Module	0.31
	Inverter	**0.04 → 0**
BOS	Electrical BOS	0.096
	Structural BOS	0.20
	Labor	0.14
	Design & Engineering	0.01
	Permitting & Interconnection	0.02
Others	Civil	0.02
	Supply Chain, Logistics & Misc.	0.03
	Taxes	0.04
	Overhead & Margin	0.14
	Total	1.046 → 1.006

(b) LCOE calculation with ATB data and calculator by NREL

Net Capacity Factor	20%
Annual Energy Production (kWh/kW)	1725
Overnight Capital Cost OCC ($/kW)	1046 → 1006
Fixed Operation & Maintenance ($/kW-year)	14
Variable Operation & Maintenance ($/MWh)	0
Capital Recovery Factor	5.2%
Calculated LCOE (cents/kWh)	**3.911 → 3.793**

For many years, a continued effort has been made to improve the inverter performance cost-effectively. However, inverters themselves have a limited impact on the LCOE of large-scale solar farms. As detailed in Table 13, a zero inverter cost only yields a 3% LCOE reduction for a 20 MW PV farm based on central inverters, a reference PV farm design provided by First Solar.

Therefore, a system perspective is required to evaluate inverters' technology holistically, where EBOS, soft costs, capacity factor, etc., should be considered, especially when integrating battery storage into PV farms. Those power conversion system (PCS) architectures that enable an extended LCOE reduction at the system level, despite a higher cost in inverters themselves in some cases, are promising candidates to help proliferate low-cost solar energy.

Figure 31 shows the fundamental elements of the SPS farm that impact LCOE. Analysis in this research takes the PV modules, structural BOS, DC system, PCS, MVAC system, and BESS into account. The impacts of financing and other common factors are out of scope.

The DC system includes DC underground cables, fuses, combiners, and disconnectors. One key parameter is the voltage level, which is primarily 1/1.5 kV today and may reach 2 kV in the future. The power conditioning unit (PCU) interfaces the DC system to the MVAC system. It contains PV inverters and line-frequency transformers, if appropriate, whose specifications depend on different PCS architectures. Comprised of cables and protection components, the MVAC system at various voltage levels (4/13/34 kV) connects the PCU to the substation. Lastly, the 20 MW/80 MWh BESS contains battery packs, as- sociated interconnection cables, converters, transformers, and protection apparatus. It can be seen that the specifications of the DC, MVAC, and battery storage systems are strongly dependent on the deployed PCU.

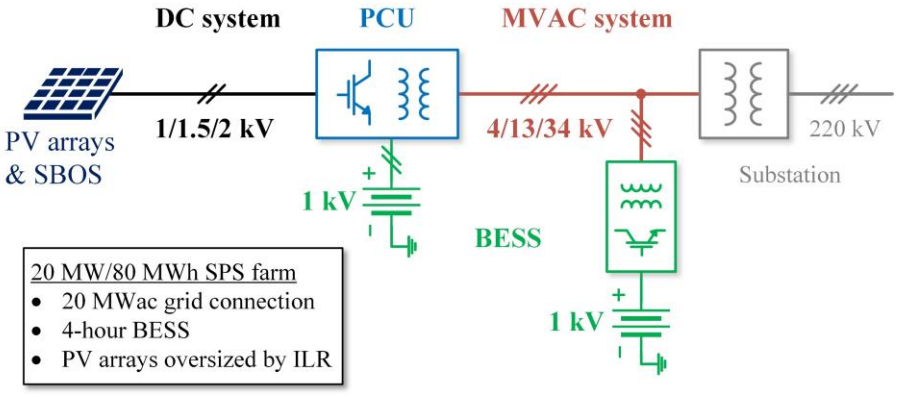

Figure 31: Basic elements of a 20 MW/80 MWh SPS farm.

The farm layout of the PV farm with traditional central inverters/string inverters and the proposed MVSI have been presented in Figures 19-21, respectively. Based on their farm, specifications of all EBOS elements in different approaches can be identified, leading to a detailed cost and loss breakdown of the SPS farms. As a result, the system-level LCOE of SPS farms with corresponding technologies can be evaluated and compared to validate the advantages of the proposed MVSI and MDCT in reducing the system-level LCOE.

AC- and DC-coupled BESS for Large-Scale PV Farms

Figure 32 presents two popular configurations to integrate battery storage into PV farms in real-world projects, namely co-located AC-coupled BESS and DC-coupled BESS. In the AC-coupled approach, additional battery converters and 60 Hz transformers are required for charging/discharging battery packs. It provides great retrofit ability and flexibility but results in extra cost and power losses.

On the other hand, the DC-coupled approach only needs an isolated DC-DC converter to interconnect the BESS to the DC bus formed by PV arrays. It is able to capture the clipped energy by PV arrays without oversizing the PV inverters and cascaded 60 Hz transformers. In addition, it features a reduced number of power conversion stages, leading to an increased roundtrip efficiency of the BESS.

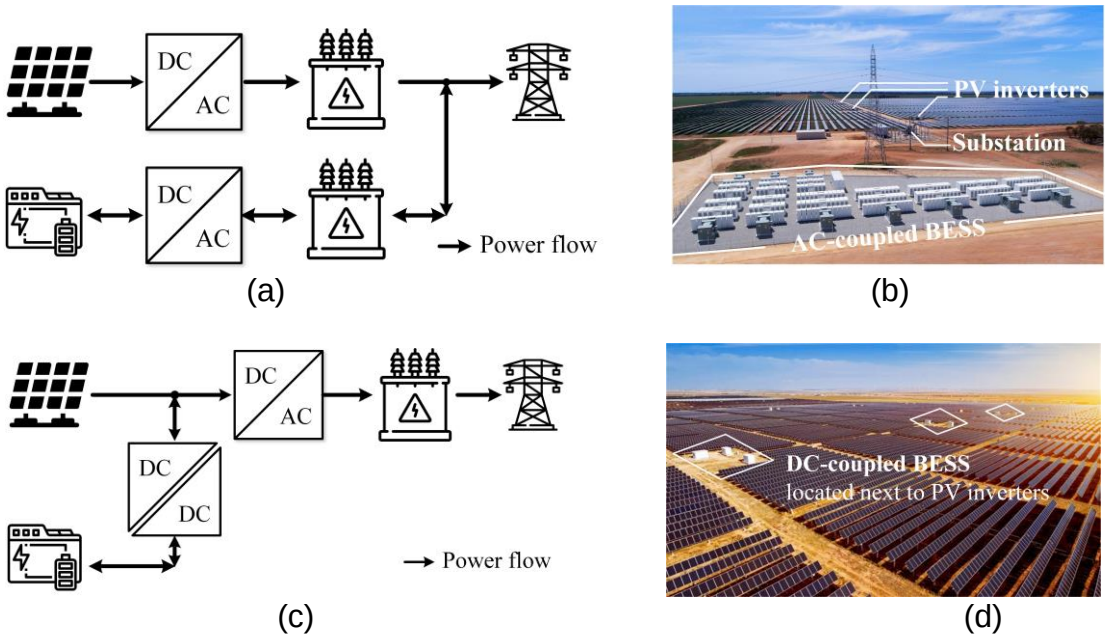

Figure 32: Layout of utility-scale PV farms with BESS. (a) and (b) Schematic and picture of AC-coupled BESS. (c) and (d) Schematic and picture of DC-coupled BESS.

Central Inverters (CI) with AC- and DC-coupled BESS

Figure 19 shows the detailed system layout of a 20 MW PV farm based on central inverters. Single-line-diagrams (SLD) of central-inverter-based PV farms with AC- and DC-coupled BESS are shown in Figure 33 to facilitate the system cost and losses analysis. The SLD shows the electrical elements from PV strings to harness, trunk, combiner boxes, inverters, 60 Hz transformers (if appropriate), and finally, MV sectionalizing cabinets, including all components of interest for system-level LCOE analysis for this task.

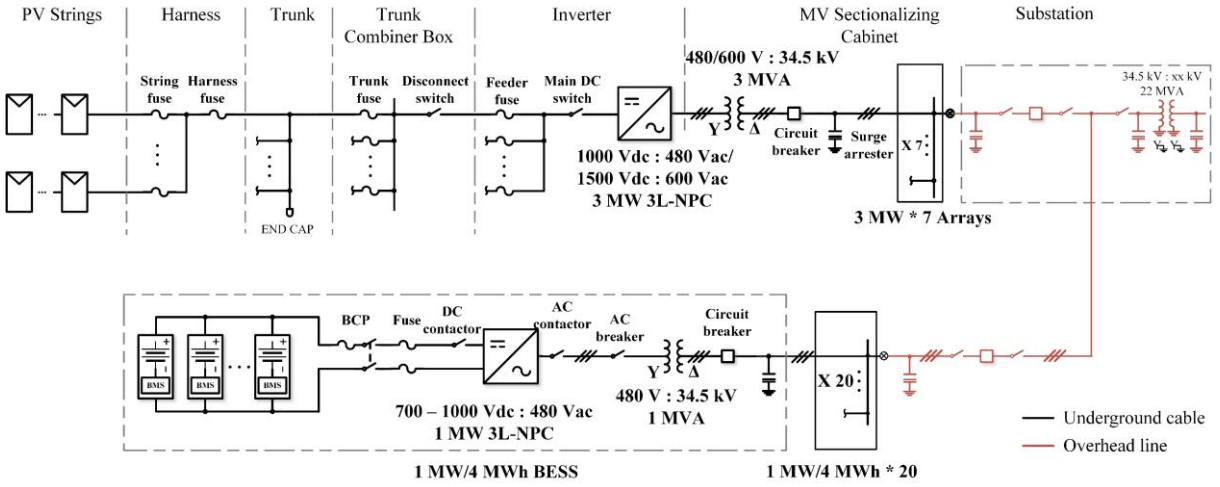

(a)

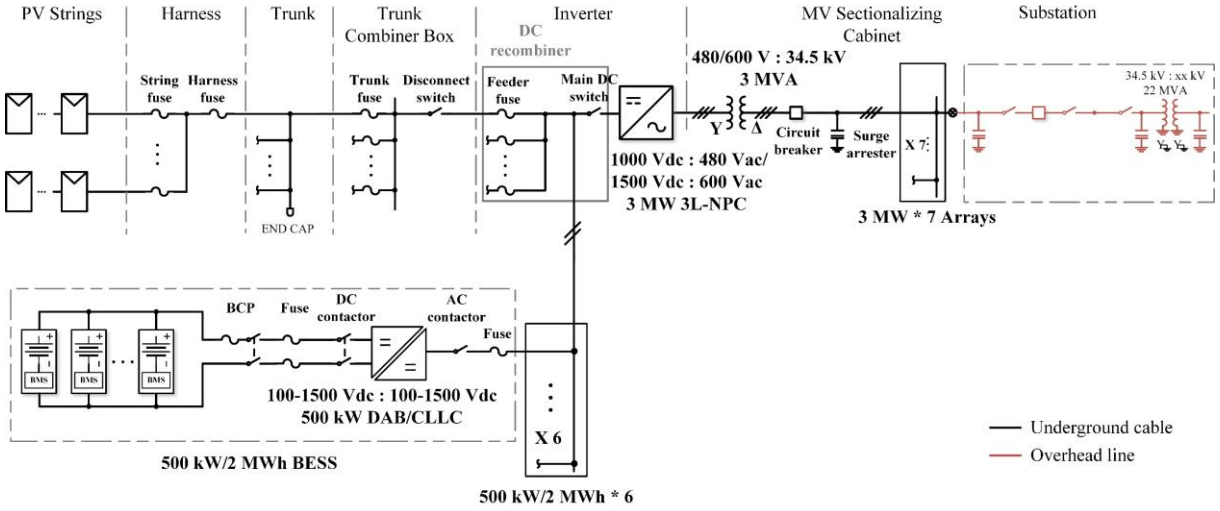

(b)

Figure 33: Single-Line-Diagram of 20 MW SPS farms with 3 MVA central inverters and (a) AC-coupled BESS (b) DC-coupled BESS.

Figure 33(a) presents the SLD of 20 MW SPS farms with central inverters (CI) and AC-coupled BESS. Seven 3 MW central inverter power electronics building blocks (PEBBs) based on three-level neutral-point-clamped (3L-NPC) converter topology are deployed, converting 1, 000/1, 500 V PV string voltage to 480/600 V three-phase AC output. The 480/600 V LVAC is elevated to 34.5 kV by 3 MVA line-frequency transformers downstream of the central inverters. The AC-coupled 20 MW/80 MWh BESS is composed of twenty BESS building blocks, each rated at 1 MW with 4 hours of storage capacity. In each BESS PEBB, the battery exchanges power with the 34.5 kV grid via a 1 MW 3L-NPC inverter cascaded by a 1 MVA line-frequency transformer. A similar three-level inverter was selected here for convenience. However, the battery voltage is not allowed to fall below 700 V due to the modulation limitation by the inverters in this case. A front-end boost stage can be added to allow a wider range of battery voltage.

Figure 33(b) shows the SLD of 20 MW SPS farms with central inverters and DC-coupled BESS. It shares the same power path from PV strings to the substation as that with AC-

coupled BESS. However, there is three primary difference existing in the configuration of BESS:

1. The point of common coupling (PCC) switches from MVAC at the substation to the DC bus formed by PV strings, eliminating the 34.5 kV line-frequency transformers and associated EBOS elements.
2. The specification of each BESS unit becomes 500 kW/2 MWh, which is the maximum standard PEBB by leading manufacturers.
3. An isolated DC-DC converter that is commonly based on Dual-Active-Bridge (DAB) converter is applied to exchange the power in an efficient way.

Centralized String Inverters with AC- and DC-coupled BESS

Centralized string inverters (SI) are another state-of-the-art PCS architecture for large-scale PV farms. Compared to central inverters employing only a single MPPT, string inverters feature string-level MPPT optimization and thus lead to higher energy yield, gaining increasing popularity in the market.

Figure 20 shows the system layout of a 20 MW PV farm based on centralized string inverters. Based on the farm layout, the SLD of a string-inverter-based PV farm with AC- and DC-coupled BESS are derived and exhibited in Figure 34.

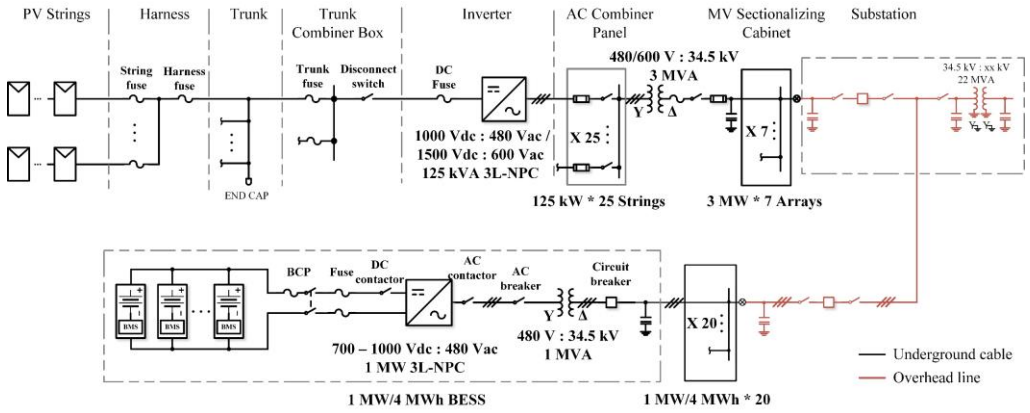

(a)

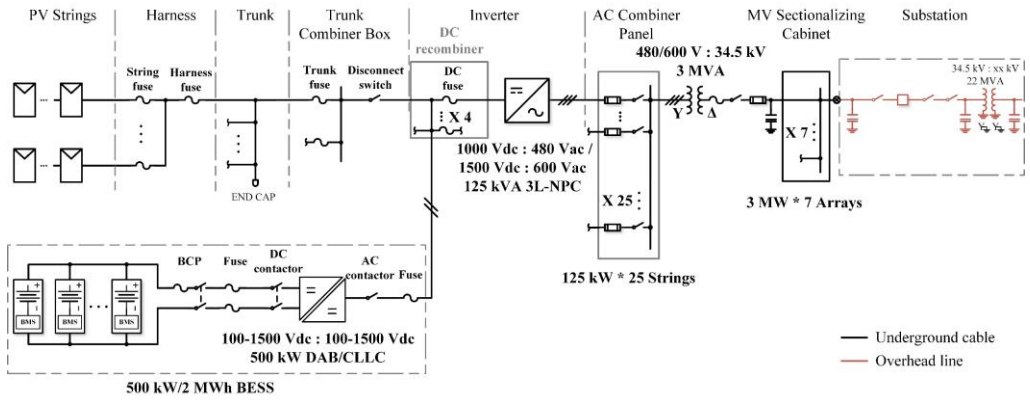

(b)

Figure 34: Single-Line-Diagram of 20 MW SPS farms with 125 kVA string inverters and (a) AC-coupled BESS (b) DC-coupled BESS.

This approach is achieved by employing 175 of 125 kW strings inverters based on 3L-NPC topology. Each SI interfaces one independent 1,000 V PV string to a 480 V three-phase LVAC output or a 1,500 V PV string to a 600 V AC output. Consequently, it reduces the number of DC combiner boxes on the DC feeders but extra AC combiner panels downstream of string inverters to bundle multiple independent PV strings. Each AC combiner panel accommodates 25 PV strings, which is followed by one line-frequency transformer for the 34.5 kV grid connection.

Figure 34(b) shows the DC-coupled BESS counterpart with the SI-based PV farms. It shares the same 500 kW/2 MWh BESS building blocks as CI-based approach, but the connection pattern differs. Each 500 kW BESS unit is shared by four 125 kVA string inverters to match the four-times difference in power ratings of BESS units and string inverters. The connection can be managed by DC re-combiner boxes consisting of DC fuses, disconnect switches for multiple inverters, and one single BESS unit.

Proposed MVSI with Localized DC-coupled BESS

Figure 21 exhibits the system layout of the 20 MW SPS farm based on the proposed 300 kVA/4 kVac MVSI. The tri-port nature of the MVSI enables localized DC-coupled BESS integration without additional BESS converters, leading to significant savings in cost and power losses. Unlike the centralized power conditioning units (PCU) in CI- and SI-based approaches, the proposed MVSI enables scalable SPS farm building blocks with PV strings, as shown in Figure 21(a), leading to a distributed PCU layout across the SPS plant. In addition, instead of using UG cables, standard and low-cost OHL are deployed to reduce the cable and laboring cost tremendously.

Figure 35 illustrates the SLD of TMVSI-based SPS farms. Every 1 MW/4 MWh BESS unit supplies three 300 kVA MVSI to match the power ratings. Additional battery storage converters are eliminated by localized DC-coupled BESS configuration enabled by the tri-port TMVSI. AC combiner panels are also removed owing to the distributed PCU layout across the SPS plant.

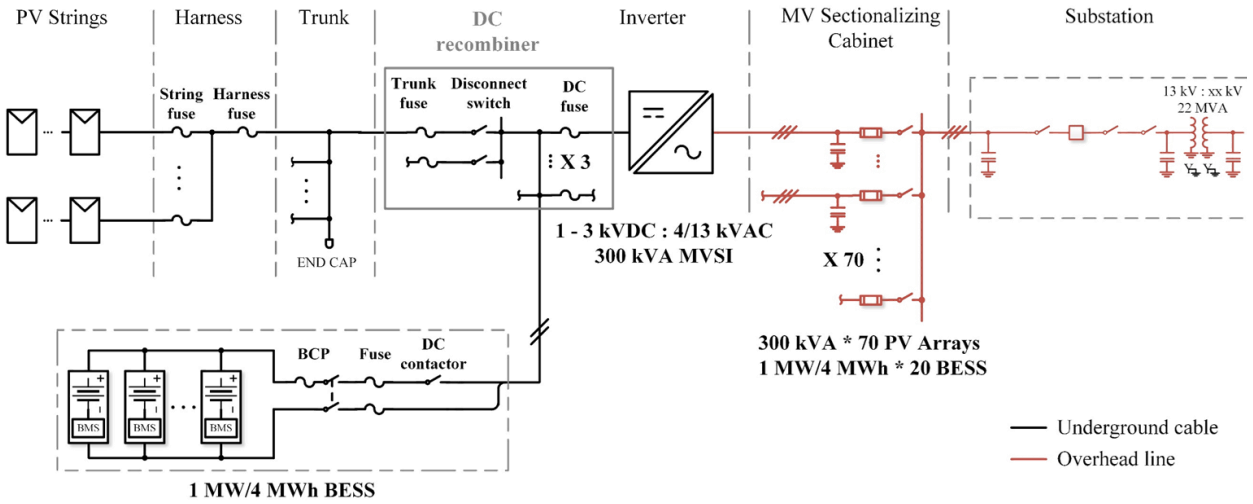

Figure 35: Single-Line-Diagram of 20 MW SPS farms with the proposed 300 kVA MVSI and localized DC-coupled BESS.

Proposed MDCT with Localized DC-coupled BESS

Multi-port DC Transformer (MDCT) that is also based on S4T converter topology is another attractive implementation approach for MVSI. Figure 36 shows the schematic of a 300 kVA /13 kVac MDCT. Without cascading multiple single-phase AC outputs in the TMVSI, the MDCT employs a 34 kV line-frequency transformer downstream of the S4T converters for MV grid connection. Multiple S4T modules are connected in an input-parallel output-parallel (IPOP) manner to achieve a higher power level. Each module converts the PV and battery power to a three-phase 575 V AC output, which is elevated to 13 kV MVAC via line-frequency transformers. As a further step, 34 kVac line-frequency transformers can be employed to further expand the benefits of the MVAC collection network.

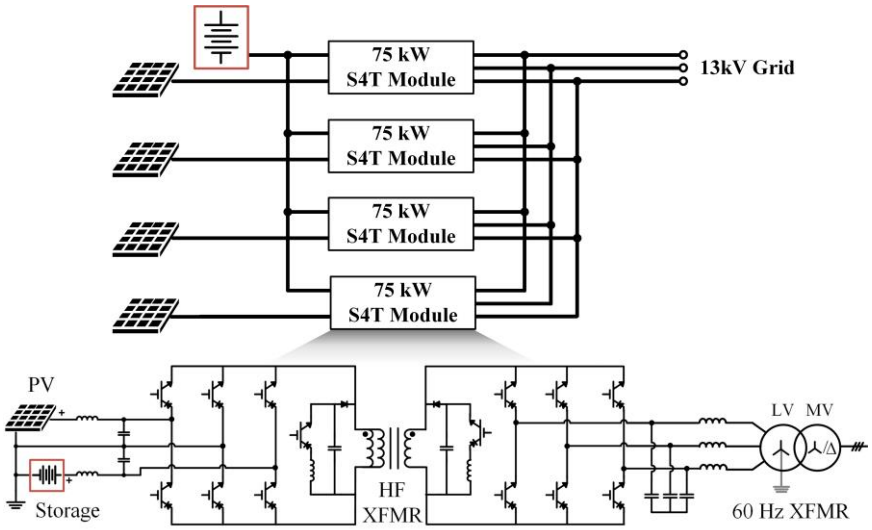

Figure 36: Circuit schematic of 300 kVA/13 kVac MDCT.

Figure 37 presents the SLD of MDCT-based 20 MW/80 MWh SPS farms. It shares a similar farm layout as the MVSI-based approach, except that each 1 MW/4 MWh BESS unit is paired with one 1 MW MDCT unit. Each 1 MW MDCT unit contains three 300 kVA MDCT PEBBs sharing one common 1 MVA 60 Hz transformer for a cost-effective design.

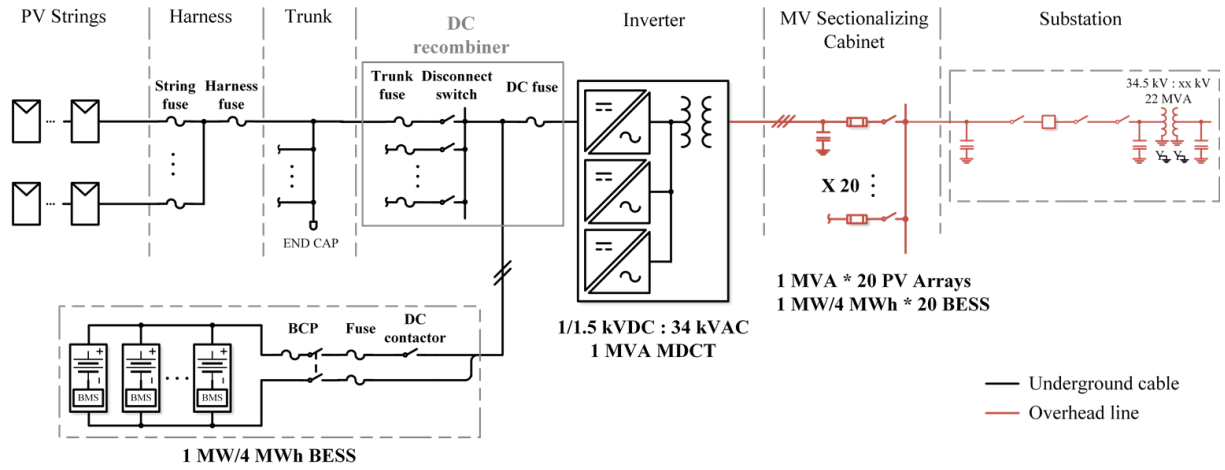

Figure 37: Single-Line-Diagram of 20 MW SPS farms with the proposed 300 kVA MDCT and localized DC-coupled BESS.

Compared to the MVSI, the MDCT features near-term commercial availability since it eliminates the use of costly high-voltage reverse-blocking devices. In addition, the integrated protection apparatus of the 60 Hz transformer relaxes the protection scheme and cost of the S4T converters. By agreement between the CDE and the DOE, a demonstration of the 300 kVA S4T MDCT was completed instead in Budge period 3.

Breakdown of System Cost and Losses

Figure 38 presents all elements of interest for SPS farms with AC- and DC-coupled BESS, including PV arrays, cables, inverters, 60 Hz transformer, and BESS. Their specifications in the four approaches under investigation are discovered in detail in this section. In this analysis, the grid connection capacity is kept constant at 20 MWac for a fair comparison among different PCS architectures. With the detailed SLDs of the overall farm based on different PCS architectures, the system cost and losses of the 20 MW/80 MWh SPS farms can be extracted piece by piece.

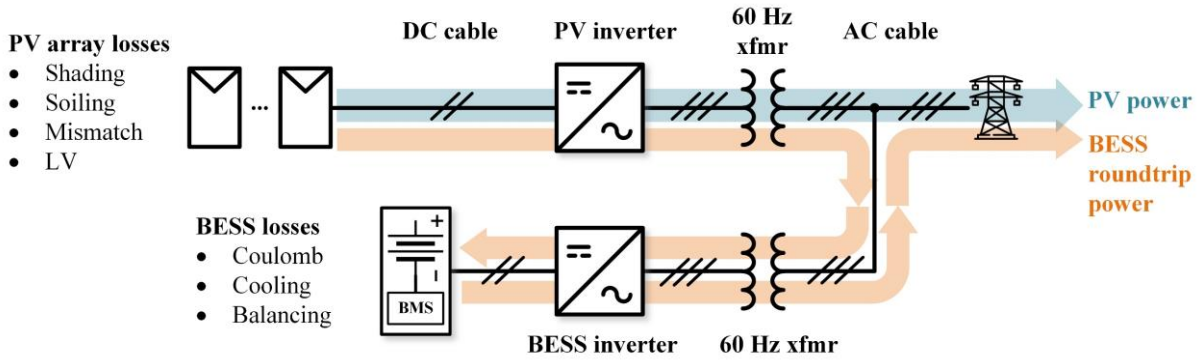

(a)

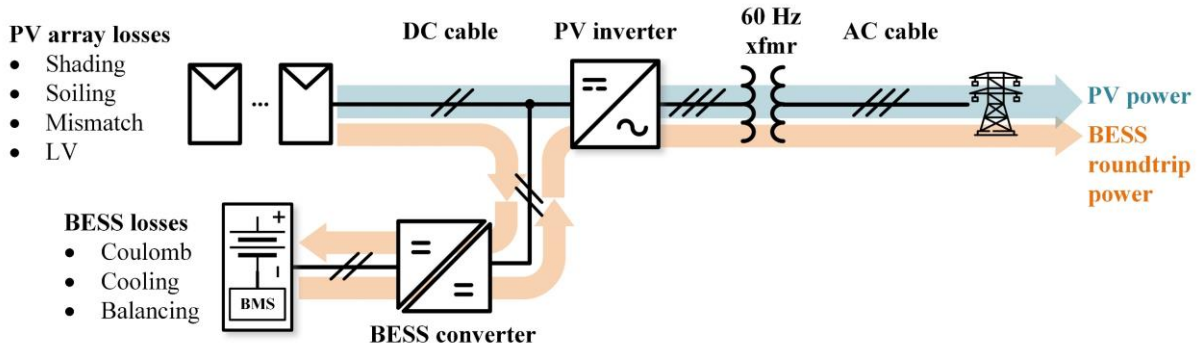

(b)

Figure 38: System losses of interest for SPS farms with (a) centralized AC-coupled BESS and (b) DC-coupled BESS.

PV Arrays with Oversizing Ratio ILR

For utility-scale SPS farms, PV arrays play a crucial role in the system losses. The 20 MW SPS farm employs a large number of PV panels to form PV arrays across the giant plant. Thus, unbalanced conditions of PV cells occur easily and frequently in shading, soiling, snow, bird dropping, module mismatches, etc., resulting in significant energy losses. Depending on the ground coverage ratio, the shading loss varies between 2% − 10% [4]. Subject to the weather and location, the soiling loss and snow could reduce the energy

revenue by 2% for regions with year-round rain seasons and 5% for regions with long dry seasons [5]. Caused by manufacturing imperfections, the PV module mismatch accounts for > 2% loss for most systems with long strings, which can be eliminated by using DC optimizers or microinverters, which will have their own losses of around 2% − 3% [6-8]. Furthermore, there are some LV losses in the early morning and late evening hours when the irradiance is so low that the MPP voltage of PV strings falls below the minimum start voltage of PV inverters. The LV losses are around 10 %, according to one case study by SolarEdge [9]. The power losses in PV arrays can be obtained by

$$P_{\text{array}} = P_{\text{shading}} + P_{\text{soiling}} + P_{\text{mismatch}} + P_{\text{LV}} \tag{10.1}$$

Figure 39 illustrates the daily power profile of PV panels with different ILRs at 1.0/1.3/1.5/2.0. For utility-scale PV farms without BESS, the ILR usually stays between 1.1 − 1.3 to maximize the utilization of PV inverters without significant power curtailment of PV arrays [10]. Otherwise, an ILR higher than 1.3 could suffer considerable clipped PV energy, even considering the PV array losses from soiling, shading, and module mismatch. This issue can be addressed in utility-scale SPS farms, where the paired BESS can capture and store the clipped energy of the PV array and dispatch it to the grid as needed. Therefore, the ILR is seen to have increased to 1.8 − 2.0 in some projects with DC-coupled BESS. In this analysis, an ILR of 1.5 is selected as a start point for the comparative analysis, and the sensitivity of the ILR to system-level LCOE is studied.

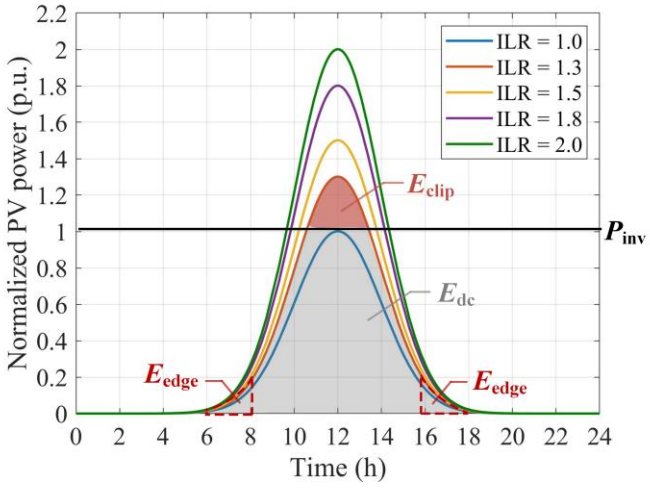

Figure 39: Normalized power generation profile of PV panels over one day.

Based on a reference design of a 20 MW solar farm by First Solar, the unit price of PV panels is given as 0.28 $/Wdc. Furthermore, the unit prices of the SBOS and labor are 0.20 $/Wdc and 0.14 $/Wdc, respectively.

Several key aspects in the four considered approaches need to be highlighted here. First of all, thanks to the current-source-converter nature, there is no minimum operating voltage for the MVSI and MDCT. Hence, the 10% LV energy losses in the early morning or late evening hours can be eliminated. Secondly, MVSI and MDCT share the same string-level MPPT and consequent shading/soiling/mismatch losses as traditional string inverters, leading to reduced shading, soiling losses, and mismatch losses than central inverters. Lastly, the labor cost could reduce by 15% − 20% for MVSI and MDCT approaches because of the reduced workload by using multi-port converters rated at hundreds of kilowatts.

PV Cables

Depending on the PCS architecture of SPS farms, DC cables include harness cables, trunk cables, and DC feeders (if any), while AC cables contain LVAC cables (if any) and MVAC cables for PV power collection. In addition, DC and AC cables for BESS inter-connection are also considered. The lengths and types of cables in different segments are elected based on the same current density of cables in corresponding parts of various PCS architectures – a rule of thumb to compromise cable losses and cost.

The specifications of selected cables and current density in CI-based and SI-based PV farms were input from solutions providers. According to the reference design, a current density of 100 A/cm^2 was selected for DC UG cables, while 170 A/ cm^2 for MVAC cables and OHL. In some segments, two different sizes of cables are cascaded to accommodate the increased flowing current over a long distance. The cable cost was quoted from cable manufacturers, and the cable losses in different segments can be calculated with

$$P_{\text{cable}} = I_{\text{cable}}^2 \cdot R_{\text{cable}} \cdot l_{\text{cable}} \qquad (10.2)$$

where I_{cable} is the flowing current in corresponding segments in ampere (A), R_{cable} is the unit resistance of different sizes of cables in Ω/m, and l_{cable} is the cable length in meter (m).

In the MVSI and MDCT approaches, DC cables' cost and loss savings stem from the immensely reduced trunk and feeder cable lengths. On the MVAC side, the cable losses and costs decrease with increased voltage levels from 4 kV to 13/34 kV. Using low-cost overhead lines completely offsets the moderate increase in AC cable length.

PV Inverters and 60 Hz Transformers

To make a fair and meaningful comparison of inverter costs, the bill of materials (BOM) cost of all selected inverters was estimated based on the same price benchmarks of each component from markets and a leading manufacturing service company.

For large-scale SPS farms based on CI, SI, and MDCT, PV inverters, as well as 34.5 kV line-frequency transformers, are required for power conditioning, while the proposed MVSI eliminates the 60 Hz transformers. Their losses were obtained from product datasheets by leading providers and reported literature.

The losses and cost of 34.5 kV 60 Hz three-phase transformers were shared by a large transformer manufacturer. The 3 MVA/34.5 kV transformers for PV inverters cost $19/ kVA and 0.5% losses.

Battery Energy Storage System (BESS)

According to the latest BNEF report in [11], $135/kW h is used to calculate the BOM cost of 80 MWh battery cells plus battery management system (BMS) for AC- and DC- coupled BESS configurations.

For the AC-coupled BESS, 10% of PV DC cable cost is assumed for DC-side interconnections of the BESS and 60% of PV AC cable cost for substation connection in a shorter length. The cable losses are calculated with (8.8). In terms of PCU, $70/kVA is estimated for the 1 MVA battery storage inverter and $29/kVA for the 34 kV 60 Hz transformers. The power losses of the inverter and transformer are 1.5% and 0.6%, respectively.

On the other hand, DC-coupled BESS eliminates the 60 Hz transformer and AC interconnection cables. Thus, only the cost of DC cables, isolated DC-DC converter, and protection apparatus remains. The same cost of DC cables as that in AC-coupled BESS was adopted. DAB converter was selected for the isolated DC-DC converter, costing $105/kVA and presenting an efficiency of 98.5%.

There are primarily three loss factors in utility-scale BESS, namely coulombic, cooling, and active cell voltage balancing losses. For state-of-the-art lithium-ion battery cells, a coulombic efficiency of > 95% is feasible [12, 13]. For large BESS containers, cooling loss accounts for around 2%, and active balancing loss stays around 5% for low C-rate charging while increasing to 10% − 20% for fast-charging scenarios [13, 14]. Consequently, the energy efficiency of battery cells, ηcell, can be calculated by

$$\begin{aligned}\eta_{\text{cell}} &= \eta_{\text{coulomb}} \cdot \eta_{\text{cooling}} \cdot \eta_{\text{balancing}} \\ &= (1-\alpha_{\text{coulomb}}) \cdot (1-\alpha_{\text{cooling}}) \cdot (1-\alpha_{\text{balancing}})\end{aligned} \quad (10.3)$$

here, α_{coulomb}, α_{cooling}, and $\alpha_{\text{balancing}}$ are coulombic, cooling, and active balancing losses, respectively.

The round-trip efficiency of BESS matters to SPS farms and determines the amount of clipped energy captured by the BESS and then delivered to the grid. In this regard, DC-coupled BESS shows advantages over its AC-coupled counterpart thanks to reducing two power conversion stages, as illustrated in Figure 37. In the AC-coupled BESS approach, the clipped energy needs to flow through one PV inverter, two 60 Hz transformers, and one BESS inverter to be stored in battery cells. To deliver the captured clipped energy to the grid, the power needs to flow through the BESS inverter and cascade the 60 Hz transformer once again. As a result, the round-trip efficiency of the AC-coupled BESS approach accounts for six power conversion stages (converters or transformers), even if we do not take the cables into account.

Alternatively, only four power conversion stages are required for the DC-coupled BESS, i.e., the BESS converter twice, the PV inverter once, and the 60 Hz transformer once, leading to improved round-trip efficiency and increased energy revenue. The round-trip efficiency of the AC- and DC-coupled BESS, $\eta_{\text{BESS,RT}}$, can be calculated by multiplying the efficiency of each stage in the power path by

$$\eta_{\text{BESS,RT}} = \begin{cases} \eta_{\text{PV,cable}} \cdot \eta_{\text{PV,inv}} \cdot \eta_{\text{PV,xfmr}} \cdot (\eta_{\text{BESS,cable}} \cdot \eta_{\text{BESS,xfmr}} \cdot \eta_{\text{BESS,inv}})^2, & \text{AC-coupled} \\ \eta_{\text{PV,cable}} \cdot (\eta_{\text{BESS,cable}} \cdot \eta_{\text{BESS,xfmr}} \cdot \eta_{\text{BESS,conv}})^2 \cdot \eta_{\text{PV,inv}} \cdot \eta_{\text{PV,xfmr}}, & \text{DC-coupled} \end{cases} \quad (10.4)$$

Please note that in the AC-coupled BESS configuration, the PV inverter, DC and AC cables, and cascaded 60 Hz transformer need to be oversized by ILR for the clipped power flowing through the PCU. Otherwise, the clipped power has to be wasted, and none of it can be stored in the BESS. Moreover, the same oversize of the BESS inverter and transformer is required to store the entire PV energy generated at maximum PV power in case of no grid demand. But in DC-coupled BESS configuration, only the BESS converter and DC cables need to be upgraded by ILR to capture full PV energy if there is no demand on the grid side.

In the proposed MVSI and MDCT approaches, the initial capital cost of BESS is primarily spent on battery packs in addition to DC cables and protection apparatus. The BESS in the kV TMVSI and MDCT approaches share the same large BESS containers as DC-coupled BESS configuration in CI- and SI-based PCS. Therefore, they share the same battery pack cost and power losses. But the MVSI and MDCT save money in extra isolated DC-DC converters. In addition, the converter loss of transferring PV power to BESS in MVSI and MDCT reduces to 1.5% because the power only circulates on one side of the HF transformer. In the MVSI and MDCT approaches, the cost of DC interconnection cables and protection is assumed to be the same as that of DC-coupled BESS configuration in CI- and SI-based counterparts. The cable loss is neglected since the BESS containers locate close to the converters with a very short cable length.

Fault Protection Elements

The protection includes fuses, disconnect switches, circuit breakers, surge arresters, contactors, and built-in elements in converters. Please note that the 34.5 kV 60 Hz transformers have already accounted for components against MVAC-side faults such as lightning strikes, leaving DC-side faults as the remaining significant challenge to the system's reliability and uptime. Hence, DC fuses and disconnect switches are the primary cost items of protection. Zero power losses are assumed for the protection apparatus for simplicity.

In the 4/13 kV MVSI architecture, the cost of protection apparatus increases, primarily stemming from the additional components against MVAC-side faults due to the absence of 60 Hz transformers. The expense increases in a further step with a rising MVAC voltage level. In comparison, the MDCT features a similar price to CI- and SI-based approaches owing to the cascaded 60 Hz transformers downstream of converters.

Comparison of System-Level LCOE

PV Energy Generation and Clipped Energy

In this analysis, a normalized PV power generation profile for one day is modeled as a bell-shape curve that can be expressed by the normal distribution with

$$P_{\mathrm{pv}} = P_{\max} \cdot e^{-\frac{(t-t_0)^2}{2\sigma^2}} = \boldsymbol{ILR} \cdot e^{-\frac{(t-t_0)^2}{2\sigma^2}} \tag{10.5}$$

$$E_{\mathrm{pv}} = \int_{t_{\mathrm{dawn}}}^{t_{\mathrm{dusk}}} P_{\mathrm{pv}} \cdot dt \approx \boldsymbol{ILR} \cdot \sqrt{2\pi} \cdot \sigma \tag{10.6}$$

where, P_{pv} is the normalized generated power by solar panels, *ILR* represents normalized maximum PV power over one day, α is the standard deviation of the normal distribution function, and t0 is the instant when PV power reaches its maximum value (noontime in the equator). Both α and t0 are geographically dependent and were defined as α = 2 and t0 = 12 for the case study. E_{pv} represents the total generated energy by the PV panel over one day, assuming no clipping occurs.

For utility-scale SPS farms, the PV arrays are usually oversized by ILR > 1.0 to maximize the value proposition of the system. Consequently, PV power clipping by the inverter would occur during noontime. As shown in Figure 38, the clipped energy E_{clip} is equal to the enclosed area by PV generation profile and PV inverter power, which can be calculated by

$$E_{\text{clip}} = E_{\text{pv}} \cdot \alpha_{\text{clip}} \tag{10.7}$$

where $E_{pv} = E_{clip} + E_{dc}$. Table 14 summarizes the normalized clipped energy of oversized PV arrays, α_{clip}, at different ILRs.

Constrained by the inverter power, only E_{dc} can be processed by the PV inverter, and E_{clip} has to be wasted if no BESS or AC-coupled BESS (without oversized PCU) is paired with the PV arrays. But E_{clip} can be captured by the DC-coupled BESS to increase the energy revenue of the PV plants. As a result, the ILR can be further increased to 2.0 and even higher with the DC-coupled BESS to maximize the return on investment of SPS applications.

Table 14: Normalized clipped energy of oversized PV arrays at different ILRs

ILR	α_{clip}
1.3	8.7%
1.5	15.4%
1.8	24.1%
2.0	29.3%

Delivered Energy to the Grid Considering System Losses

Figure 40 presents a power flow diagram of SPS farms, where power losses in PV arrays, DC/AC cables, PCU (PV inverters and 60 Hz transformers), and battery cells are considered. All losses except those in PV arrays and battery cells have been discussed in detail in previous subsections and can be extracted accordingly.

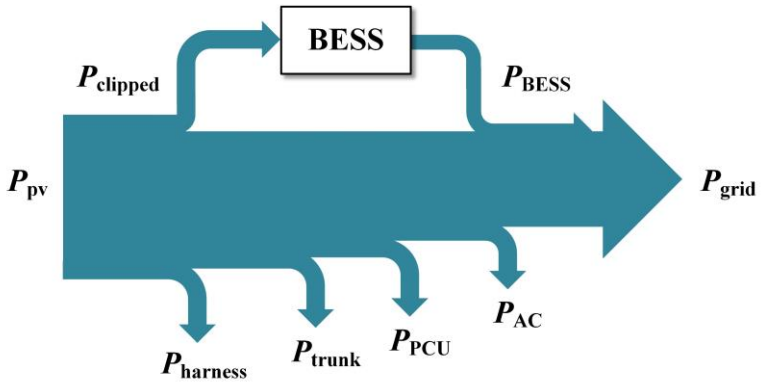

Figure 40: Power flow diagram of SPS farms from PV arrays to the Grid.

DC cable losses, including those in harness, trunk, and DC feeder cables, can be calculated by

$$P_{\text{DC,cable}} = P_{\text{harness}} + P_{\text{trunk}} + P_{\text{feeder}}$$

PCU losses contain those in PV inverters and 60 Hz transformers and can be derived with

$$P_{\text{PCU}} = P_{\text{conv}} + P_{\text{xfmr}}$$

With oversized PV arrays by ILR, the clipped power, P_{clip}, can be recycled by the paired BESS, which is otherwise wasted without added storage. As a result, extra power PBESS is delivered to the grid by the SPS farm with

$$P_{\text{BESS}} = P_{\text{clip}} \cdot \eta_{\text{BESS,RT}} \cdot \eta_{\text{cell}}$$

where $\eta_{BESS,RT}$ is the round-trip efficiency of BESS, and η_{cell} the energy efficiency of battery cells.

Based on the power flow diagram, the delivered power to the grid can be calculated by subtracting all system loss items from the PV power with

$$P_{\text{grid}} = P_{\text{pv}} - P_{\text{array}} - P_{\text{clip}} - P_{\text{DC,cable}} - P_{\text{PCU}} - P_{\text{AC,cable}} + P_{\text{BESS}}.$$

As a result, the delivered energy to the grid can be calculated by

$$E_{\text{grid,daily}} = \int_{0\ \text{h}}^{24\ \text{h}} P_{\text{grid}}$$

$$E_{\text{grid,annual}} = E_{\text{grid,daily}} \cdot 365\ \text{day/year}$$

$$E_{\text{grid,lifetime}} = E_{\text{grid,annual}} \cdot \frac{1-(1-\alpha_{\text{degrad}})^{t}}{1-(1-\alpha_{\text{degrad}})}$$

where α_{degrad} is the annual degradation rate of PV panels [15, 16], and t is the project lifetime of utility-scale PV that mostly ranges between 25 to 35 years [17]. In this analysis, t = 30 was taken to calculate the total energy production over a 30-year project lifetime. A coefficient of 20 MW needs to be considered to obtain the actual energy yield in MWh.

Comparison of System-Level LCOE of 20 MW SPS Farms based on Four Approaches

With the details discussed above, the first cost or capital expenditures (CAPEX) can be derived by summing up the cost of all components of the research interest. The total energy yield over the 30-year project lifetime, $E_{grid,lifetime}$, can be calculated as well. Hence, the system-level LCOE ($/MWh) of the selected 20 MW/80 MWh SPS farms based on CI and SI can be estimated by

$$LCOE = \frac{CAPEX}{E_{\text{grid}}}.$$

Without loss of generality, the operational expenses and all financial factors, including tax rate and incentives, inflation rate, and depreciation, are neglected for simplicity.

Figure 41 compares the CAPEX and system losses of 20 MW SPS farms based on the traditional central inverter, centralized string inverters, the proposed MVSI, and MDCT at ILR = 1.5. Both AC- and DC-coupled BESS have been considered for state-of-the-art central and string inverters. Details are listed in the tables in Appendix.

Taking the up-to-date central inverters with AC-coupled BESS as the benchmark, the proposed 4 kV TMVSI and 34 kV MDCT approaches reduce both CAPEX and system losses, leading to decreased system-level LCOE of the 20 MW/80 MWh SPS farms by 18% and 21%, respectively. However, the 13 kV TMVSI increases the cost significantly due to

the expensive HV RB devices despite lower system losses than its 4 kV counterpart and 34 kV MDCT, resulting in a 6% higher system-level LCOE than the base case.

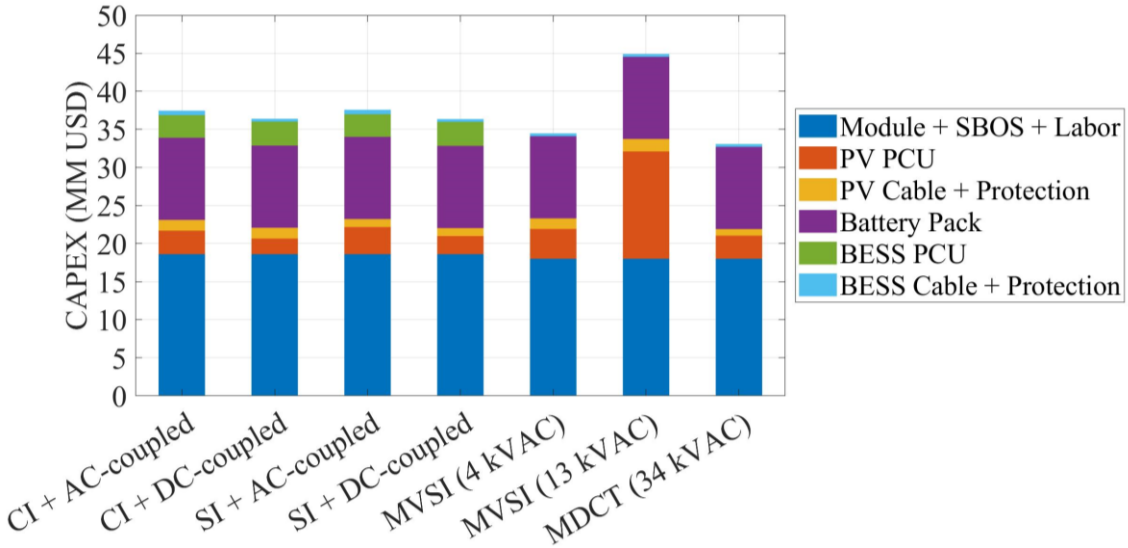

(a)

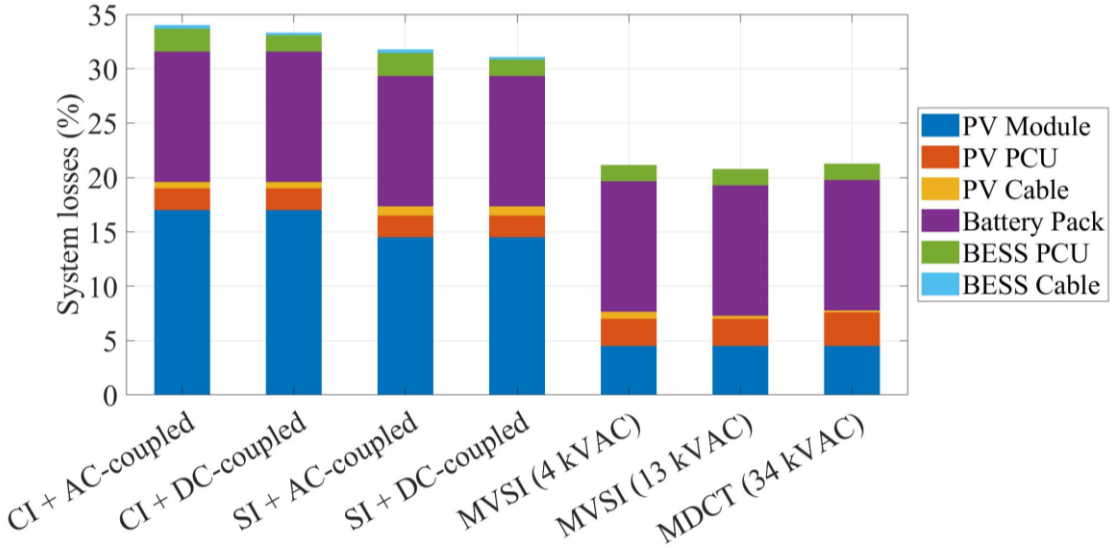

(b)

Figure 41: Comparison of (a) CAPEX and (b) system losses of 20 MW SPS farms with different PCS architectures at ILR = 1.5.

Subtask 10.2: This task is completed. To study the reliability impact on the financial analysis, the sensitivity of the system-level LCOE to different ILRs and the MVSI and MDCT inverter cost has been performed. The results suggest that the proposed 4 kV MVSI and 34 kV MDCT show a consistent LCOE reduction of 17% ~ 23% across the ILR from 1.3 to 2.0 when compared with the benchmark case (central inverter with AC-coupled BESS). In addition, a 10% increase in MVSI and MDCT inverter cost only shrinks the LCOE reductions by approximately 1%, which has a negligibly negative impact on their significant reductions in system LCOE compared to the base case.

By keeping the same grid connection capacity of 20 MW and battery storage capacity of 80 MWh, the system-level LCOE at a higher ILR can be obtained. Table 15 lists and compares

the CAPEX, delivered energy to the grid, and the system-level LCOE of the 20 MW/80 MWh SPS farms with various PCS architectures at ILR from 1.3 to 2.0.

The results in Table 15 are also plotted in Figure 42. Figure 42(a) shows the energy production over the project lifetime of 30 years and the CAPEX across ILR from 1.3 to 2.0. With an increased ILR, both CAPEX and total energy yield grow in all four approaches. Compared to those with the DC-coupled BESS, the CI and SI with AC-coupled BESS tend to saturate in their energy production, which is caused by oversized PV and BESS PCUs and a relatively lower round-trip efficiency of BESS. In this figure, the data points closer to the upper left corner suggest lower system-level LCOE. Therefore, in contrast to the CI- and SI-based architectures, the 4 kV MVSI and 34 kV MDCT indicate a reduced system-level LCOE.

Figure 42(b) demonstrates the sensitivity of system-level LCOE of various PCS architectures to the ILR from 1.3 to 2.0. Compared to the base case (the CI with AC-coupled BESS), the 4 kV MVSI reduces the LCOE by 17% − 20% over the ILR range. The LCOE reduction in the 34 kV MDCT expands to > 20%, primarily driven by the cost-effective 34 kV PCU design. The LCOE advantages of 4 kV TMVSI and 34 kV MDCT approaches are not sensitive to their inverter costs. A 10% increase in the inverter cost only shrinks their system LCOE benefits by approximately 1%, which has a little negative impact on their significant reductions in system LCOE compared to the up-to-date approaches.

Table 15: LCOE comparison of 20 MW SPS farms with four different PCS architectures across ILR from 1.3 to 2.0.

ILR		CI (AC BESS)	CI (DC BESS)	SI (AC BESS)	SI (DC BESS)	TMVSI (4 kVAC)	TMVSI (13 kVAC)	MDCT (34 kVAC)
1.3	CAPEX (M$)	33.91	33.27	34.01	33.27	31.85	42.24	30.51
	E_{grid} (MWh/day)	105.22	105.36	107.83	107.99	119.15	119.59	119.01
	LCOE ($/MWh)	**31.62**	**30.98**	**30.95**	**30.23**	**26.23**	**34.65**	**25.15**
1.5	CAPEX (M$)	37.46	36.40	37.57	36.35	34.47	44.90	33.07
	E_{grid} (MWh/day)	121.49	121.77	124.25	124.58	136.50	137.00	136.33
	LCOE ($/MWh)	**30.25**	**29.32**	**29.67**	**28.63**	**24.78**	**32.16**	**23.80**
1.8	CAPEX (M$)	42.77	41.09	42.91	40.97	38.41	48.90	36.92
	E_{grid} (MWh/day)	145.91	146.44	148.84	149.46	162.26	162.86	162.07
	LCOE ($/MWh)	**28.76**	**27.53**	**28.29**	**26.90**	**23.22**	**29.46**	**22.35**
2.0	CAPEX (M$)	46.32	44.22	46.47	44.05	41.03	51.56	39.48
	E_{grid} (MWh/day)	162.20	162.92	165.21	166.04	179.29	179.96	179.07
	LCOE ($/MWh)	**28.02**	**26.63**	**27.60**	**26.03**	**22.45**	**28.11**	**21.63**

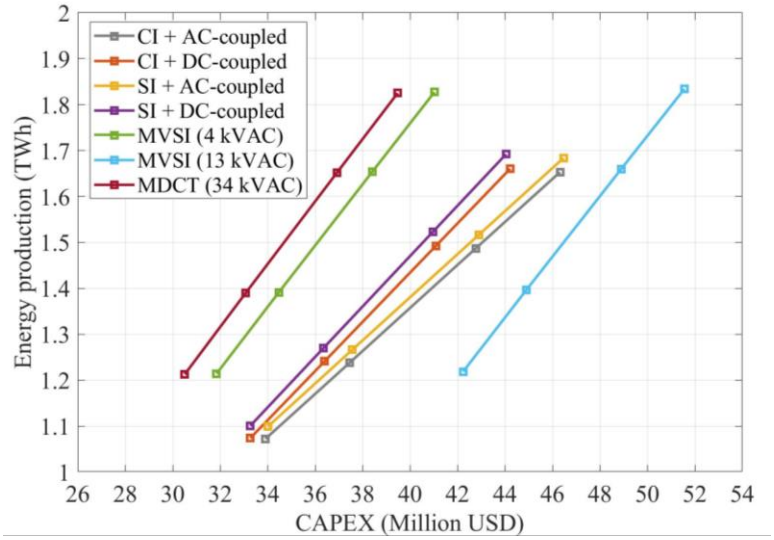

(a)

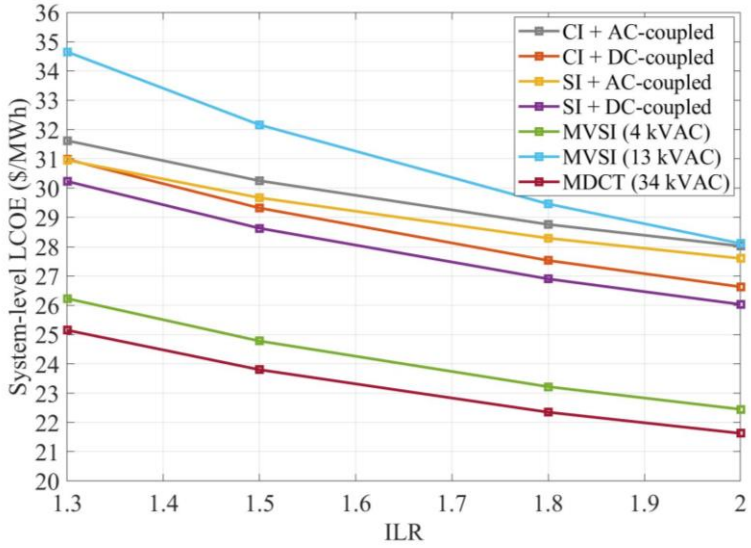

(b)

Figure 42: Sensitivity analysis of system-level LCOE to different ILR of 20 MW SPS farms with various PCS architectures.

On the other hand, despite delivering the second most energy, the 13 kV MVSI ends up with the highest LCOE among these approaches, which is dictated by the extremely expensive 3.3 kV SiC RB devices. But at ILR = 2.0, the 13 kV MVSI almost reaches the parity of the base case. As HV SiC device costs decrease in the next few years, the cost of the 13 kV MVSI is expected to drop tremendously, leading to superior LCOE over its 4 kV counterpart and at least comparable, if not better, performance compared to the 34 kV MDCT. Furthermore, the 34 kV MVSI can be developed without increased system complexity once 6.5 kV SiC RB devices are economically available. By then, the 34 kV MVSI would feature further reduced LCOE and system footprint in contrast to the 34 kV MDCT.

Please note in the comparison 1.5 kV PV strings are equipped with the CI and SI approaches, while 1 kV PV strings are connected to the MVSI and MDCT due to the limitation of standard 1.7 kV semiconductor devices. Thus, with appropriately sized

switches, the MVSI and MDCT approaches are able to interconnect 1.5 kV PV strings, triggering an extended reduction in system-level LCOE.

In short, the MVSI, which is currently viable at 4 kV AC output, has been validated to reduce the LCOE by almost 20% compared to the base case. Its 13 kV and 34 kV MVSI versions have great potential for further reduced LCOE and system footprint once the HV RB SiC devices become commercially available, featuring competitive long-term solutions. Presenting a > 20% reduction in the LCOE, the 34 kV MDCT presents an attractive MVAC PCS architecture that can be commercialized in the short term.

Task 11: MVSI Bronze prototype build and test: The proposed S4T MVSI demonstration at 300 kVA.

- Subtask 11.1: Build three S4T modules based on the bronze design at 3-phase, 1 kVac, 75 kVA
- Subtask 11.2: Test at 3-phase, 1 kVac, 75 kVA
- Subtask 11.3: Build and assemble 3-phase, 2 kVac, 150 kVA MVSI as per final golden design
- Subtask 11.4: Test 3-phase 150 kVA MVSI at 2 kVac, 150 kVA MVSI to demonstrate series stacking.
- Subtask 11.5: MVSI functional testing at 200 kVA

Results and Discussion:

Subtask 11.1: Four 25 kVA S4T modules based on bronze design were built with a custom-design medium-voltage medium-frequency transformer, 1.7 kV RB switch modules, gate drivers, and isolated gate driver power supply.

Figure 43 shows the picture of the built 25 kVA S4T module prototype. It features a dimension of 36 inches depth * 15 inches width * 7 inches height.

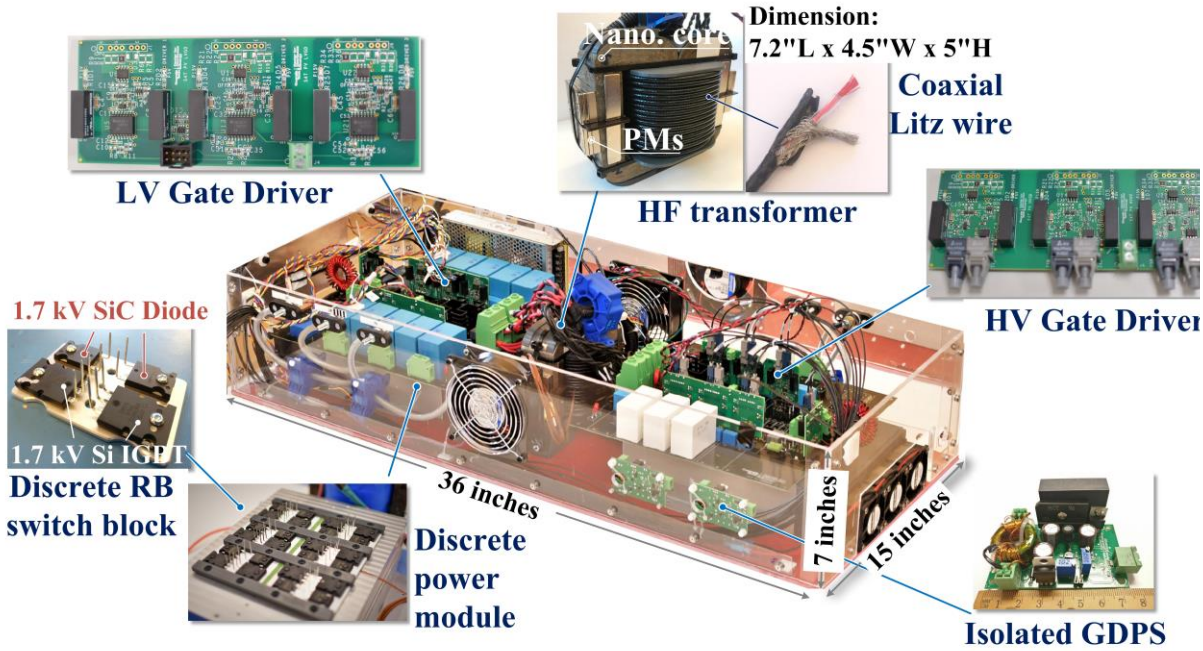

Figure 43: Prototype picture of 25 kVA S4T module for the prosed 300 kVA MVSI.

Subtask 11.2: This task is partially completed. Three 25 kVA S4T modules have been tested at 20 kVA individually. Three-phase testing at 20 kW/300 Vac has been completed.

Figure 44 presents the 100 kVA/2.4 kVac test setup with four built 25 kVA S4T modules series stacked in one phase. For functional demonstration, the PV source is emulated by a cascaded variac and rectifier, and a decoupling capacitor bank is used instead of a battery. The capacitance value was calculated by

$$C_{\text{decouple}} = \frac{P_{\text{rated}}}{2\pi f_{\text{line}} \cdot V_{\text{bat}} \cdot \Delta V}.$$

where the voltage ripple ΔV = 100 V. On the MVAC side, a resistor load bank is connected to the converters, which is controlled in an open-loop for demonstration purposes.

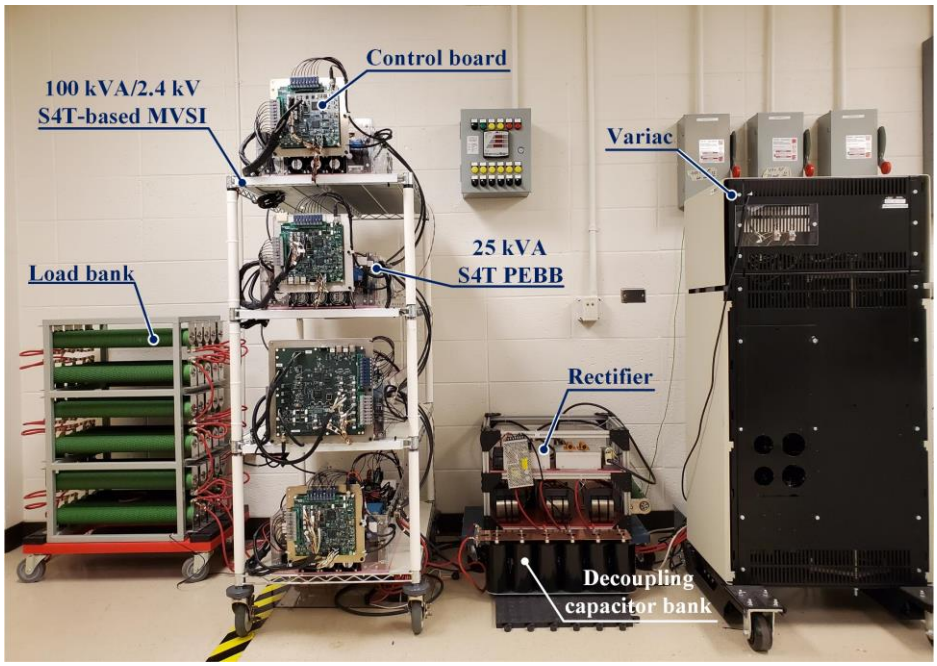

Figure 44: Test setup for the proposed TCSSS-MVSI.

Figure 45 presents the experimental results of a single PEBB at 20 kW steady-state condition, where a low total harmonics distortion (THD) of < 3% on AC current was achieved. In addition, a controlled low dv/dt < 1 kV/μs was achieved at different operating points, demonstrating its friendly feature to EMI design.

The independent control of the PV, battery, and grid ports is another attractive feature of the proposed MVSI, and its experimental validation at 10 kW is presented in Figure 46. Four different power flows scenarios, i.e., PV to load, PV to capacitor bank and load, PV and capacitor bank to load, and capacitor bank to load, are presented with power ramps and 100% step load changes. In this preliminary single-phase AC test, the decoupling capacitor bank always compensates for the pulsating reactive power at 120 Hz. Moreover, the dc-link magnetizing current, I_m, was adjusted dynamically in different load conditions to reduce conduction loss and improve converter efficiency.

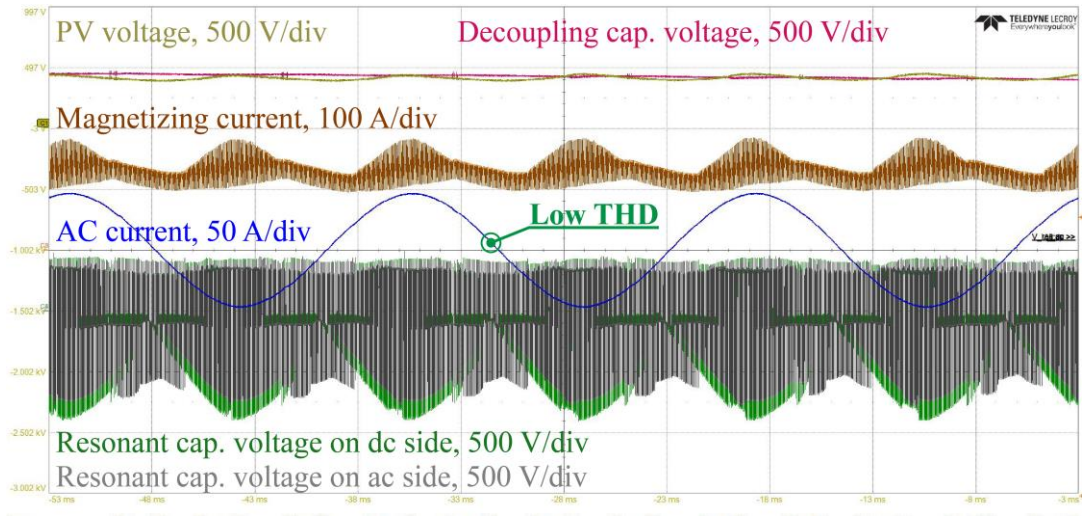

(a)

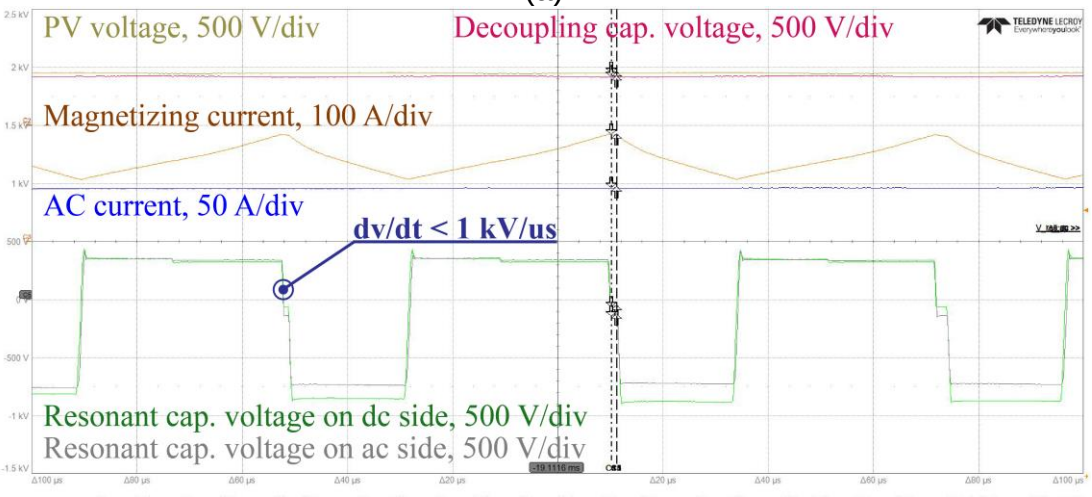

(b)

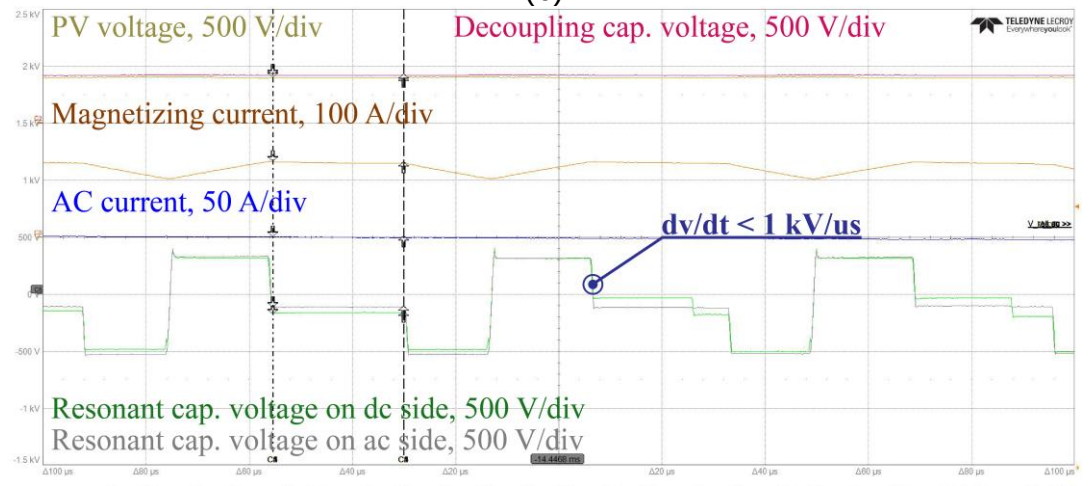

(c)

Figure 45: Experimental results of single 25 kVA PEBB at 20 kW. (a) Steady- state results at 20 kW. (b) and (c) Zoom-in views at AC peak and AC zero crossing, respectively.

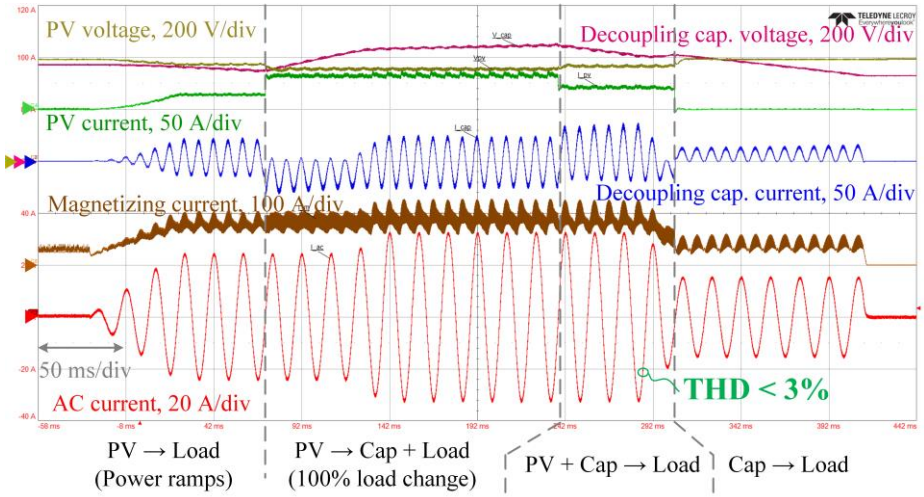

Figure 46: Experimental results of single TMVSI PEBB under dynamic operation at 10 kW. Independent power control of PV, capacitor bank, and AC load was achieved, enabling improved energy dispatchability of PV.

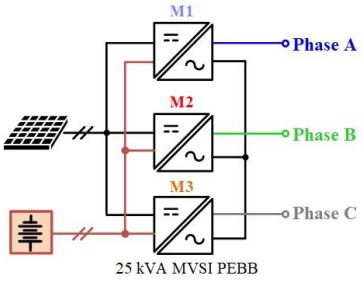

(a)

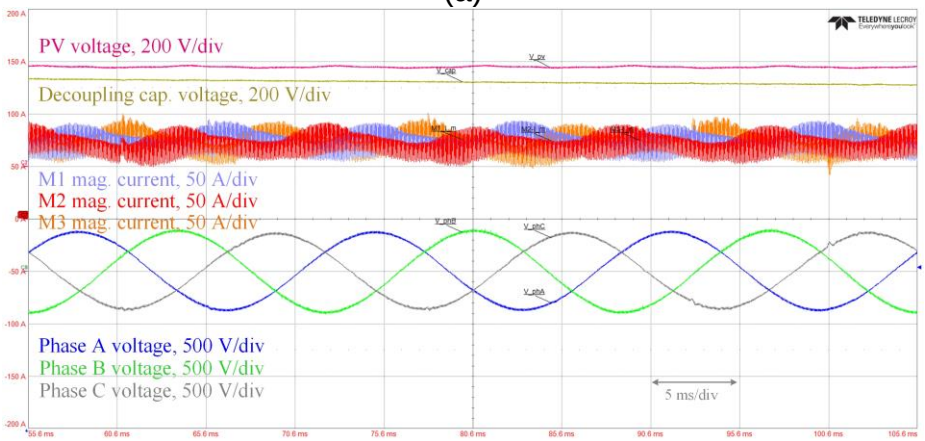

(b)

Figure 47: Experimental results of three-phase operation at 20 kW/300 Vac. The AC outputs of three TMVSI PEBBs were shifted by 120 degrees. A balanced three-phase output with THD < 3% was achieved.

After completing power testing at 20 kW individually, three S4T modules are connected in a three-phase configuration with a wye-connected resistive load to demonstrate three-phase operation, as shown in Figure 46(a). The AC outputs of the three modules were shifted by 120 degrees.

Figure 47(b) exhibits the experimental results of a three-phase operation at 20 kW/300 kVac. A balanced three-phase output with THD < 3% was achieved.

Subtask 11.3: 20 kW test with two S4T stacked in one phase was tested. Testing with three modules stacked at 600 V low power was completed. The preliminary results validate the efficacy of the proposed daisy-chained communication algorithm for the whole 300 kVA MVSI in hardware with all latency considered, addressing the biggest challenge to the system testing at full power.

Figure 48 presents the experimental results under steady-state at 20 kW and dynamic conditions at 16 kW. Similar to the single module case, a low THD < 3% on the individual

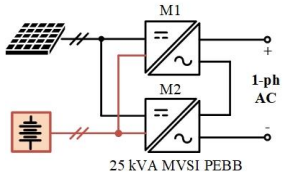

(a)

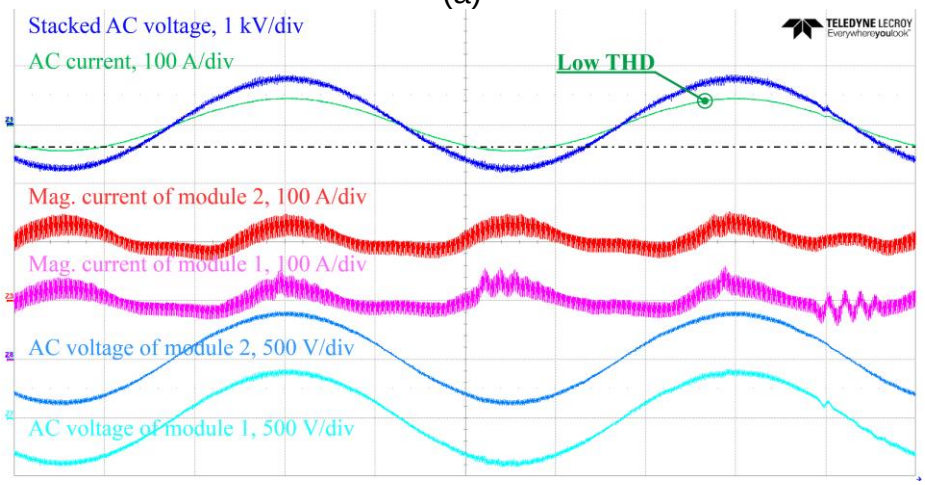

(b)

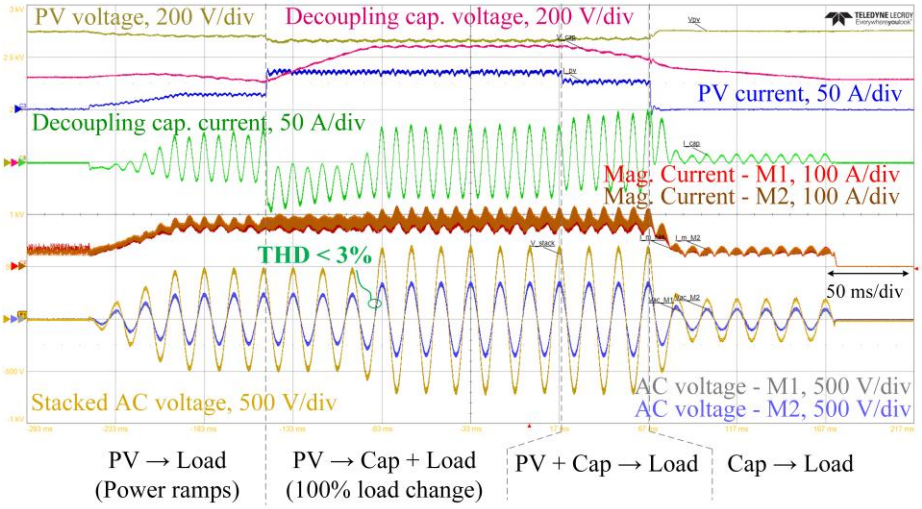

(c)

Figure 48: Experimental results of two modules in stack in one phase. (a) Test setup. (b) Steady-state results at 20 kW/600 Vac. (c) Dynamic conditions at 16 kW.

and stacked AC voltages and a low controlled dv/dt < 1 kV/µs were achieved in both modules. Furthermore, voltage balancing between two modules was always guaranteed under all dynamic conditions.

In a further step, experiments with three stacked modules were conducted, where the second controller (slave #1) was completely floating in the communication loop and relaying signals from the first controller (master) to the third one (slave #2). As presented in Figure 49, three S4T modules stacked in one phase were well synchronized with negligible phase shift during both power ramps and steady-state operation, validating the efficacy of the communication algorithm and assuring its extension to fully operational 300 kVA MVSI.

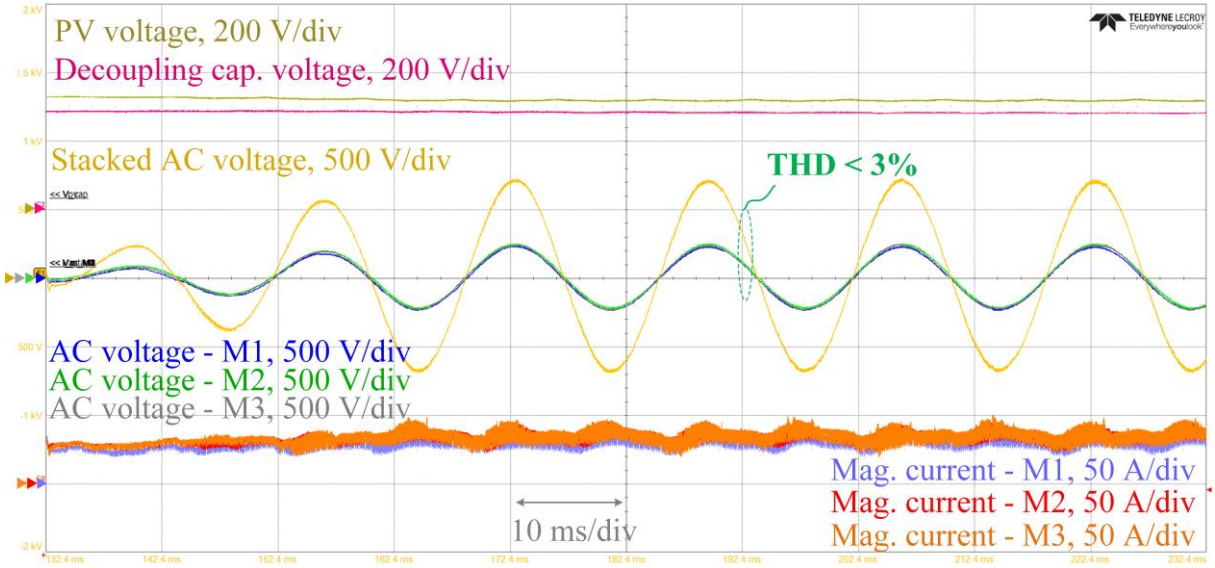

Figure 49: Experimental results of three TMVSI PEBBs in stacks under power ramps at 6 kW.

Subtask 11.4 – 11.5: By agreement between the DOE and the CDE, these two subtasks were demonstrated with 300 kVA MDCT in Budget Period 3 instead.

Task 12: Explore Regulatory Issues: It is necessary to identify the market opportunities, distribution channels, and any potential barriers to the commercialization of the proposed architecture.

Approach:

- Subtask 12.1: Explore different regulatory models to increase Utility participation in solar PV farms.
- Subtask 12.2: Commercial analysis of services and business models supported by an MVSI approach.

Results and Discussion:

Subtask 12.1: This task is completed. See Task 6 for details.

Subtask 12.2: This task is completed. See Task 6 for details.

c. Budget Period 3

Task 13: MDCT Build and Test: The proposed S4T MDCT operation demonstration at 300 kVA.

Approach:

Subtask 13.1: (M25-M27) Build of MDCT at 13 kV, 300 kVA

Subtask 13.2.1: (M27-M29) MDCT functional testing at 300 kVA

Subtask 13.2.2: (M29-M30) MDCT system impact testing at 300 kVA

Results and Discussion:

Subtask 13.1: Four 75 kVA MDCT trays were completed (built, wired, tested for signal integrity, and power tested). In addition, the rack for 300 kVA MDCT trays was built and equipped with external busbars/cables to interface the MDCT with external sources/loads.

Figure 50 shows the prototype pictures of completely assembled 75 kVA MDCT trays. All electrical and mechanical components, including semiconductor modules, gate drivers, high-frequency transformers, cold plates for cooling, controller, wirings, busbars, etc., were assembled in the tray. The enclosure is made of anodized aluminum. The key electrical component, including semiconductor modules, gate drivers, and high-frequency transformers, were characterized separately before assembly.

Figure 50: Prototype pictures of the fully assembled 75 kVA MDCT tray.

Figure 51 shows the assembly progress of two of the MDCT trays before their completion. Power modules, gate drivers, high-frequency transformers, and cooling plates were housed in the trays.

Figure 51: Assemble progress of two MDCT trays.

Subtask 13.2.1: 23 kW experimental results were obtained in one 75 kVA tray, where the DC-link current was regulated at 80 A. The zoom-in view of the switching cycle presents a controlled low dv/dt across DC-link voltage.

Figure 52 shows the test setup with the built 75 kVA MDCT tray under test. Two Magna DC power supplies were used for DC power inputs. Moreover, a resistive load bank, located on the other side of the testbench, was connected to the AC output side for functional testing. Figure 53(a) presents results under steady-state operation at 23 kW. The DC-link current was regulated at 80 A. Figure 53(b) shows the zoom-in view of the switching cycle at 9 kW, where a controlled low dv/dt was observed.

The team has power-tested all four trays at reduced power using the testbed shown in Figure 52. In addition, all trays were tested in interleaving operation.

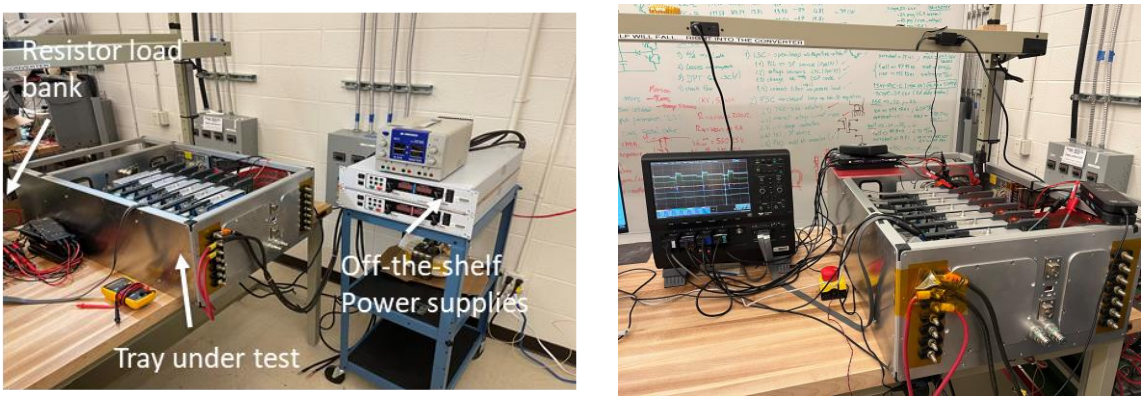

(a) (b)

Figure 52: (a) Test setup and (b) MDCT tray under test.

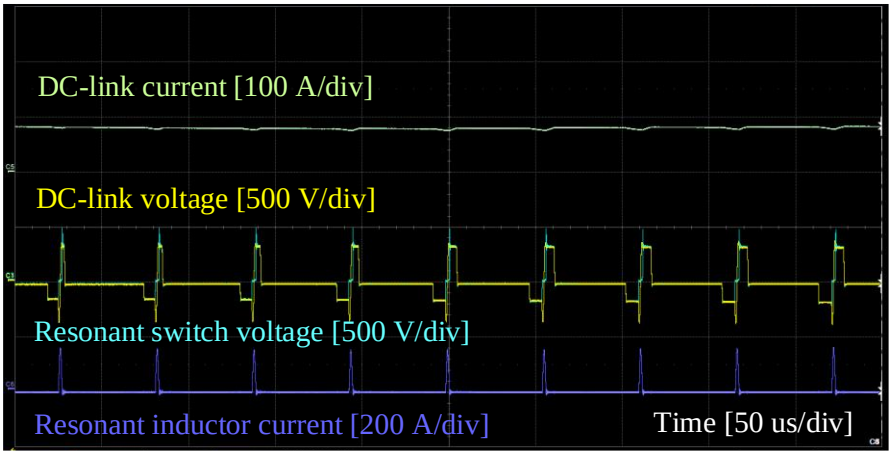

(a)

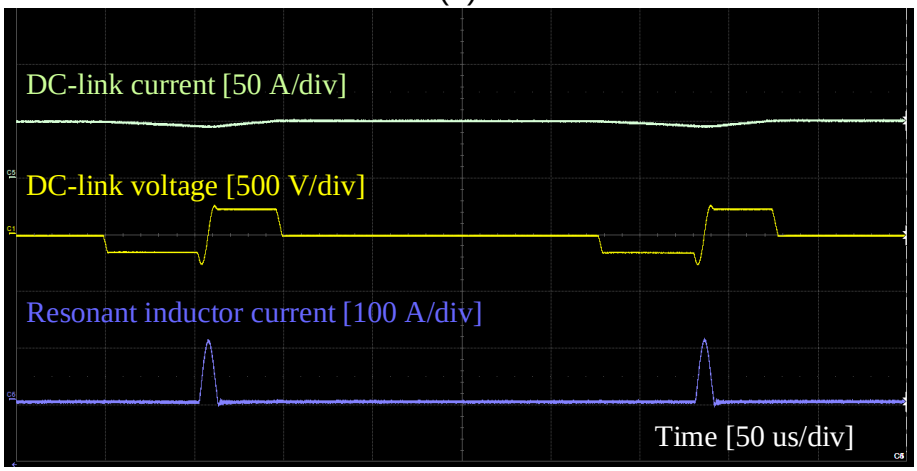

(b)

Figure 53: Preliminary experimental results with one 75 kVA MDCT tray. (a) Steady-state operation at 23 kW, 400 V DC input, 200 V DC output, Im=80 A. (b) Zoom-in view of switching cycle at 9 kW, 300 V DC input, 150 V DC output, Im=50 A

Subtask 13.2.2: The functional testing of the MDCT was performed using the experimental set-up depicted in Figure 54. Herein, the MDCT is interfacing three ports (i) a dc 750-Vdc battery emulator, (ii) a resistive load, and (iii) the ac grid.

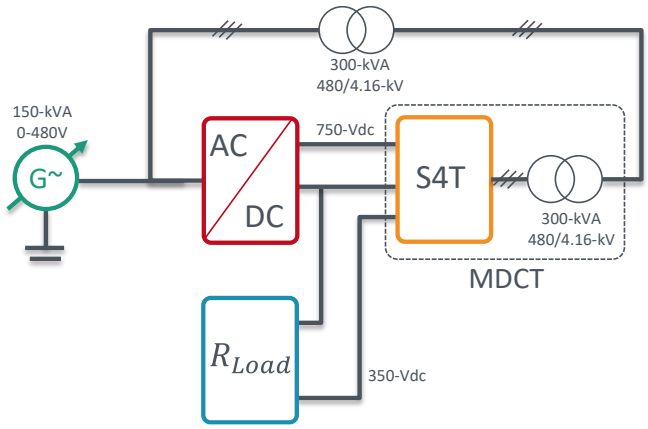

Figure 54: MDCT experimental test setup.

Following the targeted objectives for Milestone 13.2, four 75 kVA MDCT trays were tested for signal integrity, sensors, gate drivers, and thermal management. Each tray was then operated individually for up to 50% of its rated power. Figure 55 shows the four fully operational trays built throughout this project, as well as two of the trays mounted in the rack for testing using the experimental setup displayed in Figure 55. More specifically, Figure 55(a) shows the rack with the wiring, cooling, and load-sources in place.

(a) (b)

Figure 55: MDCT testing. (a) Two 75 kVA MDCT trays operating in parallel. (b) Four MDCT trays built complete.

Utilizing the test setup in Figures 54 and 55, the interleaved operation of the converters in each MDCT tray was demonstrated. In addition, the parallel operation of two trays was achieved. All configurations were tested for continuous operation at several power levels.

Figure 56: MDCT testing — two 75 kVA MDCT trays operating in parallel.

Lastly, Figures 56 and 57 depict the oscilloscope screen captures of the waveforms generated through the experimental validation of the MDCT. In detail, Figure 56 shows the switching waveforms of the MDCT trays while operating as a tri-port converter, wherein all the soft-switching transitions of the port can be confirmed. Similarly, Figure 57 displays the steady-state voltage and current waveforms of each port, once again confirming the sound operation of the converters (notice that the mild distortion on the ac waveforms is a consequence of the power quality of the local ac grid connection).

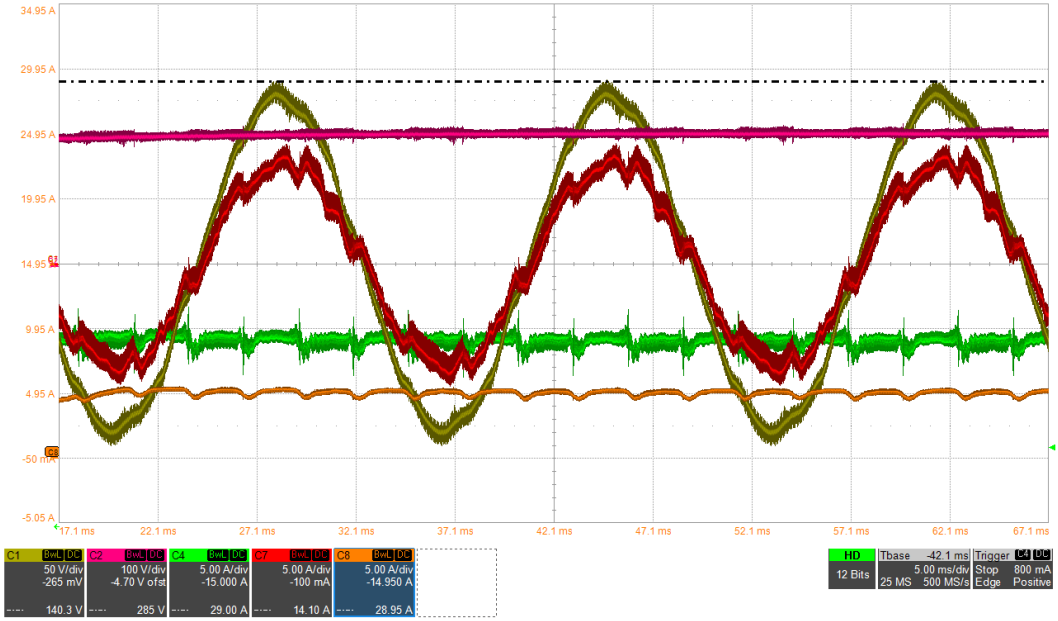

Figure 57: MDCT testing — two MDCT trays operating in parallel. Waveform legend: Yellow (Grid voltage, phase-a); Red (line-current, phase-a), Pink (PV voltage); Green (PV current); Orange (Battery current).

Task 14: Commercial Impact Study: It is necessary to identify the market opportunities, distribution channels, and any potential barriers to the commercialization of the proposed architecture.

Approach:

- Subtask 14.1: (M25-M30) Commercial impact study

Results and Discussion:

The MDCT technology has been licensed to GridBlock for its commercialization. Throughout this task, the team at Georgia Tech guided the GridBlock team through the MDCT tech-transfer process, which concluded with GridBlock completing its first multi-port converter whose design mirrors one of the MDCT trays; thus demonstrating the successful tech-transfer between the two organizations.

5. Significant Accomplishments and Conclusions

- Project explored the use of MV AC distribution architecture for hybrid PV + storage utility-scale PV farms.
- Detailed loss and LCOE analysis for AC and DC side BESS architecture, including multiple converter topologies, as well as for proposed MVSI/MDCT systems.
- MVSI was built and holds promise but needs lower-cost high-voltage SiC devices, which does not seem possible in the near term.
- MDCT provides a simpler modular building block – validated through HIL and farm-level modeling, simulation, and experimental validation.
- 300 kVA MDCT prototype built and under test. Technology is being commercialized.
- Regulatory model of utilities building PV plants, where PV panels are treated as DC generation (IPP), seems viable and can allow improved grid integration.

6. Path Forward

The core technology behind the MVSI and MDCT, i.e., the soft-switching-solid-state-transformer (S4T), has been licensed by GridBlock from the Georgia Tech Research Corporation (GTRC). This technology was conceived and developed at the Center for Distributed Energy at Georgia Tech.

As part of the ENDEAVOUR portfolio, GridBlock is taking the S4T technology to market as the industry's first plug-and-play energy router. The work conducted throughout this award was of pivotal importance in understanding and de-risking the S4T technology before it made its way to the market.

7. Products

Journal Articles:

1. Z. An, X. Han, V. R. Chowdhury, J. Benzaquen, R. P. Kandula, and D. Divan, "A Tri-Port Current-Source Soft-Switching Medium-Voltage String Inverter for Large-Scale Solar-Plus-Storage Farms," in *IEEE Transactions on Power Electronics*, vol. 37, no. 11, pp. 13808-13823, Nov. 2022
2. Z. An *et al.*, "Laminated Permanent Magnets Enable Compact Magnetic Components in Current-Source Converters," in *IEEE Transactions on Power Electronics*, vol. 37, no. 10, pp. 12391-12405, Oct. 2022.

Awards:

Zheng An received Technical Session Best Presentation Awards at IEEE APEC 2022 in Houston, TX, March 20-24, 2022. The paper titled “Farm-Level Interactions Study of a Novel Tri-Port Soft-Switching Medium-Voltage String Inverter (MVSI) Based Large-Scale PV-Plus-Storage Farms” presents improved energy dispatchability and grid-support services of the grid-connected MVSI to proliferate dispatchable and low-cost solar energy.

Conference Publications & Presentations

1. Z. An, X. Han, L. Zheng, K. Kandasamy, R. Prasad Kandula, and D. Divan, "Modular Isolated Soft-Switching Medium Voltage String Inverter for Large-Scale PV Farm," *2020 IEEE Applied Power Electronics Conference and Exposition (APEC)*, New Orleans, LA, USA, 2020, pp. 1067-1073.

2. Z. An, R. P. Kandula and D. Divan, "Feed-Forward Compensation for Model Predictive Control in Tri-port Current-Source Medium-Voltage String Inverters for PV-Plus-Storage Farms," *2021 IEEE Energy Conversion Congress and Exposition (ECCE)*, 2021, pp. 3430-3435.
3. Z. An, R. P. Kandula and D. Divan, "Comparative Investigation of System-Level Optimized Power Conversion System Architectures to Reduce LCOE for Large-Scale PV-Plus-Storage Farms," *2021 IEEE Energy Conversion Congress and Exposition (ECCE),* 2021, pp. 719-726.
4. X. Han, Z. An, M. J. Mauger, J. Benzaquen, R. P. Kandula, and D. Divan, "Laminated Permanent Magnets Enable Compact Magnetic Components in Current Source Converters," *2021 IEEE Energy Conversion Congress and Exposition (ECCE)*, 2021, pp. 5515-5522.
5. M. J. Mauger, V. R. Chowdhury, P. Kandula and D. Divan, "A Multiport DC Transformer to Enable Flexible Scalable DC as a Service," *2021 IEEE Energy Conversion Congress and Exposition (ECCE)*, 2021, pp. 1197-1204.
6. V. R. Chowdhury, Z. An, R. P. Kandula and D. Divan, "Farm-level Interactions Study of a Novel Tri-port Soft-switching Medium-Voltage String Inverter (MVSI) based Large-scale PV-Plus-Storage Farms," *2022 IEEE Applied Power Electronics Conference and Exposition (APEC)*, 2022, pp. 1956-1962.
7. Zheng An, Mickael Mauger, Joseph Benzaquen, Prasad Kandula, Deepak Divan, “A Fast-Response High-Accuracy Overvoltage Protection Circuit for Soft-Switching Current-Source Converters,” *2022 IEEE Energy Conversion Congress and Exposition (ECCE) (Presented on Oct. 2022).*
8. Zheng An, Rajendra Prasad Kandula, Joseph Benzaquen, and Deepak Divan, “Charge-based Droop Control Addressing Control Saturation for Low-Inertia Converters”, *2022 IEEE Energy Conversion Congress and Exposition (ECCE) (Presented on Oct. 2022).*
9. Vikram Roy Chowdhury, Zheng An, Rajendra Prasad Kandula and Deepak Divan, “Operation and control of Soft Switching Solid State Transformer as a Virtual Synchronous Machine for Photovoltaic application”, *2022 IEEE Energy Conversion Congress and Exposition (ECCE) (Presented on Oct. 2022).*

8. Project Team and Roles

This award was led by Prof. Deepak Divan (PI), Director of the Center for Distributed Energy at Georgia Tech, in collaboration with the following participants/collaborators:

Students and Others Trained/Supported/Supervised/Graduated (including DOE National Lab awards when applicable)

1. An Zheng, Ph.D., starting the second semester of 2018 until 05/31/2022.
2. Nishant Bilakanti, Ph.D., one semester in 2019
3. Sanaz Paran, Postdoc, one semester in 2019.
4. Karthik Kandasamy, Postdoc two semesters 2018.

5. Joseph Benzaquen, Research Faculty, one month 2022.

Participants & Collaborators:

First Solar (Mahesh Morjaria, Kevin Collins, Divyesh Mehta), ORNL (Sonny Xue), Southern Company (Andrew Ingram, Will Hobbs), EPRI (Devin VanZandt), Paul Centolella.

9. References

[1] H. Chen and D. Divan, “Soft-Switching Solid-State Transformer (S4T),” *IEEE Transactions on Power Electronics*, vol. 33, no. 4, pp. 2933–2947, 2018.

[2] L. Zheng, K. Kandasamy, R. P. Kandula, and D. Divan, “Impact of Transformer Leakage Inductance on the Soft-Switching Solid-State Transformer,” *2018 IEEE Energy Convers. Congr. Expo. ECCE 2018*, pp. 1125–1132, 2018.

[3] IEEE Standard Association, *IEEE Std. 1547-2018. Standard for Interconnection and Interoperability of Distributed Energy Resources with Associated Electric Power Systems Interfaces*. 2018.

[4] A. P. Dobos, “Pvwatts version 5 manual,” National Renewable Energy Lab. (NREL), Golden, CO (United States), Tech. Rep., 2014.

[5] Aurora Solar. “Understanding PV System Losses, Part 3: Soiling, Snow, System Degradation.” (2021).

[6] Aurora Solar. “Understanding PV System Losses, Part 1: Nameplate, Mismatch, and LID Losses.” (2021).

[7] P. Gilman, N. A. DiOrio, J. M. Freeman, S. Janzou, A. Dobos, and D. Ryberg, “Sam photovoltaic model technical reference 2016 update,” National Renewable Energy Lab. (NREL), Golden, CO (United States), Tech. Rep., 2018.

[8] S. MacAlpine and C. Deline, “Modeling microinverters and dc power optimizers in PV watts,” National Renewable Energy Lab. (NREL), Golden, CO (United States), Tech. Rep., 2015.

[9] SolarEdge. “Unique Inverter Technology Mitigates Energy Losses for 10kW Canadian Rooftop.” (accessed in April 2022).

[10] M. Bolinger, et al., “Utility-scale solar, 2021 edition: Empirical trends in deployment, technology, cost, performance, PPA pricing, and value in the united states,” Lawrence Berkeley National Lab. (LBNL), Berkeley, CA (United States), Tech. Rep., 2021.

[11] BloombergNEF, “How PV-Plus-Storage Will Compete With Gas Generation in the U.S,” Tech. Rep., 2020.

[12] J. Xiao et al., “Understanding and applying coulombic efficiency in lithium metal batteries,” Nature Energy, vol. 5, no. 8, pp. 561–568, 2020.

[13] Battery University. “BU-808c: Coulombic and Energy Efficiency with the Battery.” (2021).

[14] INSIDEEVs. “Lucid Air DC Fast Charge Follow Up: Charging Losses Explained.” (2021).

[15] J. S. Stein, C. Robinson, B. King, C. Deline, S. Rummel, and B. Sekulic, “PV lifetime project: Measuring PV module performance degradation: 2018 indoor flash testing results,” in 2018 IEEE 7th World Conference on Photovoltaic Energy Conversion (WCPEC), IEEE, 2018, pp. 0771–0777.

[16] D. C. Jordan and S. R. Kurtz, “Photovoltaic degradation rates—an analytical review,” Progress in photovoltaics: Research and Applications, vol. 21, no. 1, pp. 12–29, 2013.

[17] R. H. Wiser, M. Bolinger, and J. Seel, “Benchmarking utility-scale PV operational expenses and project lifetimes: Results from a survey of us solar industry professionals,” Lawrence Berkeley National Lab. (LBNL), Berkeley, CA (United States), Tech. Rep., 2020.

10. Appendix A — Additional tables

Table APP-1: System cost of 20 MW/80 MWh CI- and SI-based SPS farms at ILR = 1.5.

	CI (1.5 kVDC) + AC-coupled BESS	CI (1.5 kVDC) + DC-coupled BESS	SI (1.5 kVDC) + AC-coupled BESS	SI (1.5 kVDC) + DC-coupled BESS
Grid connection capacity (MWac)		20		
ILR		1.5		
P_dc (panels) (MW)		30		
Pdc/Pac	1	1.5	1	1.5
Total energy storage (MWh)		80		
Clipping energy (p.u.) @ ILR		15.4%		
PV inverter rating (MVA)	30.00	20.00	30.00	20.00
EBOS & main Xfmr (MVA)	30.00	20.00	30.00	20.00
DAB battery converter (MVA)	N/A	30.00	N/A	30.00
PV panel unit price ($/Wdc)		0.28		
SBOS unit price ($/Wdc)		0.20		
Labor unit price ($/Wdc)		0.14		
PV inverter unit price ($/kVA)	84.00	84.00	100.00	100.00
PV xfmr unit price ($/kVA)		19.00		
PV cable + protection (MM USD)	1.41	1.41	1.05	1.05
PV subtotal cost (MM USD)	**23.10**	**22.07**	**23.22**	**22.03**
Battery packs unit price ($/kWh)	135.00	135.00	135.00	135.00
Battery converter unit price ($/kVA)	70.00	105.00	70.00	105.00
Battery xfmr unit price ($/kVA)	29.00	N/A	29.00	N/A
BESS cable + protection (MM USD)	0.58	0.37	0.58	0.37
BESS subtotal cost (MM USD)	**14.35**	**14.32**	**14.35**	**14.32**
CAPEX (MM USD)	**37.46**	**36.40**	**37.57**	**36.35**

Table APP-2: System losses and LCOE of 20 MW/80 MWh CI- and SI-based SPS farms at ILR = 1.5.

		CI (1.5 kVDC) + AC-coupled BESS	CI (1.5 kVDC) + DC-coupled BESS	SI (1.5 kVDC) + AC-coupled BESS	SI (1.5 kVDC) + DC-coupled BESS
PV array	Degradation rate		0.5%		
	Shading loss	3.0%	3.0%	2.0%	2.0%
	Soiling loss	3.0%	3.0%	1.5%	1.5%
	Module mismatch loss	2.0%	2.0%	1.0%	1.0%
	LV energy loss		10.0%		
	Clipped energy in p.u. @ ILR		15.4%		
PV PCS	DC cables	0.48%	0.48%	0.51%	0.51%
	PV Inverter		1.50%		
	PV Xfmr		0.50%		
	AC Cables	0.10%	0.10%	0.33%	0.33%
	PV-to-grid efficiency	97.4%	97.4%	97.2%	97.2%
E_{array} with array losses (MWh/day)		**102.63**	**102.63**	**105.44**	**105.44**
Battery cell	Coulomb loss		5.0%		
	Cooling loss		2.0%		
	Balancing loss		5.0%		
BESS PCS	Battery converter		1.50%		
	BESS xfmr	0.60%	N/A	0.60%	N/A
	Cables	0.34%	0.24%	0.34%	0.24%
	BESS round-trip efficiency	92.8%	94.2%	92.5%	94.2%
E_{BESS} with battery cell losses (MWh/day)		**18.86**	**19.14**	**18.81**	**19.14**
Daily energy production (MWh/day)		**121.49**	**121.77**	**124.25**	**124.58**
Capacity factor		**25.3%**	**25.4%**	**25.9%**	**26.0%**
Annual energy production (MWh/year)		**44,343.29**	**44,447.65**	**45,352.68**	**45,472.94**
System-level LCOE ($/MWh)		**30.25**	**29.32**	**29.67**	**28.63**
LCOE improvement		Base case	-3.1%	-1.9%	-5.4%

Table APP-3: System cost of 20 MW/80 MWh MVSI- and MDCT-based SPS farms at ILR = 1.5.

	4 kVAC TMVSI (1 kV PV)	**13 kVAC TMVSI (1 kV PV)**	**34 kVAC MDCT (1 kV PV)**
Grid connection capacity (MWac)		20	
ILR		1.5	
P_dc (panels) (MW)		30	
Pdc/Pac		1.5	
Total energy storage (MWh)		80	
Clipping energy (p.u.) @ ILR		15.4%	
PV inverter rating (MVA)		20.00	
EBOS & main Xfmr (MVA)		20.00	
DAB battery converter (MVA)		N/A	
PV panel unit price ($/Wdc)		0.28	
SBOS unit price ($/Wdc)		0.20	
Labor unit price ($/Wdc)	0.12	0.12	0.12
PV inverter unit price ($/kVA)	196.00	705.00	123.00
PV xfmr unit price ($/kVA)	N/A	N/A	29.00
PV cable + protection (MM USD)	1.38	1.63	0.86
PV subtotal cost (MM USD)	**23.30**	**33.73**	**21.90**
Battery packs unit price ($/kWh)	135.00	135.00	135.00
Battery converter unit price ($/kVA)		N/A	
Battery xfmr unit price ($/kVA)		N/A	
BESS cable + protection (MM USD)	0.37	0.37	0.37
BESS subtotal cost (MM USD)	**11.17**	**11.17**	**11.17**
CAPEX (MM USD)	**34.47**	**44.90**	**33.07**

Table APP-4: System losses and LCOE of 20 MW/80 MWh MVSI- and MDCT-based SPS farms at ILR = 1.5.

		4 kVAC TMVSI (1 kV PV)	**13 kVAC TMVSI (1 kV PV)**	**34 kVAC MDCT (1 kV PV)**
PV array	Annual degradation rate		0.5%	
	Shading loss	2.0%	2.0%	2.0%
	Soiling loss	1.5%	1.5%	1.5%
	Mismatch loss	1.0%	1.0%	1.0%
	LV energy loss (p.u.)		0	
	Clipped energy (p.u.) @ ILR		15.4%	
PV PCS	DC cable loss	0.12%	0.11%	0.11%
	PV inverter loss		2.50%	
	PV xfmr loss	N/A	N/A	0.60%
	AC cable loss	0.53%	0.17%	0.06%
	PV-to-Grid Efficiency	96.9%	97.2%	96.8%
E_{pv} with array losses (MWh/day)		**117.39**	**117.83**	**117.25**
Battery cell	Coulomb loss		5.0%	
	Balancing loss	5.0%	5.0%	5.0%
	Cooling loss	2.0%	2.0%	2.0%
Battery PCS	Battery converter	1.5%	1.5%	1.5%
	Battery xfmr		N/A	
	Battery cables		0	
	BESS round-trip efficiency	94.0%	94.3%	93.9%
E_{BESS} with battery cell losses (MWh/day)		**19.10**	**19.18**	**19.08**
Daily E_{grid} (MWh/day)		**136.50**	**137.00**	**136.33**
Capacity factor		**28.4%**	**28.5%**	**28.4%**
Annual energy production (MWh/year)		**49821.18**	**50006.73**	**49761.52**
System-level LCOE ($/MWh)		**24.78**	**32.16**	**23.80**
LCOE improvement (compared to based case)		-18.1%	+6.3%	-21.3%

11. Appendix B — ORNL Report

Regulatory and Commercial Models for Increasing Utility Participation in Large Scale PV Installations and the Use of DC Transformer Technology

Paul Centolella & Associates

Introduction

This project supports development and demonstration of an integrated bidirectional AC / DC converter and multiport DC transformer and its application in utility-scale solar projects. This solid-state technology could become an integral component of utility-scale solar, reducing costs, managing integration with AC power systems, and helping accelerate the growth of utility-scale solar. Technological advances support continued growth in utility-scale solar and would create a market for the DC transformer technology. To date, public policy requirements and purchases by large corporate energy users have supported much the growth in utility-scale solar. However, when one looks the potential for utility-scale solar that is not the result policy mandates or corporate purchases, solar projects face commercial and regulatory hurdles. This paper describes these challenges and identifies options for addressing them.

Additionally, the bidirectional AC / DC converter and multiport transformer technology can be used to manage the integration of other DC power sources, including batteries, fuel cells, and microturbines. The technology also creates an opportunity for utilities to offer DC service for charging electric vehicles, data center operations, lighting and information technology in commercial buildings, and industrial applications that utilize direct current. In many this may include the development of a small DC microgrid that combines a battery uninterruptible power supply and / or distributed generation with loads using DC power. Today, the conversion from DC to AC distribution systems and from AC to DC to serve these loads typically occurs on the customer side of the utility interconnection and is inefficient and often performed in a piecemeal fashion. We will review regulatory implications and commercial opportunities for electric utilities to provide DC service.

Growth in Utility-Scale Solar

Utility-scale solar projects can be found in three-fourths of the states.[1] Projecting steady growth through the first half of this decade, Lawrence Berkeley National Laboratory's recent 2020 solar data trends report suggests U.S. solar power capacity could exceed 180 GW by 2025. A more conservative U.S. EIA Annual Energy Outlook reference case forecasts that solar photovoltaic (PV) generating capacity will increase from 35.7 GW in 2019 to 47.6 GW in 2020,
157.9 GW in 2030, and 309.3 GW, or 18% of total U.S. generating capacity, in 2050. EIA similarly projects growth in PV generation from 69.3 TWh in 2019 to 89.8 TWh in 2020, 364.1

[1] Bolinger et al. 2019.

TWh in 2030, and 605.2 TWh in 2050.[2] This remarkable growth in PV capacity and generation was projected to occur despite the then scheduled reductions in available Investment Tax Credits (ITC). In the December 2020 federal spending package, the ITC was extended for two additional years at 26%. This means that all solar projects that begin construction in 2021 or 2022 can receive a 26% tax credit. This will drop to 22% for all market segments in 2023.
Starting in 2024, utility and commercial solar will continue to be eligible for a permanent 10% credit, while the residential tax credit expires in 2024.[3]

The recent and projected growth of utility-scale PV reflects a 90% reduction in the unsubsidized levelized cost of utility-scale PV from 2009 to 2020 [4] and the likelihood of further cost reductions. The installed cost of the lowest-priced projects in 2018 already matched the U.S. Department of Energy's 2020 $1/W SunShot target.[5] Additional cost reductions of as much as 58% from 2019 levels are projected to occur by 2030 as well as an over a 70% reduction by 2050. Further cost reductions will reflect improvements power electronics, installation costs, and solar module performance, including the introduction of heterojunction, perovskite and bifacial technologies.[6]

Utility-scale PV enjoys significant economies of scale when compared to distributed solar.[7] The unsubsidized levelized cost of Commercial and Industrial Rooftop PV can be more than two and up to four times the cost of utility-scale projects. The unsubsidized levelized cost of residential rooftop PV is estimated to be 3 to 7 times that of utility-scale solar.[8] On the basis of the unsubsidized levelized cost of energy (LCOE), new utility scale solar is less expensive than new gas combined cycle generation and is approaching the levelized cost of energy from existing combined cycle gas units.[9]

Reflecting falling costs, solar Power Purchase Agreement (PPA) prices have steadily declined. Nationwide average levelized power purchase agreement (PPA) prices fell to $24/MWh in 2019, down 17% from 2018 and more than 80% since 2010. This includes a number of recent PPAs for a combination of PV and batteries in the mid-$20 / MWh range.[10] PPA prices include the benefit of available tax credits. At these PPA prices, PV can compete with energy provided by existing natural gas combined cycle generation.

[2] U.S. EIA 2020.
[3] Pickerel 2020, reporting on the Consolidated Appropriations Act of 2021 enacted December 28. 2020. The bill also extended until January 1, 2026 the safe harbor deadline for completing projects claiming credits based on when construction started and set a target for siting 25 GW of wind and solar on public lands. St. John 2020.
[4] Lazard 2020.
[5] Bolinger et al. 2020.
[6] NREL 2020; see also: IRENA 2019.
[7] MIT 2016; Burger et al. 2019.
[8] NREL 2020; Lazard 2020. See also: Burger et al. 2019; and Tushida 2017.
[9] Lazard 2020.
[10] Lawrence Berkeley National Laboratory, Utility-Scale Solar, available at: https://emp.lbl.gov/utility-scale-solar; Bolinger et al. 2020.

Falling costs have contributed to surge in solar interconnection requests. Total pending solar interconnection requests in ISO / RTO and utility queues has increased from less than 45 GW in 2014 to 367 GW in 2019, with new requests increasing from less than 20 GW per year in 2014 to 168 GW in 2019.[11] By the end of 2019, solar projects represented half of all new capacity under consideration in ISO / RTO and utility interconnection queues.[12] Figure 1, below, shows the growth in proposed solar capacity additions. While not all of the projects currently in the queues will be built, the figures provide an indication of the type of projects that are drawing investor attention. To put investor interest in solar in perspective, the ERCOT interconnection queue included nearly 77 GW of solar projects in August 2020, which is more than ERCOT record peak demand of almost 75 GW.[13]

Figure 1: Generation Capacity in 7 ISO / RTO and 30 Utility Interconnection Queues by Resource Type [14]

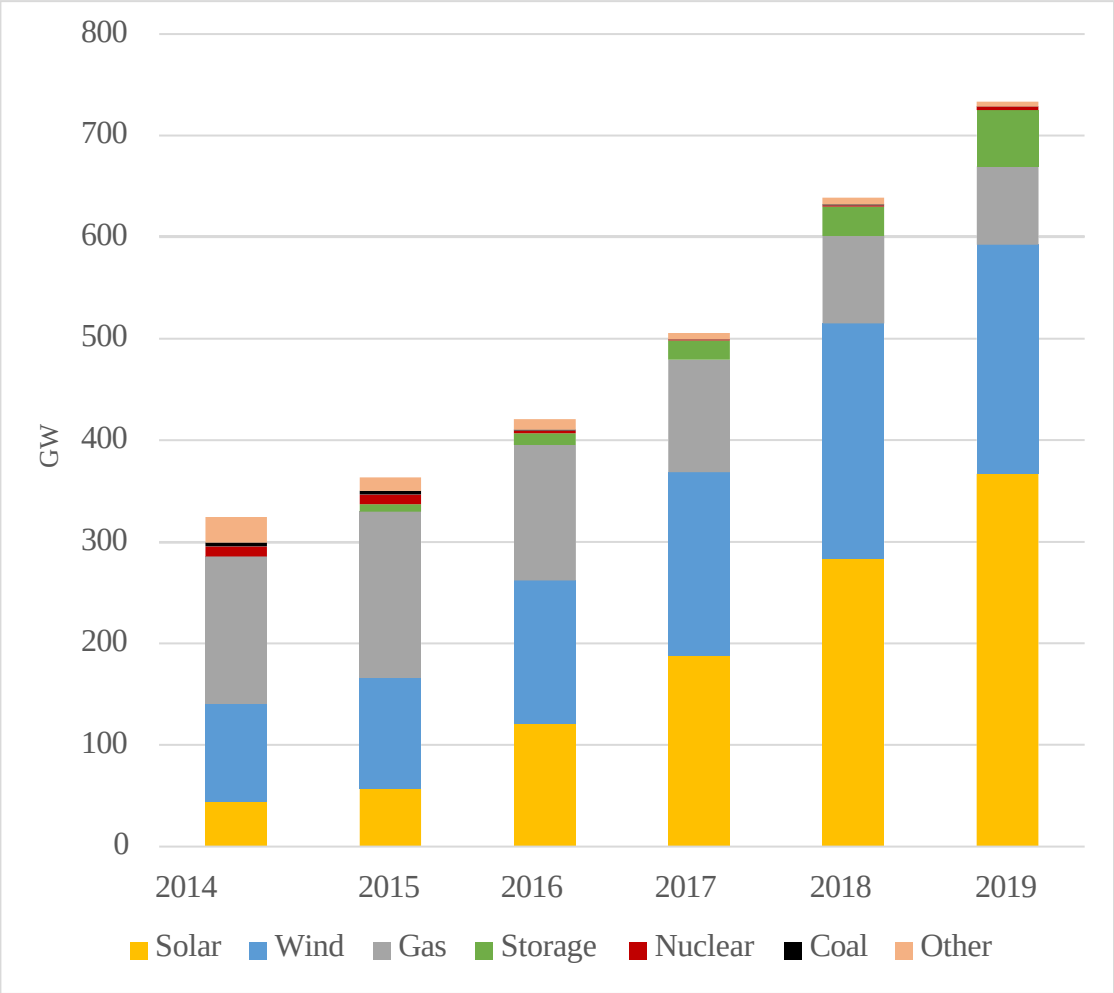

[11] Bolinger et al. 2020.
[12] Bolinger et al. 2020; Caspary et al. 2021.
[13] Rhodes 2020.
[14] Bolinger et al. 2020.

Nearly one third of the solar capacity in interconnection queues at the end of 2019 was paired with energy storage.[15] The addition of a battery in a hybrid solar and storage facility enables it to respond to dispatch and regulation signals, stabilize its power output to the grid, and help manage morning and evening ramp rates. The cost of lithium-ion batteries has fallen, and additional cost reductions are forecast. The proportion of utility-scale solar projects including battery storage is likely to increase. A mid-case NREL projection suggests that the capital costs for a four-hour lithium-ion battery could fall by 50% from 2019 to 2030.[16] However, batteries are likely to remain more expensive than flexible demand for preventing curtailments of excess solar and as an initial step in mitigating morning and evening ramps or than gas-fired generation for addressing multi-day and seasonal reductions in output. Co-locating utility-scale solar and battery storage can take advantage of shared equipment to reduce infrastructure costs by an estimated 8% and may enable the batteries to qualify for solar ITCs.[17] An integrated bidirectional converter and transformer can efficiently manage power flows between the PV panels, battery, and the larger power grid.

Recent projects and PPA prices reflect, in part, the 30% ITC available to facilities that commenced construction prior to 2020 and anticipated reductions in the amount of the tax credit. Solar capacity is expected to continue increasing despite reduced ITCs. However, the rate of growth may be lower than what would have occurred given greater tax credits.

Many of the nation's largest electric utilities have made commitments to reduce greenhouse gas emissions. Ten of the twelve largest U.S. electric companies by market capitalization have announced plans to become carbon neutral by 2050, and many these companies have significant interim emission reduction objectives.

Table 1: Large Market Capitalization Utility Carbon Reduction Goals[18]

Utility Company	**Greenhouse Gas Reduction Goals**	**Year**
NextEra Energy	Reduce by 40% - Already #2 in low carbon generating capacity	2025
Dominion Energy	Net Zero	2050
Duke Energy	Net Zero	2050
Southern Company	Net Zero	2050
AEP	Committed to an 80% reduction with an aspiration be Net Zero	2050
Exelon Corp.	Reduce 15% - Already #1 in low carbon generating capacity	2022
Sempra Energy	100% Renewable Electric	2045
Xcel Energy	100% carbon free	2050
Eversource Energy	Carbon Neutral	2030
WEC Energy Group	Net Carbon Neutral	2050
PSEG	Net Zero	2050
ConEd	100% Clean Energy	2040

[15] *Ibid.*
[16] Cole and Frazier 2020.
[17] Fu et al. 2018; St. John 2020.
[18] Whieldon and Ryser 2020.

Other electric companies that have committed to becoming carbon neutral include: Ameren, APS, Austin Energy, Avangrid, Avista, CMS Energy, DTE Energy, Edison International, Entergy, First Energy, Green Mountain Power, Hawaii Electric, Idaho Power, Los Angeles Department of Water & Power, Madison Gas & Electric, Mid-American, National Grid, New York Power Authority, NRG, Pinnacle West, Platte River Power Authority, PNM Resources, Puget Sound Energy, and Sacramento Municipal Utility District.[19]

Twenty-two states, plus the District of Columbia and Puerto Rico, have either pledged to achieve net-zero carbon emissions or set targets to rely on 100% clean or renewable energy by 2050, including California, District of Columbia, Hawaii, Maine, Minnesota, Nevada, New Mexico, New York, Puerto Rico, Vermont, Virginia, and Washington, which have done so by statute, and Arizona, Colorado, Connecticut, Illinois, Louisiana, Maryland, Massachusetts, Michigan, Montana, New Jersey, Rhode Island, and Wisconsin by executive action.[20] Many large corporations have sustainability plans for achieving net zero emissions.

Under then Chairman Chatterjee, FERC held a technical conference and issued a Notice of Proposed Policy Statement on carbon pricing in organized power markets.[21] This issue is likely to receive greater attention when a Democrat assumes the position of FERC Chair early in a Biden Administration. And, having run on a $2 trillion plan to accelerate clean energy investment with the target of achieving a carbon-free utility sector by 2035, President-elect Biden can be expected to take steps to further accelerate solar development.

The cost of energy from new utility-scale solar and solar / storage hybrids is expected to become less expensive than operating existing fossil fuel generation. However, financing requirements and regulatory policies could continue to limit development beyond policy mandated purchases and large corporate PPAs. The following sections characterize these challenges and address the commercial and regulatory developments that may be needed to help meet utility and government commitments.

Financing Utility-Scale Solar

Developers and their lenders will rarely finance the capital costs of 30 year generating assets on the basis of expected future hourly prices. This is particularly true for solar assets because solar generation a given market tends to be highly correlated.[22] As a result, project developers need to transfer facility ownership or enter long-term contracts (PPAs) with credit worthy counterparties. Today, the purchasers increasingly are large corporate electricity users.
Additionally, project developers often are not in a position to take full advantage of available

[19] See: https://sepapower.org/utilitytransformation-challenge/utility-carbon-reduction-tracker/.
[20] See: https://www.c2es.org/content/state-climate-policy/; and https://www.greentechmedia.com/articles/read/top-10-utility-regulation-trends-of-2020;
[21] FERC, Docket No. AD20-14-000, *Technical Conference regarding Carbon Pricing in Organized Wholesale Electricity Markets*, September 30, 2020 and *Notice of Proposed Policy Statement,* October 15, 2020.
[22] Bartlett 2019.

tax credits and require tax equity partners. We will look at these issues in both markets with retail competition for generation services and states with regulated vertically integrated utilities.

Contracting for Utility-Scale Solar in Competitive Retail Power Markets

Thirteen states (Connecticut, Delaware, Illinois, Maine, Maryland, Massachusetts, New Hampshire, New Jersey, New York, Ohio, Pennsylvania, Rhode Island, Texas) and the District of Columbia, accounting for approximately one-third of U.S. power consumption, have competitive retail power markets.[23] In twelve of these jurisdictions, there is also a FERC regulated ISO / RTO wholesale energy market.[24] In Texas, the state Public Utilities Commission both regulates the ERCOT wholesale market and sets the rules for retail competition.[25]

Many of the retail access states also have strong renewable portfolio standards or other greenhouse gas reduction policies. These policies may require utilities and / or retail suppliers to purchase renewable energy or Renewable Energy Credits (RECs). However, fully utilizing utility-sale solar to meet carbon reduction objectives will require addressing constraints on contracting and financing these facilities.

Generation is a competitive service in these jurisdictions. To create a level playing field for competition, investor-owned distribution utilities in retail access states typically are prohibited from owning supply resources or allowed to own only small amounts of generation and only in limited circumstances. Even with smaller distributed energy resources (DER), the New York Public Service Commission, for example, allows distribution utilities to own these resources only in the following circumstances:

1. Procurement of DER has been solicited to meet a system need, and the utility has demonstrated that competitive alternatives proposed by nonutility parties are clearly inadequate or more costly than a traditional utility infrastructure alternative;
2. A project consists of energy storage integrated into distribution system architecture;
3. A project will enable low or moderate income residential customers to benefit from DER where markets are not likely to satisfy the need; or
4. A project is being sponsored for demonstration purposes.[26]

To develop utility-scale solar in retail access jurisdictions projects that exceed state minimums, solar developers have to rely on long-term PPAs with providers of generation services.

[23] Customers of municipal utilities and rural electric cooperatives were often not covered by retail competition statutes. Additionally, portions of Texas outside of ERCOT are not included in the competitive retail market. Some additional states have allowed competition for serving a limited set of generally larger customers.

[24] ERCOT which is intra-state and regulated by the Public Utilities Commission of Texas, and the following FERC regulated markets: ISO New England, Mid-continent ISO which includes Ameren and Mid-American in Illinois, New York ISO, and PJM which includes Delaware, District of Columbia, ComEd in Illinois, Maryland, New Jersey, Ohio and Pennsylvania.

[25] With limited DC connections to the Eastern and Western Interconnections, wholesale transactions within ERCOT are not considered to be federally regulated interstate commerce.

[26] NY PSC 2015.

A comparison of the ERCOT market in Texas to those in the other retail access jurisdictions illustrates the impact market structure and regulation can have on the development of utility-scale solar and the necessary long-term solar contracts. Based on data reported to U.S. EIA for 2019, Texas accounted for 46% of the then existing utility-scale solar and 76% of the planned solar capacity in the 14 retail access jurisdictions.[27] While this, in part, reflects more sunlight than what reaches more northern states, the number of large PV facilities being added in Texas and solar's increasing share of the ERCOT interconnection queue indicate ERCOT is a favorable market for development of utility-scale solar.[28] Moreover, public policy not is the primary driver for solar investment. Texas met its Renewable Portfolio Standard requirements years ago. The other 13 retail access jurisdictions have more stringent Renewable Portfolio Standards than Texas.[29] And, in other retail access states (Massachusetts, New Jersey, and New York) that as of 2018 had installed solar capacity comparable to that in Texas, distributed PV, that is more expensive and benefits from net metering and rate design subsidies, was a majority of the solar resource. Most new solar capacity in Texas is from utility-scale facilities[30]

Two important differences in market structure help make Texas a more favorable for development of utility-scale solar. First, Texas uses scarcity pricing to ensure resource adequacy and provide a powerful incentive for forward contracting. These contracts can support solar and hybrid solar / storage projects that can provide power during periods of high demand. In the other markets, administrative capacity mechanisms that make it more difficult for solar to participate are used to address resource adequacy. Second, in Texas, distribution utilities are not the Provider of Last Resort, the market encourages retail customers to select a Competitive Retail Electric Supplier (CRES), and competitive supply prices tend to reflect near- term or, with some suppliers, real-time wholesale prices. In the other retail access markets, the distribution utility typically offers Default Service, otherwise known as Basic or Standard Offer Service, to any customer that has not selected a CRES. Default supply is typically procured through periodic auctions purchasing overlapping annual or multi-year tranches of power at a fixed price. The Default rate passes the cost of purchases on to customers in a flat kWh charge designed to remains relatively stable over time. Changes in the Default rate will lag changes the market, leading customer to move in and out the competitive market depending on whether market prices are below or above the default price. The remainder of this section discusses the implications of these differences for utility-scale solar contacts in competitive retail access markets and suggest modifications to address barriers to solar development.

In efficient competitive markets, when resources are scarce demand sets the price based on how different customers value incremental consumption. To approximate an efficient market, ERCOT prices scarcity using an operating reserve demand curve (ORDC) that increases energy and operating reserve prices to reflect an increasing probability of shortages as the market

[27] U.S. Energy Information Administration 2020a.
[28] Wesoff 2020; Wesoff 2020a; Rhodes 2020; and Keleher et al. 2020.
[29] National Conference of State Legislatures 2021.
[30] Quilici et al. 2019.

tightens. Based on estimates of the value of unserved energy to customers, the ORDC price represents the opportunity cost of reducing reserves as demand increases. As a result, ERCOT prices can increase to, and in the summer of 2019 reached, $9,000 / MWh. However, very little demand is exposed to these high prices. Scarcity pricing provides the incentive for retailers to hedge risk by entering forward contracts and working with their customers to manage demand.[31] Over 85% of energy in the ERCOT market is purchased through bilateral contracts.[32] The ERCOT model has been successful in maintaining resource adequacy.[33] And, by encouraging long-term contracts, it has supported the development of utility scale solar.

Other regional wholesale markets place a much lower ceiling on energy prices, then compensate for doing so by imposing administratively determined capacity requirements. The wholesale market operator sets the capacity requirements, creates a centralized capacity auction, purchases capacity, and assigns the costs to Load Serving Entities (LSEs). Capacity performance requirements may limit the participation of seasonal and variable resources and require aggregation, recognizing aggregations that include solar to the extent they can provide sustained and predictable performance whenever an emergency occurs.[34] Additionally, FERC also has created barriers to capacity participation by clean and renewable resources that benefit from state renewable portfolio standards, the Regional Greenhouse Gas Initiative (a multi-state carbon pricing program), and other state policies. The capacity offers from resources that benefit from state policies can be increased under a Minimum Offer Price Rule (MOPR), such that these resources may no longer qualify for capacity revenue.[35]

In the ERCOT market, competitive retail supply prices track wholesale market forward contract and / or spot prices, offering products that may include a pass through of hourly prices and various hedging options based on forward contract prices. The lack of a fixed Default rate has two important implications. First, it eliminates a boom-and-bust cycle in the competitive market with customers migrating to competitive supply when market prices are falling but returning to the default rate when the market price rises above the default option. Second, stability in the competitive market enables intermediaries to purchase and sell shares of longer term contracts to different retail suppliers. The market enables longer term contracts, in part, because the risk of customers abandoning the competitive market for a default supply is absent.[36]

[31] Gramlich and Lacey 2020.
[32] Potomac Economics 2020.
[33] Silverstein 2020; ERCOT 2019; See also: ERCOT 2020.
[34] See: Federal Energy Regulatory Commission, *PJM Interconnection, L.L.C.*, 151 FERC ¶ 61,208 (June 9, 2015). See also: Federal Energy Regulatory Commission, *ISO New England Inc.*, 147 FERC ¶ 61,172 (2014): Gramlich and Goggin 2019. [35] Federal Energy Regulatory Commission, *Calpine Corporation, et al. v. PJM Interconnection, L.L.C.,* 169 FERC ¶61,239 (December 19, 2019): Federal Energy Regulatory Commission, *ISO New England Inc.,* 173 FERC ¶ 61,161 (November 19, 2020). See also: Federal Energy Regulatory Commission, *New York Independent System Operator, Inc.* 170 FERC ¶61,121 (February 20, 2020). See also: Gramlich and Goggin 2019.
[36] Gramlich and Lacey 2020.

In the near term, the following reforms could help enable longer-term contracts and financing of additional utility-scale solar in competitive retail markets:

- Restrict the application of FERC MOPR rules to those rare circumstances in which a generator may be unable to access the larger market due to transmission constraints and a large purchaser can exercise monopsony power. Allow state policies to support the purchase of preferred resources.[37]
- Adopt robust scarcity pricing mechanisms in FERC regulated wholesale markets and require LSEs to disclose and maintain a sufficient combination of forward contracts and financial resources to meet their customer obligations in a scarcity pricing stress test.[38] As scarcity pricing increases voluntary forward contracting, it may be possible to phase out centralized forward capacity purchases.
- Make hourly wholesale spot prices the basis of the retail Default supply tariff in competitive retail markets. CRES would be encouraged to offer a range of hedging and renewable energy products that would support forward contracts. An equilibrium level at which customers select these products will emerge to support a secondary market in forward contractual commitments that includes forward contracts with utility-scale solar projects.[39]

Utility-Scale Solar in Vertically Integrated / Rate Regulated Jurisdictions

Vertically integrated utilities in rate regulated jurisdictions face a different challenge in developing utility-scale solar. On one hand, these utilities can and, at least when directed to do so by their regulator will, enter PPAs for solar energy. However, a regulated utility's profits are based on the returns allowed on the investments in the utility's rate base. The nature of an expense and its FERC accounting code determine whether a utility expenditure can be included in rate base and the utility can earn a return. A PPA is an operating cost, not a rate base asset. Therefore, the cost of the PPA is simply a pass through in rates and the utility does not earn a profit. As regulated utilities in many states are already meeting existing portfolio standard and other regulatory requirements, utility PPAs are becoming less common. "Long-term utility PPAs which take all risks off the developer are becoming scarce."[40]

Regulators could allow utilities to profit from solar PPAs by creating solar energy performance incentives. However, a substantial performance incentive would be required to enable solar to effectively compete with rate base investment opportunities in utility business plans. A complementary approach would be to enable capitalization of utility solar PPAs. Utility

[37] Except in cases involving the allocation of costs of a multi-state utility, the review of power purchasing options has traditionally been treated as a matter of state authority. *Pike County Light and Power Co. v. Pennsylvania Public Utility Commission,* 77 Pa. Cmwlth. 268, 465 A. 2d 735 (1983); *Pacific Gas & Electric Co. v. Lynch,* 216 F. Supp. 2d 1016 (N. Dist. CA 2002); *Palisades Generating Co.,* 48 FERC ¶ 61,144 (1969). This question is a separate from the issue of who can participate in wholesale power markets. While purchasing decisions can affect capacity prices, it should be noted that existing capacity mechanisms are not efficient market mechanisms in that LSEs are not voluntary buyers. The market operator determines the resources to be purchased and assigns costs to different LSEs.

[38] See, for example: Federal Energy Regulatory Commission, *PJM Interconnection, L.L.C.,* 171 FERC ¶ 61,153 (May 21, 2020).

[39] Spain adopted wholesale spot prices as the basis of retail default service supply prices in 2014. See: Ministry of Industry, Energy, and Tourism 2014; and Council of European Energy Regulators 2019.

[40] Gramlich and Lacey 2020.

regulators could create a regulatory asset allowing PPA expenditures to be capitalized. However, this is not common practice.

The regulator in the United Kingdom has an innovative approach in which network utilities capitalize a fixed percentage of their total expenditures (TotEx). TotEx regulation enables a utility to capitalize generate earnings from the fixed percentage of its revenue requirements, without regard for whether the utility uses the funds for operating expenses or capital investment. The nature of a utility's actual expenditures does not change the proportions of revenues that are capitalized or are recovered annually. TotEx regulation significantly reduces, if not equalizes, the incentive for the utility to prefer capital expenditures to operating expenses.[41] U.S. Generally Accepted Accounting Principles are a barrier to including the recovery of previously capitalized costs in TotEx regulation applied to a utility's entire revenue requirement.[42] However, there is no obvious reason why a TotEx regulation could not be adopted for new spending including expenditures on utility-scale solar.

Alternatively, a vertically integrated utility could own the solar facility. However, as a result of tax normalization, a regulated utility will not enjoy the same ITC benefit as a non-utility, which distort the utility's investment decisions.

Tax Based Financing: Impacts of Tax Normalization on Vertically Integrated Utilities

The earliest investment tax credits for the development of solar energy were enacted in the Energy Tax Act of 1978. The current Investment Tax Credit was first adopted in the Energy Policy Act of 2005 and has been repeatedly extended and modified.[43] The tax credit made a significant contribution to the development of solar energy. Extending the credit at historical levels (30%)could increase installed solar capacity in 2030, perhaps by more than 25%.[44] However, ITC for utility scale solar is now at 26%, scheduled to decline to 22% in 2023, and to 10% for projects started after 2023.[45]

Utility tax normalization rules have limited direct utility investment by preventing regulated utilities from efficiently monetizing tax credits. Tax normalization requires regulated utilities to recognize ITC tax benefits over the life of the solar assets, generally 30 years or longer. Other solar project owners can realize the full benefit of the ITC in the first year the project is in service. This delay in recognizing ITCs and related depreciation benefits can increase the cost of utility owned solar by as much as 20-30%.[46] Normalization alters the investment decisions of

[41] Ofgem 2013; Spiegel-Feld 2015.
[42] New York Department of Public Service 2015; New York Public Service Commission 2016.
[43] Sherlock 2018.
[44] Comello and Reichelstein 2015; Fraizer et al. 2019.
[45] Utility scale solar is likely to remain cost competitive given cost reductions that are anticipated to occur within this time period. The absolute value ITCs, which are based on a percentage of project costs, also will decline with the capital cost of projects. See: Fraizer et al. 2019. The tax treatment of ITCs may nonetheless continue to affect utility investments.
[46] Blank and Richardson 2020.

vertically integrated utilities. A solar project, which would be cost-effective if undertaken by a non-utility, may appear to be more expensive to the utility than gas-fired unit given the utility's inability to take full advantage of available ITCs. This can occur because:

- The delay in realizing ITC and depreciation benefits can increase the cost of utility-owned solar compared to other utility generation;
- Normalization reduces the competitiveness of utility-owned solar in wholesale power markets, such that, it can be difficult for utilities to sell power from solar assets at a competitive price;[47] and
- Even if a solar PPA is the best option for customers, the alternative, e.g., a gas-fired generator, may be more profitable for utility shareholders.[48]

Exempting utility-scale solar projects from the tax normalization rules in Internal Revenue Code Section 168 could accelerate direct investments in solar by regulated utilities.[49]

Utilities have developed two potential ways to mitigate the impact of tax normalization, although both involve additional costs and complexity.

Some utilities have partnered in tax equity investors in special project companies for the development of renewable energy projects as a means to leverage renewable tax credits. In these agreements, the tax equity investor is allocated a disproportionate share of tax benefits, and a portion of the near-term cash flow under a PPA with the utility, in return for its upfront capital contribution. The investor's contribution pays part of the cost of the project, reducing the cost to the utility and its customers. When the tax equity investor reaches an agreed target return, the utility has the option to buy out the investor, becoming the sole owner of the project. However, tax and regulatory rules governing these agreements are complex and may not be consistent with utility objectives.[50] Moreover, the pool of available tax equity investment is limited.[51] And, the addition of a tax equity investor, formation of a special project company, and required regulatory approvals increase project costs.[52] Efforts to standardize the terms of such partnerships and applicable regulatory reviews might reduce some of the related costs.

Dominion Energy pursued an alternative strategy. Under tax normalization, cost-of-service ratemaking cannot recognize the benefits of ITCs and accelerated depreciation cannot recognize more than the annual ratable portion of these benefit, determined by dividing their value by the project's useful life. Dominion pursued a three step strategy to sidestep tax normalization by removing solar assets from conventional cost-of-service regulation:

1. In 2015, Virginia adopted a statute allowing regulated utilities to charge consumers for solar power "based on a market index in lieu of a cost-of-service model."

[47] Murphy 2019.
[48] Blank and Richardson 2020.
[49] 16 U.S.C. §168 (f), Accelerated Cost Recovery System.
[50] Shaw and Shimamoto 2018; See also: Murphy 2019.
[51] Bhattacharyya 2020.
[52] *Ibid.*

2. The utility sought a private letter ruling from the IRS stating that if the Virginia Commission were to adopt a market index rate adjustment clause, solar projects would not constitute "public utility property," allowing the utility to use the ITC.
3. The company sought authority from the Commission to charge customers for utility owned solar based on the highest priced PPA proposal that the utility received in response to a 2015 request for proposals.[53]

However, this is a complex strategy that has not been broadly adopted.

Given the costs and complexity of the alternative approaches, exempting utility-scale solar from tax normalization could be important to solar development in jurisdictions where generation is subject to cost-of-service regulation. This is particularly true in jurisdictions where there are few other alternatives for the development of utility-scale solar.

State Restrictions on Third Party Power Purchase Agreements

Five states – Florida, Georgia, Kentucky, North Carolina, and Oklahoma – with significant solar resource potential appear to restrict PPAs with third party solar developers. These restrictions are based on statutes and rulings that define who is a utility and / or establish exclusive utility service territories for the retail sale of electricity.[54] This issue may need to be addressed on a state-by-state basis.

Refundable Tax Credits

Tax credits are typically non-refundable and have value only to the extent they can be used to offset the holder's tax liability. Most renewable project developers lack the tax liabilities needed to take full advantage of available tax credits and would benefit from a refundable credit.[55] Making the tax credits refundable would make them the equivalent of a grant, in this case administered through the tax system. A refundable credit would increase the value of ITCs by avoiding uncertainty regarding the ability to use credits and may eliminate the need for a developer to partner with a tax equity investor. Refundable credits would lower the cost of solar PPAs and potentially enable build – transfer agreements in which a developer uses ITCs to reduce project costs before transferring ownership to a utility.

Prior to 1980, the original federal wind and solar tax credits were refundable. Several states offer refundable tax credits for renewable energy.[56] The 2009 American Recovery and Reinvestment Act included a temporary provision allowing energy projects to receive a 30% cash grant from the Department of the Treasury in lieu of a tax credit, effectively making the

[53] Burton 2016.
[54] See: http://ncsolarcen-prod.s3.amazonaws.com/wp-content/uploads/2015/01/3rd-Party-PPA_0302015.pdf. Citing: Florida Public Service Commission Docket 860725-EU, Order 17009 (1987); Georgia Territorial Act O.C.G.A §46-3-1; Kentucky Revised Statutes 278.010 (3); North Carolina General Statutes §61-3(23); and Oklahoma 17 Okl. St. §151; O.A.C. §165.40.
[55] Bhattacharyya 2020.
[56] Heightley et al. 2019.

tax credits refundable. The 2020 Coronavirus Aid, Relief, and Economic Security (CARES) Act made the employee retention credit refundable. Potential impacts of the pandemic on tax equity financing led to proposals to make the solar ITC refundable, although this has not yet been adopted.[57]

Proposals to make ITCs refundable have raised three concerns. First, refundable ITCs would result in the loss of federal revenue. Credits that are currently carried forward and ultimately go unused could instead be immediately claimed by taxpayers. Revenue loss might be addressed by limiting the total amount of available credits as was done with the advanced energy manufacturing tax credit (Internal Revenue Code §48C) and clean coal tax credits (Internal Revenue Code §§48A and 48B). Second, to the extent refundable investment tax credit eliminates the need for tax equity investors, this could take away the evaluation of investments and project oversight provided by these investors. This might not become an issue if external equity investors are needed to fund projects or alternatively could be addressed by government monitoring of project viability. Third, refundable credits have generally been reserved for households, mostly for providing income support to low income households.[58] Making solar ITC would be an exception to common practice.

Systemic Challenges to Achieving a Low Carbon Future with Significant Utility-Scale Solar

To achieve a low carbon energy future, policymakers, utilities, and their regulators will need to address complicated issues that cannot be fully explored in this memorandum. These include:

- How to Price Carbon: Placing a price on greenhouse gas emissions throughout the economy would provide an incentive to efficiently reduce emissions.[59] However, the expected cost of reductions and potential impacts on communities that depend on carbon emitting industries have thus far blocked significant carbon pricing proposals. Policymakers may revisit this issue as clean energy becomes less expensive and options are developed to address negatively impacted communities.
- The treatment of stranded fossil fuel generation assets: As the price of renewable energy falls, additional fossil fuel units will become uneconomic to operate. In competitive markets, absent price supports these units will retire and sunk costs may have to be written off by investors. In rate regulated jurisdictions, utilities may have an incentive to defer investment in cost-effective solar to continue to earn a return on existing assets.[60] However, uneconomic capacity may be considered no longer used and useful. Typically, utilities can only include used and useful assets in rates. In such cases, the regulator and utility may face difficult questions on how to incent the development of lower cost solar while maintaining the utility's financial integrity and ability to raise capital.

[57] Bhattacharyya 2020.
[58] Heightley et al. 2019.
[59] National Academies 2016.
[60] Blank and Richardson 2020.

- Transmission planning and investment: Solar resource potential is unevenly distributed.[61] Additional transmission investments are likely to be needed to fully realize their potential. This may require changes in interregional planning and siting authority.[62]
- Resource adequacy and supply planning: Conventional resource adequacy metrics such as Loss of Load Expectation and Effective Load Carrying Capacity generally assume that the output and availability of individual generators are independent of one another. However, this is not the case for solar and wind resources or for extreme weather events, limitations on natural gas availability, cyber-security attacks, and other common mode supply disruptions. This will require the development of new tools and approaches.[63]
- Demand flexibility: Achieving an affordable clean energy future will require greater reliance on flexible demand to offset the ramps, absorb excess energy, and balance the variability of solar and wind resources. Enabling smart connected energy using devices to dynamically shape, shift, and modulate demand in response to changing system conditions will require a departure from conventional event driven demand response and rethinking retail rate design to develop efficient and equitable rates that communicate appropriate price signals.[64]

Grid Integration of Utility-Scale Solar: Utility Gathering and Interconnection Service

While the issues discussed above present barriers to larger utility participation, there may be opportunities for utilities to play the more limited role of building and owning make ready infrastructure. There is nothing inherently anti-competitive that would prevent a distribution utility in a retail access jurisdiction from developing make-ready infrastructure. Such infrastructure might include all of the wires for gathering of power and a DC transformer and DC / AC converter used to connect the facility to the grid. . A vertically integrated utility can own all or part of a solar facility.

Even to build make ready infrastructure, both the vertically integrated utility and the distribution utility in a competitive market would face financing disadvantages. For example, a third party developer could benefit from the full ITC credit on gathering, conversion, and interconnection portions of a solar project, while the utility would have to follow tax normalization rules.

Nonetheless, it may prove viable for distribution utilities to offer access to solar as a service. There are many consumers who would like to purchase solar power but are unable to affordably do so because they live in multi-family housing, don't have a suitable site, or can't afford the up front investment. Residential rooftop solar is more expensive than utility- or

[61] See: https://www.energy.gov/maps/solar-energy-potential.
[62] Weiss et al 2019; Larson et al. 2020; McCalley and Zhang 2020; and FERC Staff 2020.
[63] Centolella et al. 2021
[64] Centolella 2020.

community-scale solar and can increase costs for distribution system operators. Utilities could offer access to a community-solar alternative to meet customer demand and maintain the sales that otherwise might be lost to uneconomic rooftop PV. In this business model, the utility would build and own all of make ready infrastructure, which could be sited at an optimum location for grid integration and power production. Additionally, the utility could create a marketplace where its customers could subscribe to, lease, and potentially buy and sell fractional shares in the output of community solar. In retail access jurisdictions, the PV panels and batteries would be installed and owned by one or more third parties. The third parties, or their agent, would become the market participant in the ISO/RTO power markets. The utility marketplace would make solar shares affordable for consumers and create a liquid market to support third party investment. The utility could rate base its make ready network investments and potentially earn small transaction fees on marketplace transactions.

Grid Integration of Utility-Scale Solar: DC Transformer / Converter

A growing share of solar projects entering interconnection queues are hybrid projects combining PV and battery storage. The addition of storage reflects the opportunity to shift the timing of delivered power, the need to moderate changes in PV output, and frequency regulation requirements. Solar output is subject to both long-term variability, caused by the Earth's movement relative to the sun, and significant rapid changes in output due to cloud cover. Cloud induced fluctuations can be difficult to predict and can impact power production in a matter of seconds. For example, Figure 2 shows changes minute-by-minute average irradiance measured in a 21 MW solar facility in California on a partly cloudy day.[65]

Figure 2: Minute-averaged Irradiance

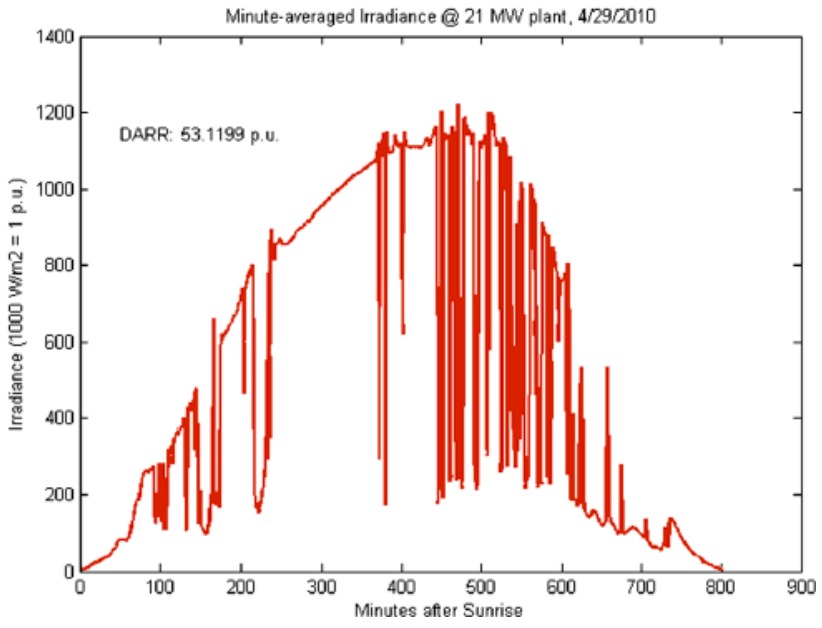

[65] Van Haaren et al. 2012. Note: DARR refers to the daily aggregate ramp rate, calculated as the sum of: minute to minute differences in average irradiation divided by a constant value for peak irradiance (1000W/m^2).

Output variability due to passing clouds affects up to 70% of daytime solar capacity.[66] Such variability has raised concerns that, as the power system becomes increasingly dependent on large-scale solar, short-term fluctuations could lead to under frequency load shedding and impact grid stability.[67]

An increase in solar and wind generation and the decline in synchronous generating capacity led the North American Electric Reliability Corporation (NERC) Essential Reliability Services Task Force to recommend in 2015 that all new generators have the capability to manage frequency.[68] At the time, the most significant standard governing primary frequency response in the United States was NERC standard BAL-003-1.1 which placed responsibility for frequency response on Balancing Authorities. There was not a uniform gird code or requirement that generators provide primary frequency response. There were different requirements in the different ISOs/RTOs and utility balancing authorities.[69] This changed with FERC Order 842, which requires all new generators, including solar, to install, maintain, and operate equipment capable of providing primary frequency response as a condition of interconnection.[70]

The multiport DC transformer and bidirectional AC / DC converter developed for this project will facilitate the integration of battery storage in utility-scale solar facilities. This is a new approach that offers greater flexibility and potential cost savings. These savings could be in addition to cost savings available from co-locating storage and solar and standard DC coupling in hybrid systems. Co-location reduces costs by avoiding the duplication of equipment and development costs. According to an NREL analysis, a conventional DC coupled hybrid system can provide additional savings compared to an AC based PV and battery system because:

- Only a single bidirectional inverter is required reducing the costs for the inverter, its wiring, and housing;
- The extra conversion between DC and AC reduces the roundtrip efficiency of the battery in a hybrid system; and
- A DC connection from the PV panels to the battery ensures that any PV generation in excess of the inverter power specification will be stored and not clipped at the inverter.[71]

In this analysis, Fu et al. assume the savings in a DC coupled hybrid system would be partially offset by battery systems having to be placed within the PV field next to the bidirectional inverter resulting in higher balance of system structural costs and greater installation labor and overhead costs.[72] However, the multiport DC transformer and integrated converter may provide additional flexibility to optimally locate the batteries and reduce these costs. Based on the analysis in Fu et al. and taking into consideration the potential flexibility provided by a multiport DC transformer / converter, a DC based power gathering and conversion system

[66] Crabtree et al. 2017.

[67] Chen et al. 2020; Alshahrani et al. 2019; Rakhshani et al. 2019; Crabtree et al. 2017.

[68] NERC 2015; See also: FERC 2016.

[69] Roberts 2018.

[70] FERC 2018.

[71] Fu et al. 2018; DiOrio and Hobbs 2018.

[72] Fu et al. 2018.

might reduce the total cost of a 100MW PV and 60 MW / 240-MWh battery hybrid facility by one to three percent compared to a comparable AC coupled hybrid facility and by 7% to 11% when compared to PV and battery systems that are not co-located.[73]

DC Transformer Technology: DC as a Utility Service

While alternating current (AC) won the "war of currents," DC power systems never fully disappeared. Pacific Gas & Electric continues to provide DC service to support variable-speed DC-motored elevators in office buildings near Market Street in San Francisco.[74] Moreover, in 2018, California amended its Public Utilities Code to require the development of standards for metering DC service, "to streamline the interconnection process and lower interconnection costs for direct current microgrid applications."[75] Some utilities may continue to provide DC service for urban transit systems.[76] Advances in power electronics, which have made DC voltage regulation a simple task, the increasing penetration of DC loads, and growth in renewable resources is leading to renewed consideration of DC service as a means to increase efficiency for portions of today's power system.[77]

The integrated bidirectional AC / DC converter and multiport DC transformer developed for this project has the potential to reduce the costs, connect DC power sources and integrate them with the AC system, control the power delivered end uses that require DC power, and support DC microgrids with the ability when necessary to island from the AC grid and balance PV, storage, or other DC power sources with DC power usage.

A growing share of electric supply including both utility-scale and distributed resources are natively DC power sources. This includes PV, fuel cells, and storage including batteries, flywheels, and ultra-capacitors. Microturbines that generate high frequency AC are more easily connected to a DC system.[78] Additionally, some wind turbines rely on an AC-to-DC-to-AC conversion to match the frequency of AC power systems. An integrated bidirectional AC / DC converter and DC transformer could support integration of systems that are natively provide DC or include a DC power stage. In some cases, different units may be connected through a DC network leading to a common converter / transformer to avoid duplication and reduce costs.
This project's PV, battery, and converter / transformer system is testing in this framework.

Many uses of electricity convert AC to DC power. Electronics including computers, phones, printers, TVs, and microwave ovens use DC power. Compact fluorescent and solid state lighting

[73] *Ibid.* The higher percentage figures assume that the offsetting cost increases estimated by Fu et al. can be avoided with the use of the multiport DC transformer and integrated bidirectional DC / AC converter. Other potential costs and savings have not been estimated.
[74] Fairley 2012.
[75] California Senate Bill 1339, adding Public Utilities Code §8371(f). See also: California Public Utilities Commission 2021.
[76] See, for example: Chicago Transit Authority 2020.
[77] Elsayed et al. 2015; Reed 2020.
[78] *Ibid.*

technologies work more efficiently on DC power. DC power is used in energy efficient washing machines, air conditioners, and a growing number of other home appliances. The Variable Speed Drives for commercial HVAC systems, pumps, elevators, and industrial applications rely on DC power. The steel industry is employing DC electric arc furnaces that consume less energy than the corresponding AC furnaces. The electrochemical industry relies on DC applications.
Data center efficiency can be improved by reducing the AC to DC conversions and operating on a DC network. DC fast charging will be important in the electrification of the transportation sector.[79] In 2012, nearly 30% of all power passed through a power electronics converter before being used, and the prediction at the time was that this percentage would increase to 80% in 10 to 15 years.[80]

A bidirectional AC / DC converter and DC transformer could be applied to provide DC power or in a DC microgrid that combines a power source and DC end uses. Initial applications with a significant DC power requirement include data centers, commercial buildings, and electric vehicle charging.

Data centers are large electricity users. Globally data centers use over 400 TWh of electricity per year, approximately 3% of the world's total electricity consumption.[81] In a traditional data center, much of this power can be wasted. A typical data center is served by a medium voltage AC line. The incoming AC voltage is first transformed to a lower voltage level, than converted to DC to power the batteries in the uninterruptible power supply (UPS) system. After powering the batteries, the current is converted back to AC and sent to the center's power distribution units that supply individual server power supplies, where it is then converted back to the DC power the servers themselves require. In each of these conversions, energy is dissipated in the form of heat.[82] To maintain efficient operations, the heat must be removed, and equipment cooled, requiring additional electricity. An average data center has a power usage effectiveness (PUE) of around 1.8. PUE is a measure of the total data center energy use divided by the energy actually delivered to computing equipment. A 1.8 PUE means that for every 10 kWh devoted to computing, 8 additional kWh are dissipated in AC / DC conversions and losses, spent on cooling, or devoted to lighting and other auxiliary uses.[83] Today, DC data centers accounts for only a tiny fraction, approximately 10MW, of the installed base of data center operations.[84] A transition to the use of DC power in data centers could provide significant advantages. DC power could avoid the multiple conversions and losses, improve efficiency, and enhance data center reliability. A detailed study led by Lawrence Berkeley National Laboratory found that:

[79] Patterson 2012; Reed 2012; and Wang 2012.
[80] Reed 2012.
[81] Bachmann 2019.
[82] *Ibid*.
[83] The most efficient data centers typically achieve PUEs below 1.2 and can achieve below 1.04. National Renewable Energy Laboratory Computational Science. See: https://www.nrel.gov/computational-science/measuring-efficiency-pue.html.
[84] Sterlace 2020.

"DC based power distribution systems can reduce the total system energy use in a data center by 5 to 7 percent compared to the most efficient AC systems and by up to 28 percent compared to typical AC distribution systems. DC distribution systems also reduce cooling loads and have the potential to improve reliability by reducing the number of possible failure points. …Additionally, because DC configurations produce less heat, they can save 28 percent of the electricity used by a building cooling system. The servers and the power distribution and cooling systems account for the bulk of the energy used in data centers; savings from DC configurations, when compared to typical AC systems, can amount to 28 percent of the electricity used by the entire facility."[85]

Compared to conventional AC powered centers, a 380 Vdc data center could have 15% lower up-front capital costs and require 33% less floor space, reducing lifetime data center costs by up to 36%.[86] DC power also offers benefits in terms of power quality and reliability. "The design of a DC power system is simpler, with fewer components (and thus fewer points of failure) than the AC alternative, and it eliminates harmonics, phase load balancing and other issues associated with AC."[87] As a result, a DC system can offer up to a 10 times improvement in reliability compared to an AC system using a single UPS per path, a common configuration.[88] The telecom industry has used DC systems for decades due to its higher reliability. The Japanese Ministry of Economy, Trade, and Industry has been pursuing a Green IT program designed, in part, to convert data centers to DC. China is committed to move to DC data centers.[89] In the U.S., the use of DC in data centers has been constrained by the absence of standards; a lack of experience with the technology among data center owners, operators, and contractors; and, as a result, limited product selection.[90] The Federal Government and industry could enable a transition to DC power by supporting standards development and training.

Commercial buildings use electricity for lighting, cooling, ventilation, information technology often including small data centers, and in other systems that can use DC and require AC to DC power conversions. "Virginia Tech's Center for Power Electronics Systems in Blacksburg estimates that more than 80% of the electricity used in office buildings passes through power electronics and experiences one or more conversions between ac and dc electricity. Defining common interfaces and standards for our dc devices … could … simplify how we use power while saving energy, offering the potential for 5–15% savings or more, depending on the ac-dc conversions we reduce or eliminate."[91] Moreover, there are small data centers in nearly every commercial office building. Small data centers can reduce their energy use by 10% to 30% by using DC power.[92] Some buildings include rooftop solar. In these buildings, "the native dc

[85] California Energy Commission 2008. See also: AILee and Tschudi 2012. For example, Duke Energy reduced the energy use in its data center by 15% on DC power. Kintner 2011.
[86] AILee and Tschudi 2012.
[87] Sterlace 2020.
[88] Shrestha et al. 2018. See also: Elsayed et al. 2015; and Sterlace 2020.
[89] AILee and Tschudi 2012.
[90] Sterlace 2020.
[91] Patterson 2012.
[92] Patterson 2012. See also: EPRI 2010.

power produced by the solar panels is inverted to ac power, just so it can be distributed in the building. Then the ac power gets converted back to dc for specific device uses, such as lighting. This double conversion wastes even more energy. After these double conversions, 15% or more of the solar energy generated is lost."[93] An integrated bidirectional AC/DC converter and transformer can match the buildings DC generation and loads and manage its interface with the AC power grid to sell surplus generation and use grid power when local PV output is insufficient. At the same time the converter could provide power conditioning and voltage regulation services to the grid.[94]

Battery costs and EV prices are expected to decline toward first cost parity between electric and conventional vehicles over the next decade. In several categories, the purchase price of EVs could fall below that of conventional vehicles before 2030.[95] Given aggressive policies to reduce greenhouse gas emissions, half of the global light duty vehicle fleet could be EVs by 2050.[96] However, for the next several years, the electrification of transportation will involve a tradeoff: EVs having higher first costs than the comparable internal combustion or diesel vehicles and enjoying lower fuel and maintenance costs over time. As a result, high usage vehicles may be among the first categories in which electrification becomes cost-effective. Fast charging will be important for high use EVs, where time spent off the road represents a significant cost and / or inconvenience. These vehicles may include transit buses, taxis, ride share and other mobility on demand vehicles, warehouse vehicles, delivery and potentially
long-distance trucks. The Los Angeles (2030), San Francisco (2035), New York (2040), Chicago (2040) Seattle / King County (2040), and several international transit systems have committed to 100% electric bus fleets. Today, the price of an electric transit bus, over $650,000, may be more than 60% higher than that for a diesel bus. However, reduced fuel and maintenance costs can result in a lifecycle cost reduction of more than $170,000 per vehicle.[97] Utilizing electric buses on longer routes may require DC fast charging to replenish the batteries' state of charge while buses stop to unload and load passengers. In some European cities, buses are being charged at 450 kW fast chargers located at stops serving multiple buses. Taxis, ride share, and other mobility on demand vehicles present another opportunity for fast charging. Minimizing the time that these vehicles are off the street for charging is critical to the economics of electrifying these fleets.[98] Major global cities have made commitments to electrifying or eliminating emissions from mobility on demand vehicles including Shenzhen China, Oslo (by 2024), Amsterdam (by 2030), and London (by 2050). Warehouse vehicles, delivery trucks, and potentially long-haul carriers also are likely to make a transition to electric vehicles. Warehouse and delivery vehicles tend to be heavily used and operate at or from a central location.
Depending on their usage schedules and relative infrastructure costs, DC fast charging may be a sensible option for these fleets. Convenient fast charging hubs located on freeways and other major highways will be an important in supporting long-distance travel in light duty EVs that

[93] *Ibid.* See also: Glasgo et al. 2016; Thomas et ql. 2012.
[94] Fairley 2012.
[95] Lutsey and Nicholas 2019. See also: https://atb.nrel.gov/transportation/2020/index.html?t=lv.
[96] MIT Energy Initiative 2019.
[97] Quarles et al. 2020.
[98] Bauer et al, 2020.

otherwise would be range limited and the electrification of long-haul trucking. In these cases, vehicles will need to be charged rapidly while drivers stop for a meal or short rest period. By combining what would otherwise be multiple components, an integrated bidirectional AC/DC converter and transformer can help reduce costs, integrate batteries where needed to manage varying demand, and integrate fast charging stations with the AC power grid.

Data centers, commercial buildings, and fast charging hubs may combine the use of DC power with batteries as either an uninterruptible power supply or means of balancing variable demand and in some cases with distributed generation. Data centers and essential end uses in commercial building (e.g., IT, lighting, elevators) may need to maintain operations when islanded from the larger AC power grid. These are examples of small microgrids. An integrated bidirectional AC/DC converter and DC transformer may be an efficient way to meet their requirements.

Increasing the use of DC power in these and other applications may require addressing certain challenges, including:

1. A lack of comprehensive application, equipment, and interoperability standards for DC power distribution;
2. The lack of a common understanding and basic knowledge in the industry on building distribution-level DC power systems;
3. Differences in safety and power protection device applications for DC systems;
4. The lack of a robust ecosystem to support the use of DC in building-level electrification; and
5. An unclear pathway for moving from AC-centric power distribution to DC-inclusive distribution schemes.

The first three challenges can be the development appropriate standards by standards development organizations (SDOs) in cooperation with government and the private sector. The fourth challenge will be addressed when with ongoing research and development, available standards, and business cases lead to a broader set of products and services. Microgrid applications can provide an opportunity to segment the introduction of direct current into high value applications before considering more difficult changes in the larger power system.[99]

[99] Patterson 2012. Emerge Alliance is an industry association working to establish standards and promote market development for DC and hybrid DC/AC microgrids. See: https://www.emergealliance.org.

References

AILee, G. and W. Tschudi. 2012. “Edison Redux: 380 Vdc Brings Reliability and Efficiency to Sustainable Data Centers,” *IEEE Power & Energy Magazine.* (November / December 2012).

Alshahrani, A., S. Omer, Y. Su, E. Mohamed, and S. Alotaibi. 2019. "The Technical Challenges Facing the Integration of Small-Scale and Large-scale PV Systems into the Grid: A Critical Review" *Electronics* 8, no. 12: 1443.

Bachmann, J. 2019. *DC Data Centers: A Necessary Paradigm Shift for Sustainability and Savings.* (November 19, 2019). Available at: https://www.connectorsupplier.com/dc-data-centers-a-necessary-paradigm-shift-for-sustainability-and-savings/.

Bartlett, J. 2019. *Reducing Risk in Merchant Wind and Solar Projects through Financial Hedges.* Washington, D.C.: Resources for the Future.

Bauer, G., C. Zheng, B. Greenblatt, S. Shaheen, and D. Kammen. 2020. “On-Demand Automotive Fleet Electrification Can Catalyze Global Transportation Decarbonization and Smart Urban Mobility,” *Environ. Sci. Technol.* 2020, 54, 12, 702, Hereafter: Bauer et al. 2020.

Bhattacharyya, B. 2020. *Renewable Energy Tax Credits: The Case for Refundability.* Washington, D.C.: Center for American Progress. (May 28, 2020).

Blank, E. and D. R. Richardson. 2020. *Solar ITC Tax Normalization: Limits Solar Growth and Favors Fossil Fuels.* April 2020.

Bolinger, M., J. Seel, and D. Robson. 2019. *Utility-Scale Solar: Empirical Trends in Project Technology, Performance, and PPA Pricing in the United States – 2019 Edition.* Berkeley, CA; Lawrence Berkeley National Laboratory.

Bolinger, M., J. Seel, D. Robson, and C. Warner. 2020. *Utility-Scale Solar Data Update 2020 Edition.* Berkeley, CA; Lawrence Berkeley National Laboratory.

Burger, S., J. Jenkins, S. Huntington and I. Perez-Arriaga, "Why Distributed?: A Critical Review of the Tradeoffs Between Centralized and Decentralized Resources," in *IEEE Power and Energy Magazine*, vol. 17, no. 2, pp. 16-24, (March-April 2019).

Burton, D. 2016. “Dominion Takes On ITC Rules,” *Solar Industry Magazine.* (April 2016).

California Energy Commission. 2008. *DC Power Distribution Cuts Data Center Energy Use: Technical Brief.* Sacramento, CA: CEC. (October 1, 2008).

California Public Utilities Commission. 2020. *Decision Adopting Rates, Tariffs, and Rules Facilitating the Commercialization of Microgrids Pursuant to Senate Bill 1339 and Resiliency*

Strategies. Order Instituting Rulemaking Regarding Microgrids Pursuant to Senate Bill 1339 and Resiliency Strategies, Rulemaking 19-09-009. (January 21, 2021).

Caspary, J., M. Goggin, R. Gramlich, and J. Schneider. 2021. *Disconnected: The Need for a New Generator Interconnection Policy.* Washington, D.C.: Americans for a Clean Energy Grid.

Centolella, P., M. Gildersleeve, A. Rudkevich, I. Shavel, and R. Tabors. Forthcoming 2021. *Exploring the Impacts of Extreme Events Natural Gas Fuel and Other Contingencies on Resource Adequacy.* Palo Alto, CA: EPRI.

Centolella, P. 2020. *The Pricing We Need: What pricing will be needed to realize an affordable clean energy future?* Presentation for Harvard Electricity Policy Group. (October 27, 2020).

Chen, X., D. Yang, E. Lim, H. Wen, K. Yan, and J. Kirtley. 2020. "Power ramp-rates of utility -scale PV systems under passing clouds: Module-level emulation with cloud shadow modeling," *Applied Energy.* Vol. 268. (June 2020).

Chicago Transit Authority. 2020. *Traction Power.* Available at: https://www.chicago-l.org/operations/power/index.html.

Cole, W. and A. W. Frazier. 2020. *Cost Projections for Utility-Scale Battery Storage: 2020 Update.* Golden, CO: National Renewable Energy Laboratory.

Comello, S., and S. Reichelstein. 2015. *The U.S. Investment Tax Credit for Solar Energy: Alternatives to the Anticipated 2017 Step-Down.* Palo Alto, CA: Stanford Graduate School of Business.

Council of European Energy Regulators. 2019. *Implementing Technology that Benefits Consumers in the Clean energy for All Europeans Package: Selected Case Studies.* CEER Report Ref: C19-IRM-16-04. (July 22, 2019).

Crabtree, G., J. Misewich, R. Ambrosio, K. Clay, P. DeMartini, R. James, M. Lauby, V. Mohta, J. Moura, and P. Sauer. 2017. "Integrating renewable electricity on the grid," *Proceedings of the AIP Conference*. Geneva, Switzerland. (September 2017).

DiOrio, N. and W. Hobbs. 2018. *Economic dispatch for DC-connected battery systems on large PV plants.* Golden, CO: National Renewable Energy Laboratory. (May 3, 2018)

Electric Power Research Institute. 2010. *DC Power for Data Centers.* Palo Alto, CA: EPRI. (November 2010).

Elsayed, A., A. Mohamed, and O. Mohammed. 2015. "DC microgrids and distribution systems: An Overview," *Electric Power Systems Research,* 119 (2015).

ERCOT. 2019. *Project No. 49852, Review of Summer 2019 ERCOT Market Performance: ERCOT's Review of Summer 2019.* Austin, TX: ERCOT. (October 11, 2019).

ERCOT. 2020. *PUC Project No. 49852, Review of Summer 2019 ERCOT Market Performance: Updated Total System Demand Response/ Price Response Results for Summer 2019 Peak Week August 12 – August 16, 2019.* Austin, TX: ERCOT. (February 6, 2020).

Fairley, P. 2012. "Dc versus ac: The second war of currents has already begun," *IEEE Power & Energy Magazine.* (November / December 2012).

Federal Energy Regulatory Commission Staff. 2020. *Report on Barriers and Opportunities for High Voltage Transmission: A Report to the Committees on Appropriations of Both Houses of Congress Pursuant to the 2020 Further Consolidated Appropriations Act.* Washington, D.C.: FERC (June 2020).

Federal Energy Regulatory Commission. 2018. *Essential Reliability Services and the Evolving Bulk-Power System—Primary Frequency Response*, Final Rule 152 FERC ¶ 61,128, Order No. 842 (February 15, 2018).

Federal Energy Regulatory Commission. 2016. *Essential Reliability Services and the Evolving Bulk-Power System—Primary Frequency Response*, Notice of Proposed Rulemaking, 154 FERC ¶ 61,117. (November 25, 2016).

Fu, R., T. Remo, and R. Margolis 2018. *2018 U.S. Utility-Scale Photovoltaics-Plus-Energy Storage System Costs Benchmark.* NREL/TP-6A20-71714. Golden, CO: National Renewable Energy Laboratory.

Frazier, A., C. Marcy, and W. Cole. 2019. "Wind and solar PV deployment after tax credits expire: A view from the standard scenarios and the annual energy outlook," *The Electricity Journal,* Vol. 32, No. 8 (October 2019).

Glasgo, B., I. Azeedo, and C. Hendrickson. 2016. "How much electricity can we save by using direct current circuits in homes? Understanding the potential for electricity savings and assessing feasibility of a transition towards DC power buildings," *Applied Energy,* 180 (2016).

Gramlich, R., and M. Goggin. 2019. *Too Much of the Wrong Thing: The Need for Capacity Market Replacement of Reform.* Washington, D.C.: Grid Strategies. (November 2019).

Gramlich, R., and F. Lacey. 2020. *Who's The Buyer? Retail Electric Market Structure Reforms in Support of Resource Adequacy and Clean Energy Development.* Bethesda, MD: Grid Strategies, L.L.C.

Heeter, J., J. Cook, And L. Bird. 2017. *Charting the Emergence of Corporate Procurement of Utility-Scale PV.* NREL?TP-6120-69080. Golden, CO: National Renewable Energy Laboratory.

Hweightley, M., D. Marples, and M. Shelock. 2019. *Tax Equity Financing: An Introduction and Policy Considerations.* Washington, D.C.: Congressional Research Service.

Keleher, M., M. Dyson, and A. Engel. 2020. *Clean Energy is Canceling Gas Plants.* Boulder, CO: Rocky Mountain Institute. (September 30, 2020).

Kintner, D. 2011. *Duke Energy – EPRI DC Data Center Demonstration: Executive Summary.* Palo Alto, CA: EPRI.

Larson, E., C. Greig, J. Jenkins, E. Mayfield, A. Pascale, C. Zhang, J. Drossman, R. Williams, S. Pacala, R. Socolow, EJ Baik, R. Birdsey, R. Duke, R. Jones, B. Haley, E. Leslie, K. Paustian, and A. Swan, *Net-Zero America: Potential Pathways, Infrastructure, and Impacts, interim report.* Princeton, N.J.: Princeton University. (December 15, 2020).

Lazard. 2020. *Lazard's Levelized Cost of Energy Analysis, Version 14.0.*

Lutsey, N. and M. Nicholas. 2019. *Update on electric vehicle costs in the United States through 2030.* Washington, D.C.: The International Council on Clean Transportation. (April 2, 2019).

MIT Energy Initiative. 2016. *Utility of the Future: An MIT Energy Initiative response to an industry in transition.*

MIT Energy Initiative. 2019. *Insights into Future Mobility: A report from the Mobility of the Future study.* Cambridge, MA: MIT.

McCalley, J. and Q. Zhang. 2020. *Macro Grids in the Mainstream: An International Survey of Plans and Progress.* Washington, D.C.: Americans for a Clean Energy Grid. (November 2020).

Ministry of Industry, Energy, and Tourism. 2014. "Royal Decree 216/2014, of March 28, establishing the methodology for calculating voluntary prices for small consumers electric power and its legal contracting regime," *State Official Newsletter.* (March 29, 2014).

Murphy, B. 2019. "Renewable energy ownership: A game plan for utilities," *Utility Dive.* (May 22, 2019).

National Academies of Sciences, Engineering, and Medicine. 2016. *The Power of Change: Innovation for Development and Deployment of Increasingly Clean Electric Power Technologies* Washington, D.C.: The National Academies Press.

National Conference of State Legislatures. 2021. *State Renewable Portfolio Standards and Goals.* (January 4, 2021). Available at: https://www.ncsl.org/research/energy/renewable-portfolio-standards.aspx.

National Renewable Energy Laboratory. 2020. *Annual Technology Baseline: Electricity.* Available at: https://atb.nrel.gov.

New York Department of Public Service. (2015) *Staff White Paper on Ratemaking and Utility Business Models.* Case No. 14-M-0101. Proceeding on Motion of the Commission in regard to Reforming the Energy Vision

New York Public Service Commission. (2016) *Order Adopting a Ratemaking and Utility Revenue Model Policy Framework.* Case 14-M-0101. Proceeding on Motion of the Commission in regard to Reforming the Energy Vision.

North American Electric Reliability Corporation Essential Reliability Services Task Force. 2015. *Essential Reliability Services Task Force Measures Report.* Atlanta, GA: NERC. (December 2015).

Ofgem. (2013) *RIIO-ED1: Strategy decision for the RIIO-ED1 electricity distribution price control Outputs, incentives, and innovation.* London, UK: Ofgem.

Patterson, B. 2012. "DC, Come Home: DC Microgrids and the Birth of the 'Enernet'," *IEEE Power & Energy Magazine.* (November / December 2012).

Pickerel, K. 2020. "Solar investment tax credit extended at 26% for two additional years," *Solar Power World.* (Updated: December 28, 2020).

Potomac Economics. 2020. *2019 State of the Market Report for the ERCOT Electricity Markets* (May 2020).

Quarles, N., K. Kockelman, and M. Mohamed. 2020. *Costs and Benefits of Electrifying and Automating Bus Transit Fleets.* Austin, TX: University of Texas.

Quilici, L., and D. Powers, G. Therrien, B. Davis, and O. Prieto. 2019. *Retail Competition in Electricity: What Have We Learned in 20 Years?* Marlborough, MA: Concentric Energy Advisors.

Rakhshani, E., K. Rouzbehi, A. Sánchez, A. Tobar, and E. Pouresmaeil. 2019. "Integration of Large Scale PV-Based Generation into Power Systems: A Survey" *Energies* 12, no. 8: 1425.

Reed, G. 2020. "9 Reasons Why DC May Replace AC," *electric industry news week.* (November 16, 2020). Available at: https://electricalindustry.ca/latest-news/1018-9-reasons-why-dc-may-replace-ac.

Reed, G. 2012. "DC technologies: solutions to electric power system advancements," *IEEE Power & Energy Magazine.* (November / December 2012).

Rhodes, J. 2020. “Even Renewables Are Bigger in Texas,” *Forbes.* (September 25, 2020). Available at: https://www.forbes.com/sites/joshuarhodes/2020/09/25/even-renewables-are-bigger-in-texas/amp/.

Roberts, C. 2018. *Review of International Grid Codes.* Berkeley, CA: Lawrence Berkeley National Laboratory. LBNL-2001104. (February 2018).

Shaw, S. and S. Shimamoto. 2018. *The Emergence of Utility-Owned Renewable Energy Under Build-Transfer Agreements.* New York, N.Y.: Skadden.

Sherlock, M. 2018. “The Energy Credit: An Investment Tax Credit for Renewable Energy,” *In Focus.* Washington, D.C.: Congressional Research Service (November 1, 2018).

Shrestha, B., U. Tamrakar, T. Hansen, B. Bhattarai, S. James, and R. Tonkoski. 2018. "Efficiency and Reliability Analyses of AC and 380 V DC Distribution in Data Centers," *IEEE Access*, vol. 6, pp. 63305-63315.

Silverstein, A. 2020. *Resource Adequacy Challenges in Texas: Unleashing Demand-Side Resources in the ERCOT Competitive Market.* Austin, TX: Environmental Defense Fund. (May 2020).

Spiegel-Feld, D. and B. Mandel. (2015) *Reforming Electricity Regulation in New York State: Lessons from the United Kingdom.* New York University School of Law.

St. John, J. 2020. “What Renewable Energy and Energy Storage Did, and Didn’t, Get from Congress This Week,” *Green Tech Media.* (December 24, 2020.)

Sterlace, D. 2020. *Direct Current in the data center: are we there yet?* (January 6, 2020). Available at: https://www.abb-conversations.com/2020/01/dc-in-the-data-center-are-we-there-yet/.

Thomas, B., I. Azevedo, and G. Morgan. 2012. “Edison Revisited: Should we use DC circuits for lighting in commercial buildings?” *Energy Policy,* 45 (2012).

U.S. Energy Information Administration. 2020. *Annual Energy Outlook 2020.* Available at: https://www.eia.gov/outlooks/aeo/index.php.

U.S. Energy Information Administration. 2020a. *EIA-860 Detailed State Data, Annual Data*. (September 22, 2020). Available at: https://www.eia.gov/electricity/data/state/.

Van Haaren, R., M. Jorjaria, and V. Fthenakis. 2012. “Empirical assessment of short-term variability from utility-scale solar PV plants,” *Progress in Photovoltaics: Research and Applications.*

Wang, P., L. Goel, X. Liu, and F. Hoong Choo. 2012. “Harmonizing AC and DC,” *IEEE Power & Energy Magazine.* (November / December 2012).

Weiss, J., J.M. Hagerty, and M. Castañer. 2019. *The Coming Electrification of the North American Economy: Why We Need a Robust Transmission Grid.* Boston, MA: The Brattle Group (March 2019).

Wesoff, E. 2020. “The best little utility-scale solar roundup in Texas,” *PV Magazine.* (August 12, 2020).

Wesoff, E. 2020a. “Texas gusher of massive utility-scale solar development,” *PV Magazine.* (September 2, 2020).

Whieldon, E., and J. Ryser. 2020. “Path to Net Zero: Cracks appearing in natural gas’ role as bridge fuel,” *S&P Global Market Intelligence.* (July 28, 2020).

12. Appendix C — EPRI PV Farm-level Study Report Slides

MDCT Modeling in OpenDSS

Paulo Radatz, Principal Investigator, pradatz@epri.com
Wei Ren, wren@epri.com
Roger Dugan, rdugan@epri.com

Electric Power Research Institute, Inc, Power Systems Studies
Distribution Operations & Planning
942 Corridor Park Blvd, Knoxville, TN 37932

Georgia Institute of Technology (GIT) Contract:
AWD-102315-S1/RK356-S1

January 31, 2022

This material is based upon work supported by the U.S. Department of Energy's Office of Energy Efficiency and Renewable Energy (EERE) Under the Solar Energy Technology Office Award Number DE-EE0008351.

OpenDSS-Python Model

Interpretation of the Georgia Tech Simulink Model

- Three major control objectives
  - Grid side power regulation (through controlling D_{AC})
  - PV Maximum Power Point Tracking – MPPT (through controlling D_{PV})
  - Magnetizing current regulation (through controlling D_{BATT})
- Extremely fast control response by tracking instantaneous AC current reference
  - Open loop control for grid power regulation and PV MPPT with equivalent delay of half switching frequency cycle (16kHz)
  - Proportional control for magnetizing current regulation with equivalent time constant of 56us ($\models \frac{L_m \cdot i_m^*}{v_{batt}}$)
- These ultra fast dynamics are simplified in OpenDSS simulation as a controlled current source with instant response

Flow Chart for OpenDSS Implementation of MDCT Model

The flowchart presents the steps necessary to model the Simulink model behavior using Python and OpenDSS.

The model behavior is modeled in Python, and the grid (simple Thevenin equivalent model) is modeled in OpenDSS.

Python controls OpenDSS to update the grid and current sources, perform power flow, and obtain results for each time-step.

With a full circuit, a fault can be applied and/or cleared in the system.

OpenDSS solves the power flow of the circuit.

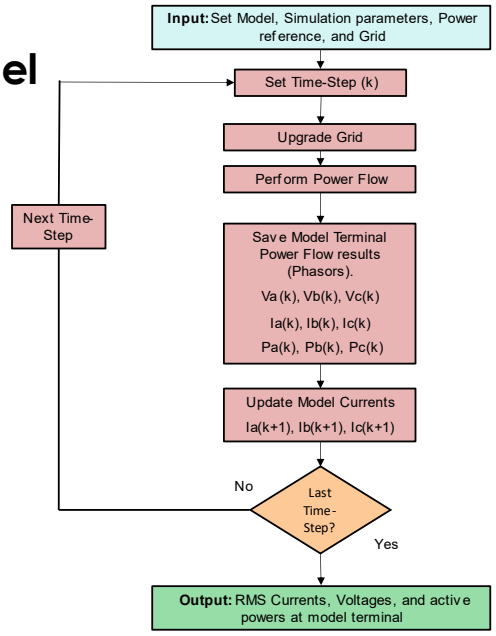

Update Model Currents

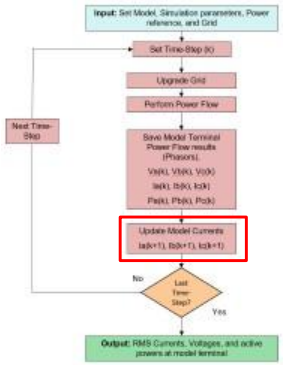

- Operation without Fault
  - $\dot{I}'x_{(k+1)} = \frac{Px_{(k+1)} - j * Qx_{(k+1)}}{\dot{V}x_{(k)}}$, where x can be phases a, b, and c
  - $\dot{I}x_{(k+1)} = a * \dot{I}'x_{(k+1)} + (1-a) * Ix_{(k)}$
  - Where *a* is a smoothing factor used for more numerical stability
- Operation under fault. Fault included at iteration (k) and phase a
  - Balanced current
    - $\dot{I}'x_{(k+1)} = \dot{I}x_{(k)}$
    - $\dot{I}x_{(k+1)} = a * \dot{I}'x_{(k+1)} + (1-a) * Ix_{(k)}$
  - Oscillation free power
    - $\dot{I}a_{(k+1)} = -j * \dot{I}a_{(k)}$
    - $\dot{I}b_{(k+1)} = \dot{I}b_{(k)}$
    - $\dot{I}c_{(k+1)} = \dot{I}c_{(k)}$

Cases Description

- Case 1 – Operation under Cloud Cover with battery smoothing effect
- Case 2 – Grid Fault and Reactive power support
  - A single line to ground fault has been presented and the model is made to deliver reactive power during the fault to support the voltage.
  - A 50% sag in the nominal voltage of phase -a has been considered.
- Case 3 – Grid Voltage Sag and its effect
  - During unsymmetrical voltage sag balanced sinusoidal current is transferred to the grid

Case 1 – Operation under Cloud Cover

OpenDSS Model Results

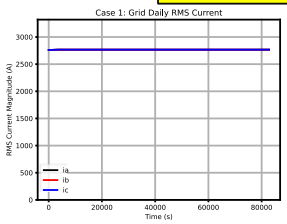

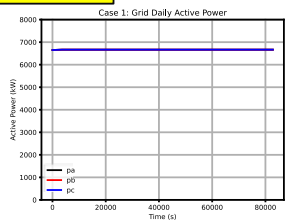

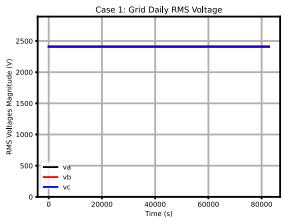

OpenDSS Model Grid Daily Active Power is the sum of the PV and the battery active power

Run case1.py

Simulink Model Results:

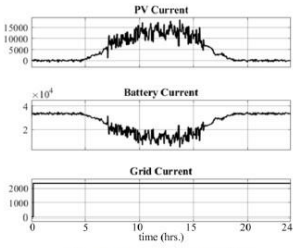

Current at each port with battery smoothing

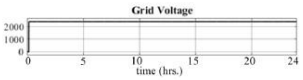

Voltage at each port

Battery to compensate for PV power fluctuation and maintain constant total output

Case 2 – Grid Fault and Reactive power support

OpenDSS Model Results

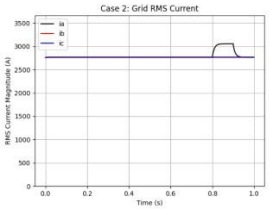

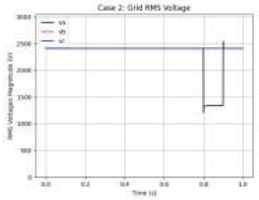

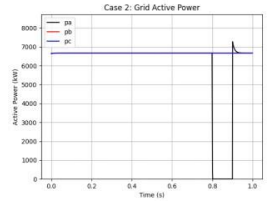

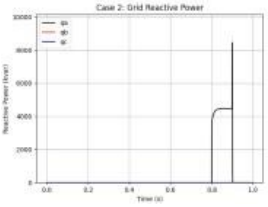

Run case2.py

Simulink Model Results:

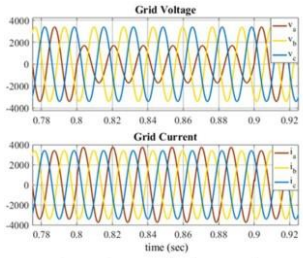

Three-phase grid voltage and current during fault

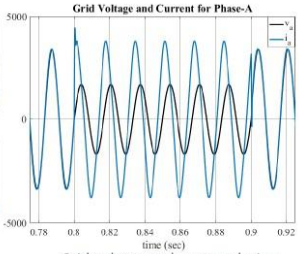

Grid voltage and current during fault for the faulted phase-a

During this fault, inverter shifts current by 90 deg to provide reactive support

Case 3 – Grid Voltage Sag and its effect

OpenDSS Model Results

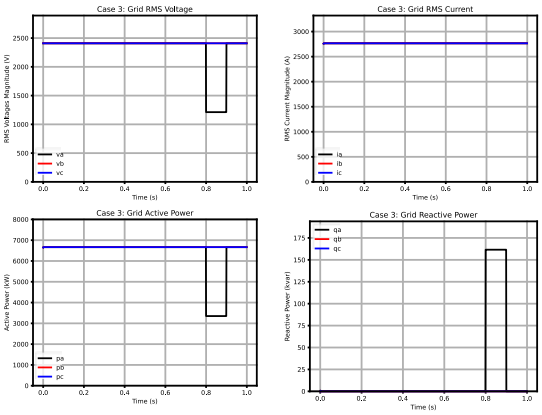

Run case3.py

Simulink Model Results:

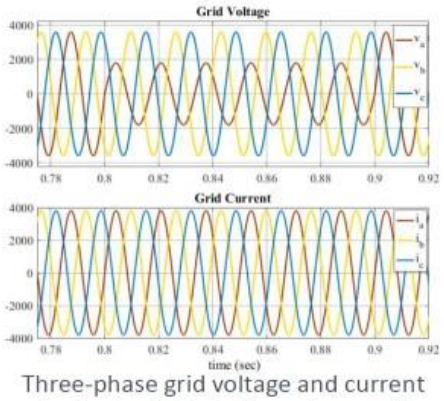

Three-phase grid voltage and current during fault (for balanced current)

At low voltage sag, inverter maintains the prefault current injection

Base Case

- System connected to bus 671
  - P rated = 20 MW
  - V rated = 4.16 kV
- Simulation Characteristics
  - Total simulation time = 1 s
  - Time-step = 0.001 s

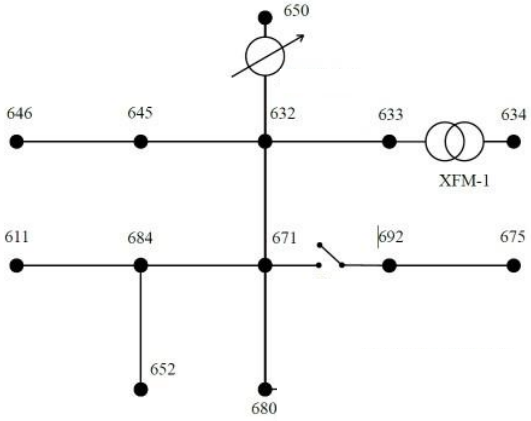

Case 1 – Operation under Cloud Cover

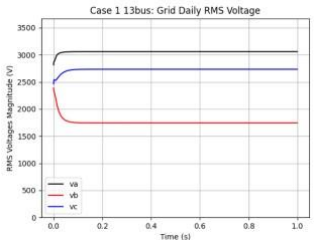

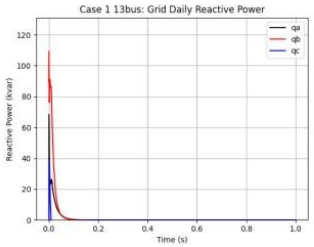

Run case1_13bus.py

Battery to compensate for PV power fluctuation and maintain constant total output

Case 2 – Grid Fault and Reactive power support

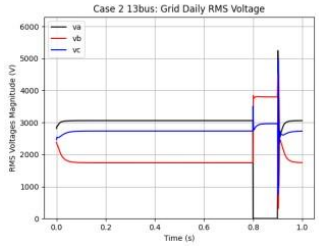

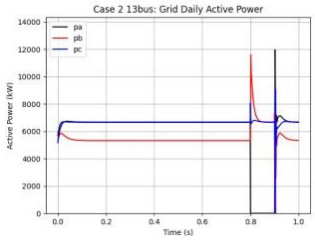

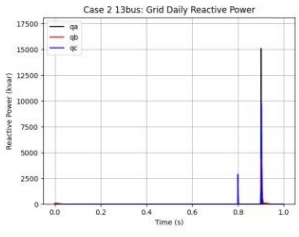

Run case2_13bus.py

- Disturbance Characteristics
  - Single-phase Fault
  - Bus 671 – Phase A
  - Time on = 0.8s
  - Time off = 0.9s

During this fault, inverter shifts current by 90 deg to provide reactive support

Case 3 – Grid Voltage Sag and its effect

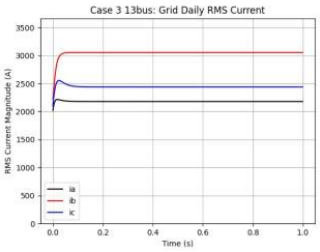

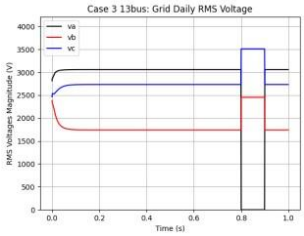

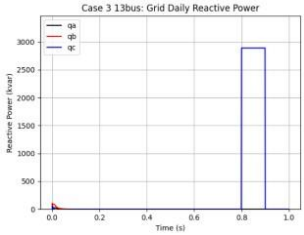

Run case3_13bus.py

- Disturbance Characteristics
  - Single-phase Fault
  - Bus 671 – Phase A
  - Time on = 0.8s
  - Time off = 0.9s

At low voltage sag, inverter maintains the prefault current injection